Robust Shape Optimization for solid mechanics and fluid mechanics

Salah-Eddine Zerrouq

SCIENCES EXACTES ET LEURS APPLICATIONS

UNIVERSITÉ DE PAU ET DES PAYS DE L'ADOUR

THÈSE DE DOCTORAT DE

L'UNIVERSITÉ DE PAU ET DES PAYS DE L'ADOUR

ÉCOLE DOCTORALE N° 211
Sciences exactes et leurs applications
Spécialité : *Mathématiques*

Par
Salah-Eddine Zerrouq

Optimisation de forme robuste pour la mécanique des solides et des fluides.

Thèse présentée et soutenue à PAU, le 05/12/2022
Unité de recherche : Laboratoire de Mathématiques et de leurs Applications de Pau

Rapporteurs avant soutenance :

Eric BONNETIER Professeur des universités - Université Grenoble-Alpes.
Yannick PRIVAT Professeur des universités - Université de Strasbourg.

Composition du Jury :

Président :	Marco MONTEMURRO	Professeur des universités - ENSAM Bordeaux.
Examinateurs :	Eric BONNETIER	Professeur des universités - Université Grenoble-Alpes
	Yannick PRIVAT	Professeur des universités - Université de Strasbourg.
	Julien DAMBRINE	Maître de Conférences - Université de Poitiers.
	Idriss MAZARI	Maître de Conférences - Université Paris-Dauphine.
Dir. de thèse :	Marc DAMBRINE	Professeur des universités - Université de Pau et des pays de l'Adour.
Co-dir. de thèse :	Bénédicte PUIG	Maître de Conférences - Université de Pau et des pays de l'Adour.
Co-enc. de thèse :	Morgan PIERRE	Maître de Conférences HDR - Université de Poitiers.

Invité(s) :

Boris ANDREIANOV Professeur des universités - Université de Tours.

Remerciements

À tout seigneur, tout honneur, commençons par remercier les gens qui ont aidé de près comme de loin à la réalisation de ce travail. Je ne trouverai sûrement pas les mots nécessaires pour exprimer ma gratitude, étant donné l'obligation de tout rédiger en français, mais aussi du fait de mon excès de reconnaissance.

D'abord les responsables directs de ma thèse, qui m'ont donné la chance de réaliser mon rêve et rédiger une thèse de mathématiques. Je suis, et resterai éternellement reconnaissant envers mes directeurs de thèse, Marc Dambrine et Bénédicte Puig, pour ce qui est la meilleure période de ma vie. Ils ont été très patients avec moi, le temps de découvrir l'optimisation de forme. Ils m'ont formé, et aidé à faire de la recherche scientifique, tout en me laissant la liberté de découvrir ce qui m'intéresse. Je les remercie pour tous leurs efforts, et pour leur attitude chaleureuse et parentale qui m'a marqué le long de ma thèse.

Je remercie mon co-encadrant, Morgan Pierre, d'avoir transformé un stage de 3 mois en une belle et chaleureuse expérience de 2 ans, qui m'a appris beaucoup de choses. Je le remercie pour nos réunions webex hebdomadaires, sa patience quand il a fallu débuguer des centaines de lignes de code, et pour son attitude très amicale.

Je suis honoré que Yannick Privat et Eric Bonnetier aient accepté de rapporter mon travail de thèse. Je suis très reconnaissant envers Marco Montemurro, Julien Dambrine et Idriss Mazari, d'avoir accepté de faire partie du jury de soutenance.

Je remercie Charles Dapogny pour son aide précieuse. Je le remercie pour toutes ses contributions théoriques et numériques qui m'ont inspiré pour réaliser ce travail.

Un grand merci à Jean-Léopold Vié pour son travail de thèse, qui m'a beaucoup éclairé. Je le remercie également d'avoir pris le temps de discuter et de répondre à mes questions.

Je remercie Fabien Caubet pour son aide, que ce soit pour détailler un calcul, lire mon travail ou le corriger. Fabien m'a toujours accueilli avec le sourire, et je lui en suis très reconnaissant.

Un grand merci à Mathieu Haefel, Cherif Amerouche, ainsi qu'à l'ensemble du personnel du LMAP : Bruno, Gilles, Jean-Matthieu, Isabelle, Guy, Jonathan, Sophie, Jackie, Charles, de m'avoir bien accueilli au sein du labo.

Je tiens à remercier mes collègues de bureau de m'avoir supporté pendant 3 ans.

Merci Adrien pour toutes les fois où tu m'as aidé. Merci Nicolas, notre fournisseur officiel de templates tex, et merci Sarah pour les énigmes pendant le confinement. Je remercie Aymeric et Giulio, mes compagnons de route, pour nos aventures en train, à traverser la France pour aller en conférence.

S'il a fallu chercher des réponses auprès de la communauté scientifique, c'est auprès de ma famille et mes amis que j'ai trouvé le courage, et la motivation pour vivre mon aventure de thésard. Je remercie mes parents pour leurs sacrifices, qui m'ont permis de venir en France et de poursuivre mes études. Merci pour votre confiance et votre patience avec moi. Tous mes remerciements vont à ma fiancée Elise, qui a partagé cette aventure avec moi et qui a supporté mes indisponibilités, que ce soit en période de lecture ou de rédaction. Merci pour tes encouragements et ton aide au quotidien. Un grand merci à toute ma belle-famille, pour les réunions familiales qui m'ont permis de me ressourcer avant de reprendre mon travail. Je suis très reconnaissant envers mes amis, qui m'ont toujours soutenu, avant et pendant la thèse. Un grand merci à la famille Donadio, qui m'a motivé à poursuivre mon rêve et à venir à Pau. Merci d'être venus me voir à plusieurs reprises, et pour tous les beaux souvenirs qui m'ont réchauffé le cœur. Un grand merci à la famille Fouhami de m'avoir vite adopté à mon arrivée en France. Merci pour tous les moments chaleureux en famille, et pour votre soutien pendant toutes ces années.

Pour finir, je tiens à remercier Boris Andreianov de m'avoir ouvert la porte de la recherche, et de m'avoir montré la beauté des mathématiques appliquées. Merci pour le professeur exceptionnel que tu es, pour la belle personne que tu es, et pour ta confiance en moi. J'espère un jour pouvoir, à mon tour, transmettre cette passion à quelqu'un, comme tu l'as fait avec moi.

Table of Contents

Résumé

Le but de cette thèse, est d'étudier et de résoudre quelques problèmes physiques de design robuste dans un contexte d'optimisation de forme, en appliquant les deux approches proposées dans la littérature : déterministe ou stochastique.

Elle est composée de deux parties. La première partie s'intéresse au design de matériaux dans deux travaux :

— Un premier travail sur le design robuste de matériaux légers, prenant en compte des incertitudes sur la géométrie de la micro-structure du matériau, en utilisant l'approche déterministe. **Ce travail donné dans le chapitre 2, fait l'objet d'un article en collaboration avec mon encadrant Marc Dambrine, qui est soumis en publication**.

— Un deuxième travail sur le design optimal de matériaux composites piézoélectriques. **Ce travail individuel donné dans le chapitre 3, fait l'objet d'un deuxième article qui sera soumis en publication après finalisation des résultats numériques**.

La deuxième partie de la thèse s'intéresse au problème de design robuste de carènes de bateaux, en utilisant une approche stochastique, pour prendre en compte les incertitudes par rapport à la vitesse du bateau. Cette partie donne des résultats théoriques et numériques sur les formes de carènes minimisant l'espérance de la résistance totale de l'eau au bateau, par rapport à une distribution probabiliste des vitesses données, dans les chapitres 7 et 9. Un autre résultat principal de cette partie est le développement d'un nouvel algorithme de second ordre pour l'optimisation de forme, basé sur une simple discrétisation de la méthode de Newton, donné dans le chapitre 8. **L'essentiel des chapitres 7, 8 et 9 fait l'objet d'un troisième article en collaboration avec mon encadrant Morgan Pierre, qui sera soumis en publication**.

L'ensemble des travaux de cette thèse a donné lieu aux présentations suivantes :

— **Inverse homogenization for elastic structures, Décembre 2021**. Rencontre en calcul des variations : Université de Lorraine, Nancy, France.

— **Some theoretical and numerical difficulties in robust shape optimization, Mai 2022**. Séminaire EDP. Laboratoire de Mathématiques et Applications

: Université de Poitiers, France.

— **Méthode de Newton pour le calcul de carènes optimales basée sur la formule de Michell pour des vitesses aléatoires, Juin 2022**. 45ème Congrès National d'Analyse Numérique, Evian, France.

Introduction en Français

Le design optimal de structures mécaniques pour accomplir un objectif physique est souvent réduit à l'optimisation des propriétés matérielles de la structure, de sa forme et de sa topologie. Cela fait appel à des outils numériques et théoriques qui reposent sur un modèle mathématique pour décrire le comportement physique de la structure (souvent une EDP). Par exemple, les équations d'élasticité sont résolues afin de modéliser le déplacement d'un objet élastique chargé d'un poids. La connaissance de ce déplacement est ensuite utilisée pour le design optimal de mécanismes compliants. Le modèle mathématique dépend à son tour de plusieurs paramètres :

— la géométrie de la structure, ce qui représente le domaine 2D ou 3D du modèle,
— les propriétés matérielles de la structure,
— les différentes forces appliquées à la structure : pression, friction, chargement...

En pratique, ces paramètres clé sont rarement connus de façon exacte (ce qui est assumé par le modèle mathématique). Ils sont souvent considérés avec un certain degré d'incertitude, pouvant influencer les performances finales du design. Ainsi, dans une époque où les produits sont conçus pour surpasser leurs performances presque annuellement, le design robuste a été développé pour mieux prendre en compte ces incertitudes. De façon générale, le design robuste emploie les mêmes outils théoriques et numériques que ceux utilisés pour le design optimal. La robustesse est atteinte en transformant le critère d'optimalité (généralement l'objectif physique de la structure, ou une contrainte sur la structure) en un critère robuste, qui permettra toujours de satisfaire l'objectif physique de la structure, tout en prenant en compte les incertitudes sur les différents paramètres. Dans le contexte de l'optimisation de forme, deux approches sont considérées :

1. Une approche stochastique, où la robustesse peut être atteinte de deux façons différentes. L'idée la plus naturelle est peut-être de considérer comme critère robuste, l'espérance de l'objectif par rapport au paramètre incertain, ou une somme pondérée de ses moments. Intuitivement, cela signifie que la structure robuste aura des bonnes performances en moyenne. Une autre solution est de s'assurer que la structure restera performante dans toutes les configurations perturbées possibles, en maximisant sa fiabilité. Celle-ci est définie comme la probabilité d'un système à réaliser sa fonction,

en une durée spécifique et dans des conditions de service spécifiques. Dans les deux cas, l'approche stochastique suppose la connaissance d'une distribution probabiliste des incertitudes (souvent obtenue via des études statistiques), et coûte généralement cher en calcul. En effet, il faut évaluer l'objectif plusieurs fois pour calculer ses différents moments de probabilités.

2. L'approche déterministe est utilisée lorsqu'on ne dispose pas d'informations statistiques sur les perturbations, autres qu'une borne sur leur magnitude. Ainsi, un design de pire scénario possible est recherché, en minimisant la pire valeur possible de l'objectif, parmi tous les designs perturbés. Cela est souvent formulé comme un problème de "min-max", difficile à résoudre et coûteux en matière de calcul.

Cette thèse examine l'application des deux approches, pour deux problèmes physiques différents. Dans la première partie, l'approche déterministe est utilisée pour le design robuste de matériaux composites. Dans la deuxième partie, l'approche stochastique est utilisée pour le design robuste de carènes de bateaux. Les résultats généraux de chaque partie sont ensuite discutés sans références, et le lecteur est renvoyé vers les différents chapitres pour la bibliographie. Avant de commencer, une référence doit cependant être citée, pour le lecteur découvrant l'optimisation de forme, et peut-être l'optimisation en général. Celle-ci est l'excellent travail de thèse de Jean-Léopold Vié [77], et ses références. Bien sûr, ce travail ne remplace pas d'autres livres de référence sur l'optimisation de forme, mais le travail de monsieur Vié propose des applications détaillées des différents outils théoriques et numériques de l'optimisation de forme, à différents problèmes physiques. Ceci peut être utile pour s'approprier facilement ces outils, souvent donnés dans un cadre plus théorique. Ainsi, aucun chapitre n'est dédié aux rappels d'optimisation de forme, mais des références seront données pour chaque outil utilisé le long de la thèse.

Partie 1

La première partie est composée de trois chapitres, elle étudie le design optimal et robuste de matériaux composites.

— Le chapitre 1 introduit le problème général : le design de structure mécanique optimale, à la fois au niveau de la forme et des propriétés du matériau de la structure. On étudie le design d'un matériau optimal au niveau de la microstructure pour deux problèmes différents : des matériaux élastiques légers, et des composites piézoélectriques.

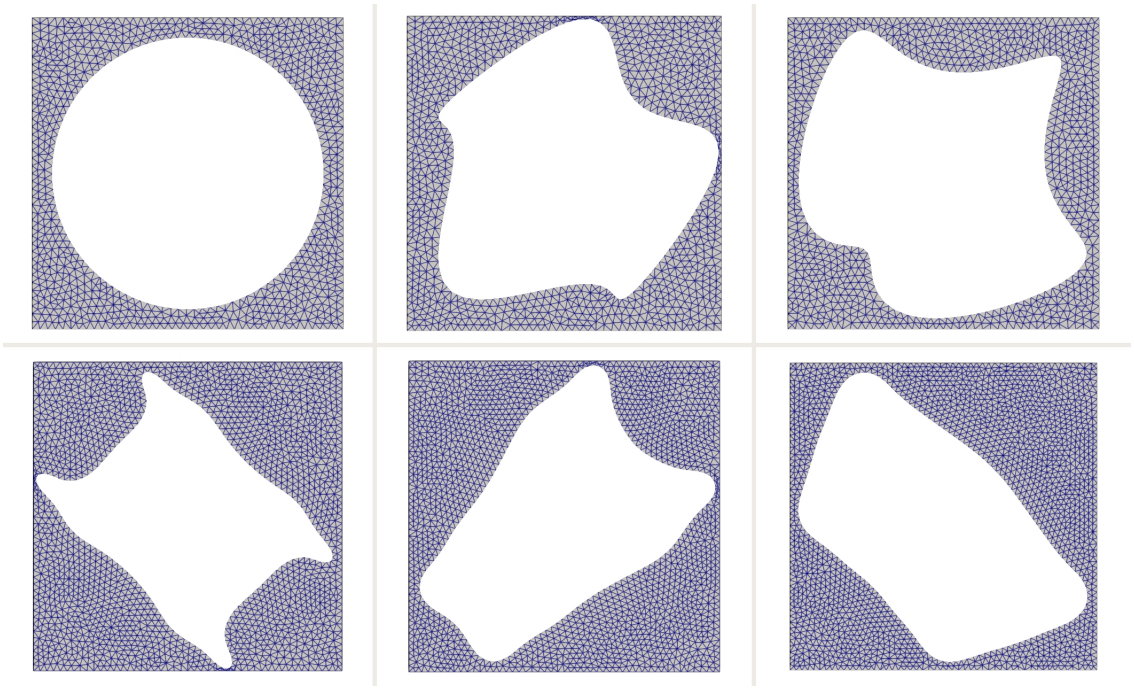

Figure 1 – The computed optimal holes for the matching of the upper bound of the effective tensor A^* with a material density $\theta = 0.4$.

— Le chapitre 2 est dédié au light-weight design de microstructures élastiques, d'abord dans une perspective optimale, ensuite dans une perspective robuste. La microstructure est représentée par une cellule perforée, remplie d'un matériau élastique. Celles-ci peuvent être "collées" cote-à-cote pour former la structure perforée globale. Mathématiquement, les propriétés du matériau sont représentées par une matrice A. Les propriétés matérielles de la structure globale, A* sont obtenues par homogénéisation (moyenne) des propriétés du mélange matériau-vide. Ainsi, étant donnée une matrice B, représentant les propriétés matérielles désirées, la forme optimale du trou dans la microstructure est recherchée afin que A* soit le plus proche de B dans le sens des moindres carrées. Les résultats numériques montrent que ce problème admet une infinité de solutions, comme exposé dans la figure 1. Bien que les microstructures calculées aient des valeurs très petites (10^-5) pour le critère de matching J, elles possèdent différentes sensibilités par rapport aux perturbations géométriques. La forme la plus robuste, moins sensible aux perturbations, est alors recherchée en minimisant une approximation du pire scénario

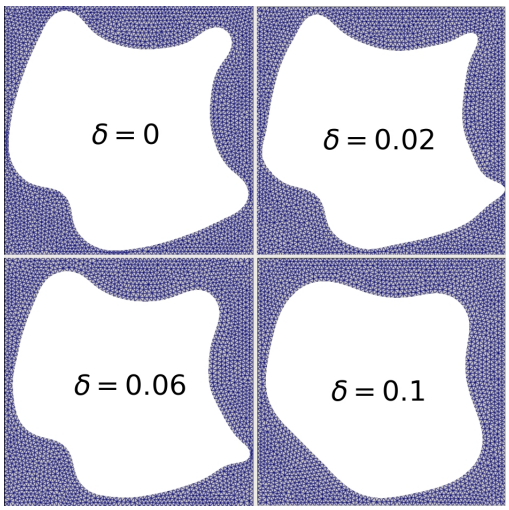

Figure 2 – The computed robust for the matching of the upper bound of the effective tensor A^* with a material density $\theta = 0.4$ for different values of δ.

possible donnée par :

$$\mathcal{J}_{rob} = J(\Omega) + \delta \|J'(\Omega; \xi)\|, \tag{1}$$

où $\delta \in (0, 1]$ représente la magnitude des perturbations géométriques. L'idée est, que pour des valeurs élevées de δ, la norme de la dérivée de forme qui modélise la sensibilité par rapport à la forme, est plus dominante. Ainsi, les formes résultantes seront moins sensibles aux perturbations géométriques. Les résultats numériques suggèrent que la robustesse se traduit par un manque de détails sur le bord de l'inclusion, comme montré dans la figure 2.

Nos résultats numériques suggèrent qu'il n'est pas possible d'être à la fois robuste et optimal pour le critère J en utilisant l'approximation (1) pour le pire scénario possible. Au final, cela reste une somme pondérée de deux fonctionnelles n'ayant pas nécessairement la même direction de descente au voisinage d'un point critique, comme le montre la figure 3. Des expérimentations numériques montrent que des meilleures formes, couplant robustesse et optimalité, peuvent être obtenues en alternant entre minimisation du critère de matching J et lissage du bord de l'inclusion.

— Le chapitre 3 étudie le design optimal des composites piézoélectriques dans l'esprit du chapitre 2. Un matériau piézoélectrique possède à la fois des propriétés élastiques et électriques. Celles-ci sont couplées, de façon à ce qu'un déplacement élastique produise de l'électricité par mouvement des électrons, et vice-versa. La

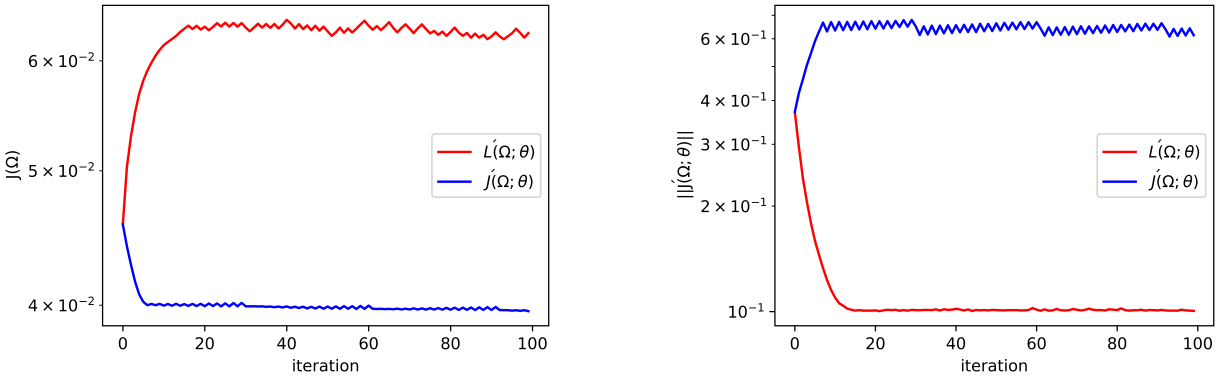

Figure 3 – Convergence results for the matching objective $J(\Omega)$ (left), and the norm of its shape derivative $L(\Omega) = \|J'(\Omega;\xi)\|$ (right) using their respective shape gradients.

modélisation des différents comportements piézoélectriques complique le problème d'homogénéisation, au moins d'un point de vue numérique. Dans ce chapitre, seul le matching optimal des propriétés élastique et diélectrique est traité.

Partie 2

La deuxième partie est dédiée au design robuste de carènes de bateaux, en utilisant l'approche stochastique. Elle se compose de 6 chapitres :

— Le chapitre 4 construit une introduction générale au design de bateaux, et une revue de la littérature sur le sujet. Il s'agit de concevoir des vaisseaux pouvant avancer dans l'eau avec une résistance minimale. Cette résistance est composée de deux parties : une résistance visqueuse due à la pression de l'eau sur la surface du bateau, et la résistance des vagues. La première est une fonction de la surface mouillée du bateau et du coefficient de viscosité de l'eau. La seconde dépend de la géométrie du vaisseau et de sa vitesse V, et peut être modélisée par différentes EDP.

— Le chapitre 5 est dédié à la modélisation de la résistance des vagues utilisée dans ce travail. Elle est donnée par une formule intégrale obtenue par le mathématicien J.H Michell en 1889. La résistance de Michell est une formule permettant d'estimer avec précision, sur certaines gammes de vitesse du bateau, la résistance des vagues pour un coût faible en calcul.

— Le chapitre 6 donne les deux problèmes principaux à résoudre pour le design de

carènes robustes. Comme énoncé précédemment, la résistance totale est la somme de la résistance visqueuse et de la résistance des vagues au bateau. Chacune dépend, à des degrés différents, de la vitesse du navire. Ainsi, une carène optimale pour minimiser la résistance totale à une vitesse fixée, pourrait perdre en optimalité lorsque la vitesse change. En pratique, la vitesse d'un navire varie sur un intervalle de vitesse minimale et maximale défini. Cette variation peut être vue comme une distribution de probabilités. Nous cherchons donc des coques robustes, qui permettraient une bonne réduction de la résistance totale "en moyenne", pour une gamme de vitesses donnée. Pour cela, le critère de robustesse est défini comme l'espérance de la résistance totale au navire par rapport à la vitesse, et notre stratégie est de la minimiser en deux étapes :

1. D'abord, la carène du bateau est représentée par une fonction du plan xOz (le plan vertical au milieu du navire). Un domaine D est fixé comme support de la carène, puis la carène optimale pour minimiser l'espérance de la résistance totale est recherchée.
2. La deuxième étape est de faire varier le domaine D dans un compact. Le support optimal de la carène optimale minimisant l'espérance de la résistance totale est donc recherché.

— Le chapitre 7 étudie la minimisation de l'espérance pour un support fixe. Un résultat d'existence d'une carène optimale et de sa régularité est donné, avant de la calculer. Cette tâche est coûteuse en calcul. L'espérance est donc calculée de façon déterministe, pour différentes distributions des vitesses (uniforme, ou centrée à gauche de l'intervalle de vitesses). Les résultats numériques comparent la carène optimale pour minimiser l'espérance u_D^*, à une carène optimale $\bar{u}_D$ calculée pour une vitesse fixée, qui est la vitesse moyenne sur l'intervalle. Pour une distribution uniforme des vitesses, les carènes calculées sont étonnament différentes, comme exposé dans la figure 4. Ces deux carènes sont ensuite testées pour différentes vitesses, et comme espéré, la carène robuste a de meilleures performances sur quasiment toute la gamme de vitesse, comme le montre la figure 5.

— Le chapitre 8 est dédié à l'algorithme de Newton. Une nouvelle et simple discrétisation de la méthode de Newton est proposée pour des domaines lisses, basée sur une matrice hessienne diagonale facile à construire, et à inverser. Vu le coût élevé en calcul des différentes approches de robustesse, déterministe et stochastique, des algorithmes d'ordre supérieur sont nécessaires pour accélérer le pro-

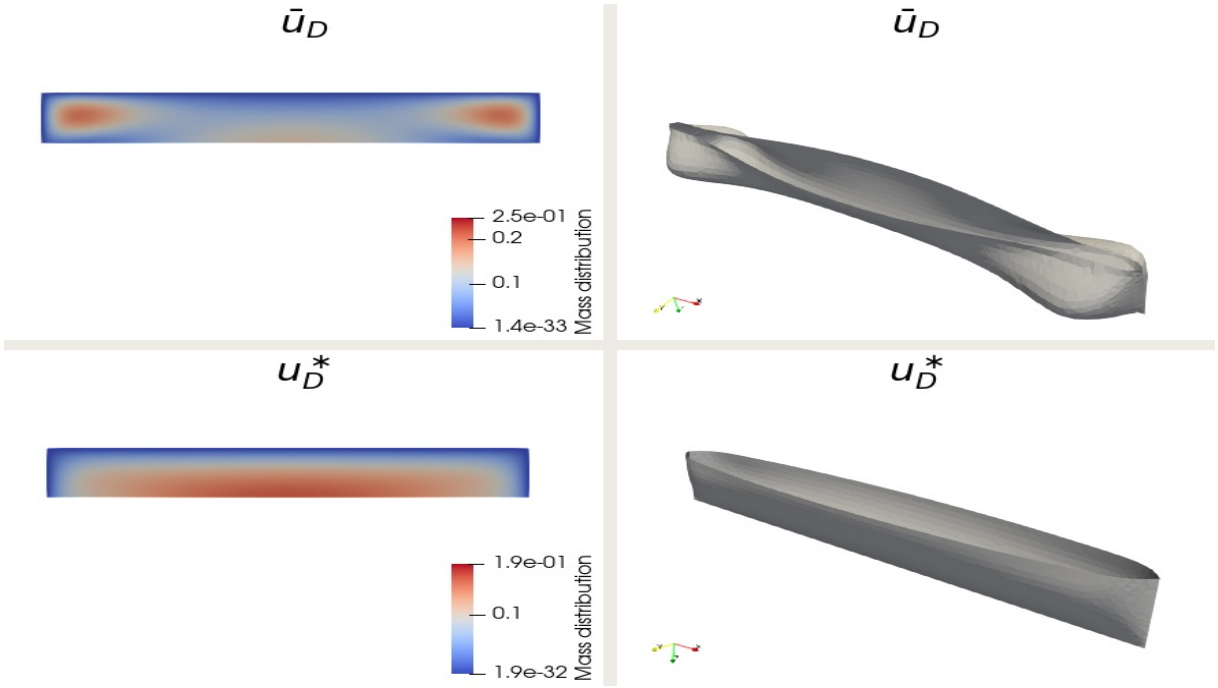

Figure 4 – The optimal hull for minimizing the expectation of the water resistance u_D^* with a uniform distribution of the velocity V and the optimal hull for minimizing the water resistance $\overline{u}_D$ on a fixed velocity $V = \frac{V_{\max}+V_{\min}}{2}$.

cessus d'optimisation. Il est connu que l'implémentation numérique de ces algorithmes pour l'optimisation de forme est difficile. Souvent, à chaque degré de liberté du maillage, un problème différent pour les dérivées de formes locales est à résoudre. Ce n'est pas le cas ici, car la discrétisation proposée permet de construire la matrice hessienne sur le bord Γ du domaine, sur lequel l'expression de la dérivée de forme est connue explicitement. La discrétisation est testée pour des fonctionnelles géométriques et des fonctionnelles dépendantes d'une EDP, avec ou sans contrainte, et elle converge dans un petit nombre d'itérations. Nos résultats numériques suggèrent que les contraintes sont bien préservées et que l'algorithme est stable, comme montré dans la figure 6, qui donne les normes $\mathbb{L}_\infty$ et $\mathbb{L}_2$ de la direction de descente θ_h pour la minimisation de l'énergie Dirichlet. La vitesse de convergence est quadratique dans le cas d'une fonctionnelle géométrique. Tous les outils numériques utilisés pour l'implémentation de l'algorithme sont donnés dans l'annexe A.

— Le chapitre 9 utilise la méthode de Newton pour le calcul de carènes robustes avec un support variable D. Seul un résultat d'existence d'une carène optimale est donné

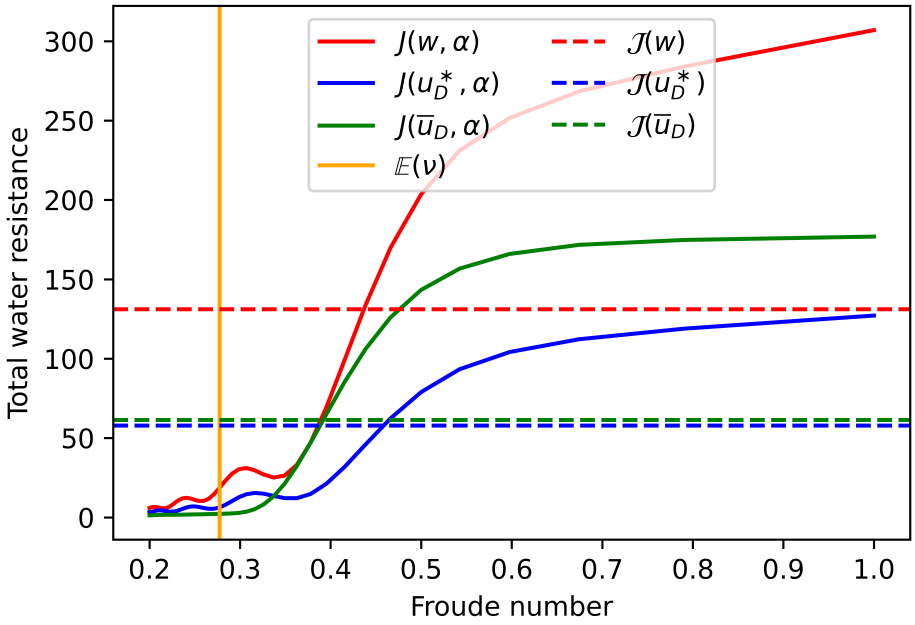

Figure 5 – The computed total water resistance for different hulls u_D^*, $\overline{u}_D$ and a standard Wigley hull w for different Froude numbers.

(le support optimal n'existe pas sur certaines gammes de vitesse). La méthode de Newton est ensuite comparée à la méthode du Lagrangien augmenté. Comme le montre la figure 7, la méthode de Newton permet une convergence plus rapide, une meilleure préservation de la contrainte et une meilleure stabilité.

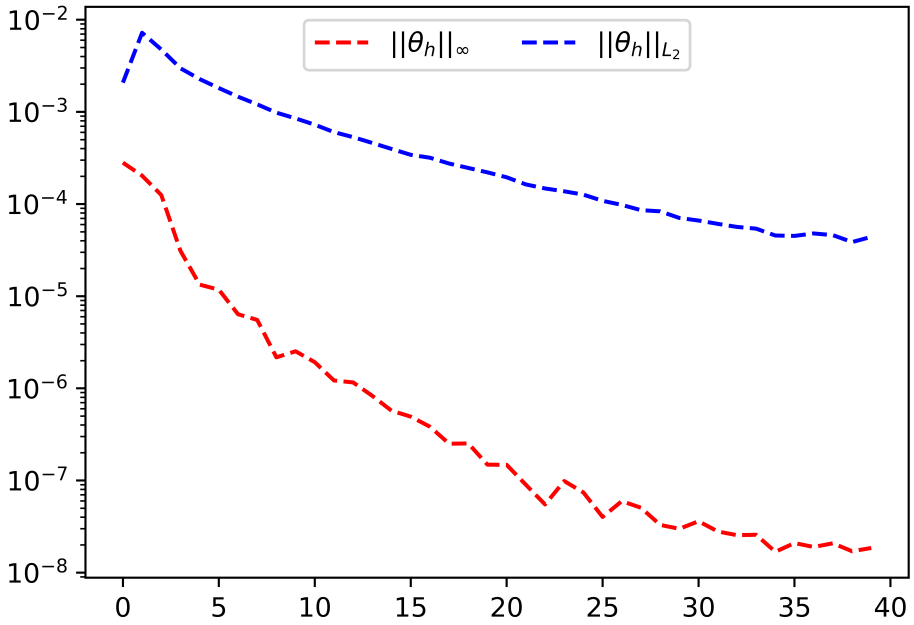

Figure 6 – The $\mathbb{L}_2$ and $\mathbb{L}_\infty$ of the descent direction θ_h for the minimization of the Dirichlet energy using Newton's method

s

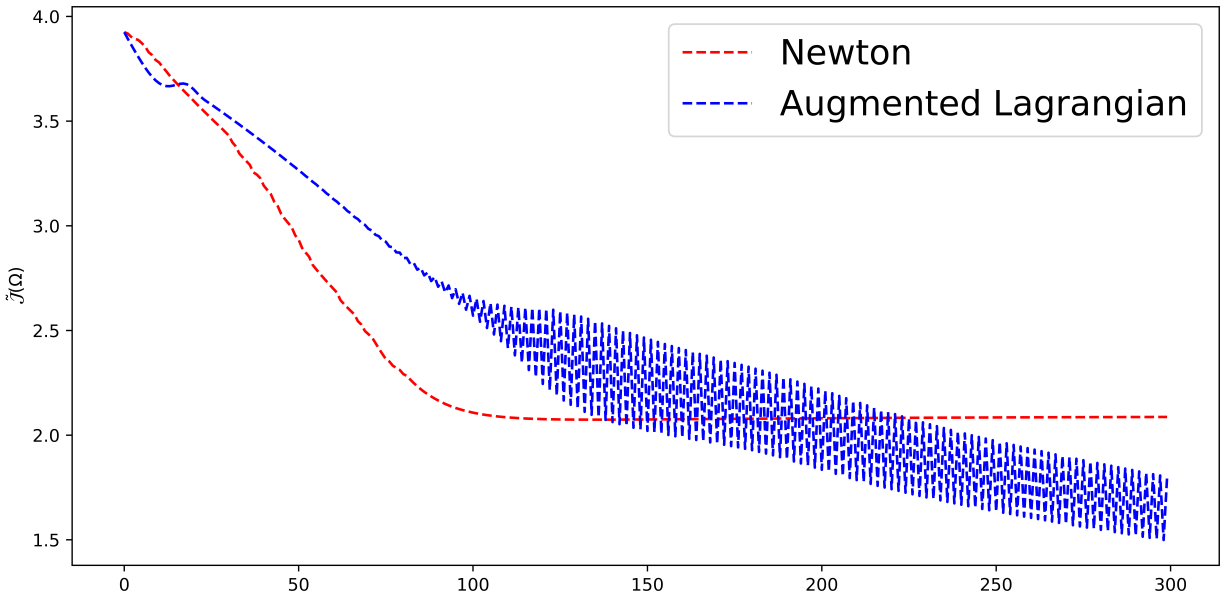

Figure 7 – Convergence results for the expectation of the water resistance using both Newton and the augmented Lagrangian algorithms.

Part I

Shape optimization for composite materials

Chapter 1

Introduction

In the industry, mechanical structures are designed to fulfill their physical purpose in an optimal way. Optimality can be sought for different criterias, for example, one can look to design structures that are mechanically robust and won't fail during use, another widely considered criteria are the weight and volume of the structure which helps to save raw materials and space. In practice, these optimality criteria are often dependent on a mathematical model that describes the physical behavior of the structure (typically a PDE problem). Such a problem is defined on the domain Ω of the structure and its material properties that we denote by ℓ. This means that optimizing a criterion $J(\Omega, \ell)$ is a matter of finding both the optimal domain and the optimal material.

The search for optimal domains for mechanical structures, despite Its difficulty, is extensively studied, we dispose of theoretical and numerical tools to solve shape optimization problems, and we invite the interested reader to study the reference book of Allaire [4] on the matter. On the other hand, the optimization of the material properties, while an easier and more "traditional" approach, is getting more challenging due to the critical demand for materials with special properties. For example, Poisson's ratio is a measure of the deformation of a material in directions perpendicular to the applied deformation force. Most materials have Poisson's ratio ranging between 0 and 0.5. For sensors, having a Poisson's ratio of -1 instead of the ordinary value of 0.3 will increase their sensitivity by one order of magnitude. Components made of homogenous materials rarely possess such special properties, and recently attention has shifted towards heterogeneous materials (composites) for their tailorable properties. For example, piezoelectric composites can be designed to have negative Poisson's ratio and are today widely used for sensors.

A long term goal of this work is the design of optimal structures with respect to both variables (geometrical domain and material properties). This is nothing new, to our knowledge this was first studied in [22], the idea is to first optimize the material properties through a steepest descent algorithm, then use the resulting optimal material to perform shape optimization of the structure. Although simple It may seem, the authors

highlight the lack of systematic and effective methods to design these optimal materials, which prevents from using them for the rest of the optimization process. Today, the design of heterogeneous material is a hot topic and different approaches are being develloped, and perhaps the most advanced one is topology optimization. Here we propose a different approach through the shape optimization of a matching criterion. That is, given a desired material properties and two materials for a potential matching composite, we search for the optimal inclusion of the two materials that minimizes the gap between the desired properties and an average of the composite's properties that is computed by Homogenization (see [5]). Our strategy can then be summarized in the following steps:

1. Compute the optimal material properties through a steepest descent.
2. Given two materials, compute the optimal inclusion (microstructure) to match the optimal material properties.
3. Compute the optimal global domain (macrostructure).

The last step is the general goal of shape optimization and its difficulty is often dependent on the physical problem and criterion to be optimized. An example for a general elasticity criterion can be found in [9], here we concern ourselves with steps 1 and 2. Let us give some results for the sensitivity analysis with respect to the material properties.

1.1 Sensitivity with respect to the material

We give the first and second order derivatives with respect to the material properties that shall be used for steepest descent algorithms. Throughout the section we set B a Banach space (for the material properties ℓ) and V a separable Hillbert space (for the state function solution of the physical problem) and let $T : B \times V \times V \longrightarrow \mathbb{R}$ a trilinear operator such that :

1. T is symmetric with respect to the 2^{nd} and 3^{rd} arguments :

$$\forall\, \ell \in B, \forall\, u, v \in V \quad T(\ell, u, v) = T(\ell, v, u)$$

2. T is continuous : $\exists\, \beta(\ell)$ such that

$$|T(\ell, u, v)| \leq \beta(\ell)\|u\|_V \|v\|_V.$$

3. T is coercive : $\exists\, \alpha(\ell)$ such that

$$|T(\ell, u, u)| \geq \alpha(\ell)\|u\|_V^2$$

We then have the following Lemma :

Lemma 1.1.1. $\forall\, \ell \in B, \forall\, m \in V^*$ *(the topological dual of* V*),* $\exists\, !u \in V$ *such that*

$$\forall\, v \in V, \quad T(\ell, u, v) = m(v) \tag{1.1}$$

$$\textit{moreover} \quad \|u\|_V \leq \frac{1}{\alpha(\ell)}\|m\|_{V^*} \tag{1.2}$$

Proof. The existence and uniqueness is easily given by the Lax-Milgram Theorem, taking u as a test function we have :

$$\alpha(\ell)\|u\|_V^2 \leq T(\ell, u, u) = m(u) \leq \|m\|_{V^*}\|u\|_V.$$

□

Lemma 1.1.1 allows us to define the parameter-to-state map as

$$\begin{array}{rccc} \mathscr{S}: & B & \longrightarrow & V \\ & \ell & \longrightarrow & u(\ell) \quad \text{solution of (1.1)}, \end{array}$$

then the state function u is differentiable with respect to ℓ, in fact we have the following Lemma :

Lemma 1.1.2. *the map* $\mathscr{S}$ *is* C^∞

Proof. We shall apply the implicit function theorem to

$$\begin{array}{rccc} \mathscr{Q}: & B \times V & \longrightarrow & V^* \\ & (\ell, u) & \longrightarrow & T(\ell, u, .) - m \end{array}$$

where

$$\begin{array}{rccc} T(\ell, u, .): & V & \longrightarrow & \mathbb{R} \\ & v & \mapsto & T(\ell, u, v). \end{array}$$

By assumption $T(\ell, u, .) \in V^*$, and for all ℓ we have :

$$\mathscr{Q}(\ell, u(\ell)) = 0.$$

For a fixed ℓ we have :

$$\partial_u \mathscr{Q}(\ell, u).h = T(\ell, h, .)$$

by linearity of T with respect to the second argument. Let us prove that $\partial_u \mathscr{Q}(\ell, u)$ is an isomorphism :

— Surjectivity : $\forall\, m \in V^*\, \exists!\, h | T(\ell, h, .) = m$, by Lemma 1.1.1.

— Injectivity : $T(\ell, h, .) = 0 \Longrightarrow T(\ell, h, h) = 0 \Longrightarrow h = 0$.

Thus by the implicit function Theorem the map $\mathscr{S}$ is of class C^∞. □

The final Lemma gives the first and second order derivatives with respect to the material properties ℓ

Lemma 1.1.3. *The map $\mathscr{S} : \ell \mapsto u(\ell)$ has the derivatives defined by the variational characterisation*

— $1^{st} order : \forall\, v \in V, \quad T(\ell, Du(\ell).h, v) = -T(h, u(\ell), v)$.

— $2^{nd} order : \forall\, v \in V, \quad T(\ell, D^2u(\ell)[h, h], v) = -2T(h, Du(\ell).h, v)$

Proof. It suffices to differentiate by the chain rule the relation :

$$T(\ell + th, u(\ell + th), v) = m(v) \qquad \forall\, v \in V.$$

we get

$$\begin{aligned} \frac{d}{dt} T(\ell + th, u(\ell + th), v) &= T(h, u(\ell + th), v) + T(\ell + th, \frac{d}{dt} u(\ell + th), v) \\ &= 0 \end{aligned}$$

so that at $t = 0$ we get the characterization of $Du(\ell).h$

A second derivation leads to

$$T(h, \frac{d}{dt} u(\ell + th), v) + T(h, \frac{d}{dt} u(\ell + th), v) + T(\ell + th, \frac{d^2}{dt^2} u(\ell + th), v) = 0,$$

so that at $t = 0$ we have :

$$2T(h, Du(\ell).h, v) + T(\ell, D^2u(\ell)[h, h], v) = 0.$$

□

An example for an elastic material

Let Ω be a bounded open subset of $\mathbb{R}^d$ with a boundary $\Gamma = \partial\Omega$ made of two disjoint parts

$$\Gamma = \Gamma_D \cup \Gamma_N.$$

With Dirichlet boundary conditions on Γ_D and Neumann boundary conditions on Γ_N. We assume that Ω is an elastic body, subjected to body forces f and we denote by A a fourth order tensor satisfying the usual symmetries of elasticity

$$A_{ijkl} = A_{klij} = A_{jikl} = A_{ijlk},$$

and which is also positive definite:

$$\exists\alpha(A) > 0, \qquad \alpha(A)|\xi| \leq A\xi : \xi = \sum_{i,j,k,l=1}^{N} = A_{ijkl}\xi_{ij}\xi kl,$$

for all symmetric matrices ξ with entries ξ_{ij}. We introduce for any $u \in \mathbb{H}^1(\Omega)$, the symmetrized gradient

$$\varepsilon(u) = \frac{1}{2}\big(\nabla u + {}^t\nabla u).$$

The elastic displacement u is solution to the following PDE problem:

$$\begin{cases} -div(A\varepsilon(u)) &= f & \text{in } \Omega \\ u &= 0 & \text{on } \Gamma_D \\ A\varepsilon(u).n &= 0 & \text{on } \Gamma_N, \end{cases} \tag{1.3}$$

and we have the following lemma for the derivatives of the mapping $\mathscr{S} : A \mapsto u(A)$:

Lemma 1.1.4. *the map $\mathscr{S} : A \mapsto u(A)$ has the derivatives defined by the variational formulation :*

— 1^{st} *order :* $\forall\, v \in \mathbb{H}^1(\Omega) \quad \int_\Omega A\varepsilon(Du(A).h) : \varepsilon(v) = -\int_\Omega h\varepsilon(u(A)) : \varepsilon(v).$

— 2^{nd} *order* : $\forall\, v \in \mathbb{H}^1(\Omega) \quad \int_\Omega A\varepsilon(D^2u(A).[h,h]) : \varepsilon(v) = -2\int_\Omega h\varepsilon(Du(A).h) : \varepsilon(v).$

Proof. Taking a test function $v \in \mathbb{H}^1(\Omega)$ in problem (1.3), and integrating by parts we find that u is solution to the following variational formulational :

$$\int_\Omega A\varepsilon(u) : \varepsilon(v) = \int_\Omega fv.$$

Let $T(A,u,v) = \int_\Omega A\varepsilon(u) : \varepsilon(v)$, then we have :

— T is trilinear and symmetric with respect to u and v due to the symmetry of the elastic tensor A.

— It is a well-known result (see [37]) that there exists $\beta(A)$ such that

$$A\xi : \xi \leq \beta(A)|\xi|^2,$$

which immediately gives the continuity of T

— The coerciveness of T is given by Korn's inequality (see the proof of Theorem 2.7 in [62]), indeed by coerciveness of A, there exists $\alpha(A)$ such that :

$$T(A,u,u) = \int_\Omega A\varepsilon(u) : \varepsilon(u) \geq \alpha(A)\|\varepsilon(u)\|^2_{\mathbb{L}^2(\Omega)},$$

and by Korn's lemma, there exists $C > 0$ such that :

$$\|u\|_{\mathbb{H}^1(\Omega)} \leq C\|\varepsilon(u)\|_{\mathbb{L}^2(\Omega)},$$

thus T is coercive and the derivatives of the map $\mathscr{S} : A \mapsto u(A)$ are an immediate consequence of Lemma 1.1.2.

□

1.2 Matching of material properties.

Our contributions focuses on two types of materials, perforated elastic materials which are used for the design of light-weight structures, and piezoelectric composites which englobes many types of composites with or without a piezoelectric effect, since an elastic material can be seen as a piezoelectric material with a zero piezoelectric coupling and dielectric properties. We give the main results obtained for these problems:

— chapter 2 deals with the inverse homogenization of light-weight elastic microstructures. Here we are given an elastic material of which the properties are represented by a fourth order tensor A. We search for a lighter structure, by putting a periodic distribution of holes in the structure. The question is then to find the optimal microstructure (a hole inside a unit cell) that will yield a certain global desired elastic properties. For example the upper bound of the global resulting properties for a mixture of the elastic material with proportion $0 \leq \theta \leq 1$, and air with proprtion $1 - \theta$. The global resulting properties are computed by Homogenization and are represented by the effective elastic tensor A^*, and our matching criterion $J(\Omega)$ is defined as a least-squares matching of the two tensors. To this end, we give an existence result for an optimal shape and prove the shape differentiability of the state functions before computing the shape derivatives of the homogenized effective elasticity tensor $A^*_{ijkl}(\Omega)$, and perform a steepest descent algorithm to compute optimal shapes for our matching criterion.
Numerical results show that the matching problem has infinite solutions which brings us to the main contribution of the work : The robust matching of these properties. Indeed, since the problem admits many solutions, we seek the most robust one with respect to geometrical incertitudes. That is we search for the optimal structure that will not loose optimality for slight geometrical perturbation that are intended to happen either due to manufacturing issues or worn-out. We thus follow the approach of [6] and minimize a worst case scenario of our matching functional defined as

$$\mathcal{J}_{rob}(\Omega) = J(\Omega) + \delta \|J'(\Omega; \delta)\|$$

where $J(\Omega)$ is the matching criterion, $\|J'(\Omega; \theta)\|$ is the operator norm of its shape derivative and $0 < \delta \leq 1$ a penalization parameter representing the magnitude of the geometrical perturbations. The idea is that minimizing the norm of the shape derivative corresponds to desensitizing the microstructure to geometrical perturbations. We then give the shape derivative of the robust matching and demonstrate the applicability of this approach by numerical results.
Numerical results show that one cannot hope to have a good matching of the desired properties and robustness as these two criterions do not necessarily have the same descent direction around a critical shape of $J(\Omega)$, thus at some point of the optimization process one has to make a tradeoff choice between optimal matching or robustness.

— Chapter 3 studies the matching of piezoelectric composites in the spirit of chapter 2. Here It is the nature of the physical problem that makes the matter more difficult. Indeed, the piezoelectric cell problems (that one has to solve in order to compute the global effective tensors) use three different tensors for the different elastic, dielectric and piezoelectric properties of the composite. We give an existence result of an optimal shape and we prove the shape differentiability of the state functions of which the shape derivatives do not live in the space $\mathbb{H}^1_{\#}(Y)$ of sobolev periodic functions due to having a jump on the boundary of contact between the two materials. We then give an expression for the entries of the different tensors that does not involve the shape derivatives of the state function nor any adjoint problem. Numerical results are being studied.

Chapter 2

Robust shape optimization for light-weight design of elastic microstructures.

2.1 Introduction

The design of periodic microstructures has become a fundamental research area in structural optimization. For elasticity problems, mathematical homogenization is used to determine the effective properties of microstructures and, in the case of composite materials, their theoretical limits. The optimality of these limits has been examined in various works (see [67],[46]), and the idea of constructing microstructures whose performances exactly meet these limits, or more generally, any prescribed property is called *inverse homogenization*. The so-called inverse homogenization problem was first addressed by Sigmund in 1995 in [69] and subsequently generates a large literature (see for example [11]). One of the main characteristics of this inverse problem is the non-uniqueness of its solutions. Therefore, the numerical design, usually computed by a minimization algorithm, depends strongly on the starting structure and the underlying parameterization. This also means that additional requirements can be added. Note that often, for applications, not only do we need optimization tools for the micro-structure and the macro-structure, but also, these procedures must be coupled (see [12, 71, 39, 36]).

In practical applications, the computed designs suffer from a loss of optimal performance due to uncertainties in the physical parameters of the optimization problem. These uncertainties can be either geometric in nature (manufacturing, reliability, wear, etc.), elastic material properties (manufacturing, change in environment altering material stiffness, etc.), or the magnitude and orientation of body forces or surface loads exerted on the structure. These uncertainties must be taken into account when designing optimization tools for microstructures. In [53], the authors use isogeometric shape optimization

to construct nearly efficient microstructures under perturbations in elastic material properties. In this chapter, we are interested in taking geometric uncertainties into account. When no information is available on these perturbations, but limits can be set on their magnitude, so-called worst-case design approaches are preferred. We consider the worst-case design of elastic microstructures with respect to small perturbations on the geometry in the spirit of the unified framework for the worst-case design of elastic structures given by Allaire and Dapogny in [6]. In other words, we try to compute a microstructure that generates the desired homogenized tensor and that should be as insensitive as possible to small geometric perturbations.

Let us present the approach we propose. For the sake of completeness and brevity, only a few important results on the homogenization theory are recalled here, the interested reader will find more details and proofs in the monograph [5]. Assume that, in a given macroscopic domain, there is a periodic distribution of holes inside an isotropic elastic solid phase, with constant elasticity tensor A. The periodicity size is denoted $\alpha > 0$. Let $Y = [0,1]^N$ be the rescaled unit periodic cell, where N is the space dimension. Inside this unit periodicity cell, the solid domain is the subset $\Omega \subset Y$, its complement being holes with boundary $\Gamma = \partial\Omega$. When $\alpha \to 0$, the medium can be considered homogeneous, with an effective constant elasticity tensor A^*. To compute this homogenized tensor A^*, one needs so-called correctors $w_{ij} \in \mathbb{H}^1_\#(Y)$ (defined below in sub-section (2.2.1)), corresponding to the local displacement in the cell Y, defined for each pair $(i,j) \in \{1,2,\dots,N\}^2$ as the solutions of the following cell problems

$$\begin{cases} div\Big(A(e_{ij} + \epsilon(w_{ij}))\Big) &= 0 \quad \text{in } \Omega \\ A(e_{ij} + \epsilon(w_{ij})) \cdot n &= 0 \quad \text{on } \Gamma \\ y \mapsto w_{ij}(y) & \quad [0,1]^N - periodic \end{cases} \tag{2.1}$$

where $e_{ij} = \frac{1}{2}(e_i \otimes e_j + e_j \otimes e_i)$ is a basis for symmetric tensors of order 2, n is the normal to the boundary Γ in Ω, and $\epsilon(w_{ij}) = \frac{1}{2}\Big(\nabla w_{ij} + {}^t\nabla w_{ij}\Big)$ is the symmetric strain tensor. The Lax-Milgram theorem ensures the existence and uniqueness of the solutions w_{ij} to these cell problems for $1 \leq i,j \leq N$. The family of functions w_{ij} can be used to define the effective tensor $\mathbf{A}^* = [A_{ijkl}]_{i,j,k,l=1}^N$ in accordance with

$$A^*_{ijkl}(\Omega) = \int_Y A(e_{ij} + \epsilon(w_{ij})) : (e_{kl} + \epsilon(w_{kl}))dy \qquad \forall i,j,k,l \in \{1,2,\dots,N\}. \tag{2.2}$$

Let us consider a given tensor $\mathbf{G} \in \mathbb{R}^{N\times N}_{sym}$ describing the desired material properties. The robust inverse homogenization problem is then: can we find a periodic hole structure (that is a domain Ω) such that the effective tensor is as close as possible to $\mathbf{G}$, while being the least sensitive to geometric perturbations? Let us make this vague statement precise.

We follow the strategy of [28] we choose the Frobenius norm on matrices to make precise the notion of closeness between matrices and we define the main objective $J(\Omega)$

$$J(\Omega) = \frac{1}{2}\|\mathbf{A}^*(\Omega) - \mathbf{G}\|_F^2 = \frac{1}{2}\sum_{1\leq i,j\leq d}\Big(A^*_{ijkl}(\Omega) - G_{ijkl}\Big)^2, \tag{2.3}$$

as a least square matching of the desired properties. In the seminal work on worst-case design in shape optimization by Dapogny and Allaire in [6], they propose to minimize a worst-case scenario functional $\mathcal{J}(\Omega)$ of a cost functional $J(\Omega)$ defined by :

$$\mathcal{J}(\Omega) = \sup_{\substack{\theta\in\mathbb{W}^{1,\infty}(\mathbb{R}^N,\mathbb{R}^N)\\ \|\theta\|_{\mathbb{W}^{1,\infty}(\mathbb{R}^N,\mathbb{R}^N)}\leq\delta}} \Big(J(\Omega) + J'(\Omega)(\mathcal{X}\theta)\Big), \tag{2.4}$$

for $\delta > 0$, $\mathcal{X}$ a cutoff function of the domain Ω, and $\theta \in \mathbb{W}^{1,\infty}(\mathbb{R}^N,\mathbb{R}^N)$ a perturbation vector of magnitude $\|\theta\|_{\mathbb{W}^{1,\infty}(\mathbb{R}^N,\mathbb{R}^N)} \leq \delta$, and where

$$J'(\Omega)(\theta) = \int_\Gamma (\theta\cdot n)k(\Omega) \tag{2.5}$$

is the shape gradient of $J(\Omega)$ in the direction θ, and $k(\Omega)$ is a scalar field depending on $J(\Omega)$. This writing is canonical by the structure theorem of shape gradients (see the monograph [50]). An important remark is that $\mathcal{J}(\Omega)$ can be rewritten as

$$\mathcal{J}(\Omega,\delta) = J(\Omega) + \delta\int_\Gamma |k(\Omega)|,$$

and that $\mathcal{J}(\Omega)$ is only going to be shape differentiable for domains Ω such that $k(\Omega) \neq 0$. A difficulty raised by this approach is that for a critical point Ω^* of J, we have $J'(\Omega^*)(\theta) = 0$, and thus $\mathcal{J}(\Omega^*) = J(\Omega^*)$ is not sensitive to the change in the norm of the shape derivative J'. The inverse homogenization problem presents this pathology since it admits in general many solutions. To get around this difficulty, we consider a slightly different approach that calls for the use of the $\mathbb{L}_p$ norm of $k(\Omega)$ the kernel of the shape gradient defined in

(2.5). Precisely, for a cost functional $J(\Omega)$, we define the (p, δ) robust functional $\mathcal{J}_p$ by

$$\mathcal{J}_p(\Omega, \delta) = J(\Omega) + \delta \|k(\Omega)\|^p_{\mathbb{L}^p(\Omega)}. \tag{2.6}$$

where $\delta \in]0, 1]$ is fixed, and $p \in \mathbb{N}$. Notice that $\mathcal{J}_p(\Omega, \delta)$ is differentiable for all Ω, and that the Allaire Dapogny cost $\mathcal{J}(\Omega)$ is nothing but $\mathcal{J}_1(\Omega, \delta)$. We also expect that the best choice corresponds to $p = 2$ since the higher is p the flater is the additional term, and will only focus on $\mathcal{J}_2(\Omega, \delta)$.

This allows us to state our problem as :

Problem 1. *Given a class of admissible domains $\mathcal{A}(Y)$, and a positive real number δ, find $\Omega^* \in \mathcal{A}(Y)$ such that*

$$\mathcal{J}_2(\Omega^*, \delta) = \min\{\mathcal{J}_2(\Omega, \delta); \Omega \in \mathcal{A}(Y)\}. \tag{2.7}$$

The main challenge in building a first order descent algorithm to solve Problem 1 is that computing the shape derivative of $\mathcal{J}_2$ requires the computation of the second order derivative of the initial objective since the robustness is enforced through a penalisation of the operator norm of the first order derivative of the initial objective. To make numerical simulations easier, a main contribution of this work is to compute new, simple, and easy to implement formulas for both functionals $J(\Omega)$ and $\mathcal{J}_2(\Omega, \delta)$.

The current paper is organized as follows. In section 2.2, we briefly recall useful definitions and properties that we will use in the paper. We address the question of the existence of solutions to the inverse homogenization problem in Section 2.4. Then Section 2.3 is dedicated to shape-calculus : we compute the shape derivatives of the effective elastic tensor entries $A^*_{ijkl}(\Omega)$, that we then use to compute the shape derivatives of our cost-functionals. Finally, numerical results are given in Section 2.5 to test these new derivatives, illustrate the non-uniqueness of solutions and exhibit the most-efficient ones.

2.2 Notations and useful known results.

2.2.1 On periodic functions

In order to work with cell problems, we need Korn's inequality for periodic function. We quote the one stated by Oleinik (See [62, p.23]).

Lemma 2.2.1 (Korn's inequality for periodic functions)**.** *Let D be an unbounded domain with a 1-periodic structure, set $Y = (0,1)^N$ and let $D \cap Y$ be a domain with a Lipschitz boundary. Then for any*

$$v \in \mathbb{H}^1_{\#}(D) = \left\{ v \in \mathbb{H}^1(D),\ v \text{ is } Y-\text{periodic}, \int_{D\cap Y} v dx = 0 \right\}$$

the inequality

$$\|v\|_{\mathbb{H}^1(D\cap Y)} \leq C \|\epsilon(v)\|_{\mathbb{L}^2(D\cap Y)} \tag{2.8}$$

holds with a constant C independent of v.

2.2.2 On the class of admissible domains.

To prove the existence of a solution to problem 1, we are going to enforce some regularity on our class of admissible shapes $\mathcal{A}(Y)$. The idea is that we often expect optimal shapes to be regular. Therefore, it does not seem too restrictive to a priori require some regularity constraints on the set of admissible shapes.

We are going to consider the class of domains satisfying a uniform cone condition, which is a convenient point of view in shape optimization, since the works of D. Chenais.

Definition 2.2.1. *Let y be a point in $\mathbb{R}^N$, ξ a unit vector, and ε a positive real number. Let $C(y,\xi,\varepsilon)$ be the cone of vertex y(without its vertex), of direction ξ and dimension ε, defined by*

$$C(y,\xi,\varepsilon) = \{z \in \mathbb{R}^N,\ (z-y,\xi) \geq \cos(\varepsilon)|z-y| \quad \text{and} \quad 0 < |z-y| < \varepsilon\}.$$

An open set Ω is said to have the ε-cone property if

$$\forall x \in \partial\Omega,\ \exists \xi_x \text{ unit vector such that } \forall y \in \overline{\Omega} \cap B(x,\varepsilon),\ C(y,\xi_x,\varepsilon) \subset \Omega.$$

We thus define the class of admissible domains $\mathcal{A}_\varepsilon(Y)$ that will be used throughout the rest of the paper as follows

$$\mathcal{A}_\varepsilon(Y) = \{\Omega \subset Y,\ \Omega \text{ open with the } \varepsilon\text{-cone property}\}. \tag{2.9}$$

We now recall very classical results from shape optimization and the calculus of variations,

that we state here without a proof, and the interested reader can see the corresponding references for a detailed proof.

Proposition 2.2.1 (Chenais, see [23]). *Let $\varepsilon > 0$. Then there exists $k \in (0, \infty)$ such that*

$$\begin{cases} \text{for all } \Omega \subset \mathcal{A}_\varepsilon(Y), \text{ there exists a linear continuous extension operator} \\ P_\Omega \text{ of } \mathbb{H}^1(\Omega) \text{ into } \mathbb{H}^1(Y) \text{ with } \|P_\Omega\|_{\mathbb{H}^1(\Omega)\to\mathbb{H}^1(Y)} \leq k. \end{cases}$$

We also define the Hausdorff convergence and the convergence of characteristic functions.

Definition 2.2.2 (Hausdorff convergence). *let $(\Omega_n)_n$ and Ω be open sets included in Y. We say that the sequence Ω_n converges in the sense of Hausdorff to Ω if*

$$d^H(Y \setminus \Omega_n, Y \setminus \Omega) \longrightarrow 0 \quad \text{when } n \to \infty. \tag{2.10}$$

with

$$\begin{cases} \forall x \in Y \quad d(x, K_1) & := \inf\limits_{y \in K_1} d(x, y), \\ \rho(K_1, K_2) & := \sup\limits_{x \in K_1} d(x, K_2), \\ d^H(K_1, K_2) & := \max(\rho(K_1, K_2), \rho(K_2, K_1)), \end{cases}$$

where K_1 and K_2 are two non-empty compact sets in Y.

Definition 2.2.3. *Let $(E_n)_n$ and E be measurable sets in $\mathbb{R}^N$. We say that E_n converges in the sense of characteristic functions to E when n goes to ∞ if*

$$\mathcal{X}_{E_n} \longrightarrow \mathcal{X}_E \quad \text{in } \mathbb{L}^p_{loc}(\mathbb{R}^N), \quad \forall p \in [1, \infty). \tag{2.11}$$

where $\mathcal{X}_E$ denotes the characteristic function of E (by definition this function is equal to 1 inside E and 0 outside of E).

The connection between both notions is done through the following result that states that the class of admissible shapes $\mathcal{A}_\varepsilon(Y)$ equipped with the Hausdorff topology has some compactness properties.

Proposition 2.2.2. *(See [50, p.59])*
Let Ω_n be a sequence of open sets in the class $\mathcal{A}_\varepsilon(Y)$ defined in (2.9). Then there exist an

open set $\Omega \in \mathcal{A}_\varepsilon(Y)$ *and a subsequence* Ω_{n_k} *that converges to* Ω *in the sense of Hausdorff and in the sense of characteristic functions. Moreover* $\overline{\Omega}_{n_k}$ *and* $\partial\Omega_{n_k}$ *converge in the sense of Hausdorff respectively to* $\overline{\Omega}$ *and* $\partial\Omega$.

2.2.3 On shape calculus.

Finally, we define the notion of shape differentiability as follows :

Definition 2.2.4. *Let* $k \geq 1$ *and* $E(\Omega)$ *be a function from*

$$\mathcal{O}_k = \{\Omega \subset \mathbb{R}^N \,|\, \Omega \text{ is a bounded open set of class } C^k\}$$

into $\mathbb{R}$. *We define*

$$\begin{aligned} \mathcal{E} \,:\, \mathbb{W}^{k,\infty}(\mathbb{R}^N,\mathbb{R}^N) &\longrightarrow \mathbb{R} \\ \theta \qquad\quad &\longmapsto E\Big((Id+\theta)(\Omega)\Big). \end{aligned}$$

The function E *is said to be shape-differentiable at* Ω *if* $\mathcal{E}$ *is Fréchet-differentiable at* 0, *that is, if there exists a continuous linear map* $\mathcal{E}'(0;\cdot)\ \mathbb{W}^{1,\infty}(\mathbb{R}^N,\mathbb{R}^N) \to \mathbb{R}$ *such that :*

$$\mathcal{E}(\theta) - \mathcal{E}(0) - \mathcal{E}'(0;\theta) = o\Big(\,\|\theta\|_{\mathbb{W}^{k,\infty}(\mathbb{R}^N,\mathbb{R}^N)}\,\Big).$$

We denote $E'(\Omega;\theta) = \mathcal{E}'(0;\theta)$.

Definition 2.2.5. *The function* E *of Definition 2.2.4 is said to be twice shape-differentiable at* Ω *if* $\mathcal{E}$ *is Fréchet-differentiable in a neighborhood* $\mathcal{U}$ *of* 0 *in* $\mathbb{W}^{k,\infty}(\mathbb{R}^N,\mathbb{R}^N)$ *and if the first derivative* $\mathcal{E}'$ *defined by*

$$\begin{aligned} \mathcal{E}' \,:\, \mathcal{U} &\longrightarrow \Big(\mathbb{W}^{k,\infty}(\mathbb{R}^N,\mathbb{R}^N)\Big)' \\ \theta &\longmapsto \mathcal{E}'\Big(\theta;\cdot\Big), \end{aligned}$$

is Fréchet-differentiable at 0. *We denote by* $\mathcal{E}''(0;\theta,\xi)$ *the second Fréchet derivative at* 0, θ *and* ξ *being respectively the first and second directions of derivation. We also denote* $E''(\Omega;\theta,\xi) = \mathcal{E}''(0;\theta,\xi)$. *In that case,* $\mathcal{E}$ *has a second-order Taylor expansion at* 0 *and*

$$\mathcal{E}(\theta) = \mathcal{E}(0) + \mathcal{E}'(0;\theta) + \frac{1}{2}\mathcal{E}''(0;\theta,\theta) + o\Big(\,\|\theta\|^2_{\mathbb{W}^{k,\infty}(\mathbb{R}^N,\mathbb{R}^N)}\,\Big)$$

Before discussing the existence of optimal shapes for the robust matching functional, we need the knowledge of the shape derivative of the matching functional for us to define it properly. The next section studies the sensitivity of both the matching and robust functionals with respect to the shape.

2.3 Shape differentiation of the effective tensor entries

2.3.1 Shape differentiability of the state functions and main tools.

We introduce a vector field $\theta : \mathbb{R}^N \to \mathbb{R}^N$ that vanishes on the boundary ∂Y of the reference cell but whose action may deform the interior surface Γ. We consider the perturbation of the identity $(Id + \theta)$, where $\theta \in \mathbb{W}^{1,\infty}(\mathbb{R}^N, \mathbb{R}^N)$ and is close to 0 in the norm of this space, so that $(Id + \theta)$ is a bi-Lipschitz homeomorphism. We denote by $\Omega_\theta = (Id + \theta)(\Omega)$, and $Y_\theta = Y \cap \Omega_\theta$. $A(\theta) = A((Id + \theta)(y))$ and $w_\theta = w_{ij}^\theta \in \mathbb{H}^1_\#(Y_\theta)$ the solution to the cell problem (2.1) in Ω_θ.

The first result states the shape differentiability of the solution of the cell problem (2.1). The proof relies on the Implicit Function Theorem following the lines presented in [50, Chapter 5].

Theorem 2.3.1. *Assume Ω is open, bounded and of class C^3. Then the mapping, $\theta \mapsto w_\theta$ is of class C^2 in the variational space $\mathbb{H}^1_\#(Y)$.*

Proof. The variational formulation of the cell problem in Ω_θ, satisfies :

$$\int_{\Omega_\theta} A(\theta)\epsilon(w_\theta) : \epsilon(v_\theta) + \int_{\Omega_\theta} A(\theta)e_{ij} : \epsilon(v_\theta) = 0 \qquad \forall v_\theta = v \circ (Id + \theta)^{-1} \in \mathbb{H}^1_\#(Y_\theta) \quad (2.12)$$

Set $\tilde{w}_\theta = w_\theta \circ (Id + \theta)$, then :

$$\nabla \tilde{w}_\theta = (I + {}^tD\theta)\nabla w_\theta \circ (Id + \theta), \quad \text{and} \quad \nabla v_\theta = (I + {}^tD\theta)^{-1}\nabla v \circ (Id + \theta)^{-1}$$

Then, (2.12) can be rewritten as :

$$\int_\Omega B_\theta \epsilon(w_\theta) : \epsilon(v) + \int_\Omega C_\theta e_{ij} : \epsilon(v) = 0 \quad (2.13)$$

with

$$\begin{cases} B_\theta &= (I + {}^tD\theta)^{-1}\,(I + D\theta)^{-1} A(\theta)\, det(I + D\theta), \\ C_\theta &= (I + {}^tD\theta)^{-1} A(\theta)\, det(I + D\theta). \end{cases} \tag{2.14}$$

We define two operators $\mathcal{B}_\theta, \mathcal{C}_\theta$ from $\mathbb{H}^1_\#(Y)$ to its dual $\mathbb{H}^1_\#(Y)'$ by the expressions: for all w in $\mathbb{H}^1_\#(Y)$, $B_\theta(w)$ is the linear form defined by

$$\forall v \in \mathbb{H}^1_\#(Y), \quad \langle \mathcal{B}_\theta(w), v\rangle = \int_\Omega B_\theta \epsilon(w) : \epsilon(v);$$

and C_θ is the affine form defined by

$$\forall v \in \mathbb{H}^1_\#(Y), \quad \langle \mathcal{C}_\theta, v\rangle = \int_\Omega C_\theta e_{ij} : \epsilon(v).$$

Consider now the mapping F defined as

$$\begin{array}{rccc} F: & \mathbb{W}^{1,\infty}(\mathbb{R}^N, \mathbb{R}^N) \times \mathbb{H}^1_\#(Y) & \to & \mathbb{H}^1_\#(Y)' \\ & (\theta, w) & \mapsto & \mathcal{B}_\theta(w) + \mathcal{C}_\theta. \end{array}$$

so that the function $\tilde{w}_\theta$ satisfies the relation $F(\theta, \tilde{w}_\theta) = 0$ in $\mathbb{H}^1_\#(Y)'$. We shall apply the Implicit Function Theorem around $\theta = 0$.

First, we check that F is of class C^2 for θ small enough. Indeed :

— $\theta \mapsto det(I + D\theta) \in \mathbb{L}^\infty(Y)$ is of class C^∞ since $\theta \mapsto I + D\theta \in \mathbb{L}^\infty(\mathbb{R}^N, \mathcal{M}_N)$ is linear and continuous and therefore C^∞.
— The mapping $M \mapsto det(M)$ is multilinear and therefore differentiable since the dimension of $\mathcal{M}_N$ is finite.
— Similarly $\theta \mapsto (I + D\theta)^{-1} = \sum_{j\geq 0} (-1)^j (D\theta)^j \in \mathbb{L}^\infty(\mathbb{R}^N, \mathcal{M}_d)$ is also C^∞.

Since F is linear with respect to the second argument w, its partial derivative with respect to w is simply

$$\Big(D_w F(0, w).h\Big)(v) = \langle \mathcal{B}_0(h), v\rangle = \int_\Omega A\epsilon(h) : \epsilon(v).$$

Once again Korn's inequality for periodic functions (see [62]) gives that there exists non negative numbers α, β such that

$$\alpha \left\|\phi\right\|^2_{\mathbb{H}^1(Y)} \leq a(\phi, \phi) = \int_\Omega A\epsilon(\phi) : \epsilon(\phi) \leq \beta \left\|\phi\right\|^2_{\mathbb{H}^1(Y)}.$$

Thus, a is coercive, and by the Lax-Milgram Theorem, $D_w F(0,w)$ is an isomorphism. The Implicit Function Theorem can be applied and provides that there exists a C^3 map φ on a neighborhood of 0, such that $F(\theta,\varphi(\theta))=0$ and $\varphi(0)=w$. This proves the C^3 regularity of $\theta\mapsto\tilde{w}_\theta$ and the C^2 regularity of $t\mapsto w_\theta$. □

By the chain rule and the second order shape differentiability of the state function w_θ, we get that the functional $A^*_{ijkl}(\Omega)$ is twice differentiable with respect to the domain. In general, the shape derivative w'_θ appears after differentiation of the objective, and one has to solve a separate problem for w'_θ, or introduce an adjoint state. For the effective tensor entries, the objective is self-adjoint and no problem has to be solved to compute the shape derivative of the entries $A^*_{ijkl}(\Omega)$ or the matching functional $J(\Omega)$, for the robust matching functional $\mathcal{J}_2(\Omega,\delta)$, we use the formal method of Céa to compute the shape derivative, which yields 3 adjoint problems to solve in 2D, and 6 problems in 3D.

We now recall the ingredients of the computation of the shape derivative, namely Hadamard's formulas for domain integrals and surface integrals that we quote from [50]:

Proposition 2.3.1. *Let Ω be a measurable bounded open set of $\mathbb{R}^N$. Let $f\in\mathbb{W}^{1,1}(\mathbb{R}^N,\mathbb{R}^N)$. The functional $F(\Omega)=\int_\Omega f(x)dx$ is shape-differentiable with*

$$\forall\theta\in C^{1,\infty}(\mathbb{R}^N,\mathbb{R}^N),\qquad F'(\Omega;\theta)=\int_\Omega div(f\theta). \tag{2.15}$$

If, in addition, Ω has a Lipschitz boundary, one can write

$$F'(\Omega;\theta)=\int_{\partial\Omega}(\theta\cdot n)f. \tag{2.16}$$

And for functionals defined by a boundary integral :

Proposition 2.3.2. *Assume that Ω is a bounded Lipschitz domain of class C^2. Let also $g\in\mathbb{W}^{2,1}(\mathbb{R}^N,\mathbb{R}^N)$. Then the functional $G(\Omega)=\int_{\partial\Omega}g(x)dx$ is shape-differentiable with*

$$\forall\theta\in C^{1,\infty}(\mathbb{R}^N,\mathbb{R}^N),\qquad G'(\Omega;\theta)=\int_{\partial\Omega}(\theta\cdot n)\Big(\partial_n g+\mathcal{H}g\Big). \tag{2.17}$$

2.3.2 Shape sensitivity of the effective tensor entries.

In this section, we compute the derivatives of the effective tensor entries

$$A^*_{ijkl}(\Omega)=\int_\Omega A(e_{ij}+\epsilon(w_{ij})):(e_{kl}+\epsilon(w_{kl})).$$

In a first step, we intend to obtain an expression of these quantities more convenient for the computation. To this end, we introduce the functions

$$u_{ij}(x_1, x_2, \dots, x_N) = (0, \dots, \overset{\text{i-th column}}{\overset{\downarrow}{x_j}}, 0, \dots) \qquad 1 \leq i, j \leq N,$$

so that $\nabla u_{ij} = e_{ij}$ which provides a more condense expression

$$A^*_{ijkl}(\Omega) = \int_\Omega A(y)(e_{ij}(y) + \epsilon(w_{ij}(y))) : (e_{kl}(y) + \epsilon(w_{kl}(y))) = \int_\Omega A\epsilon(\phi_{ij}) : \epsilon(\phi_{kl})$$

thanks to the change of state function

$$\phi_{ij}(y) = (u_{ij} + w_{ij})(y), \tag{2.18}$$

this helps rewrite the cell problem (2.1) as

$$\begin{cases} -div(A\epsilon(\phi_{ij})) & = 0 \qquad \text{in } \Omega \\ A\epsilon(\phi_{ij}) \cdot n & = 0 \qquad \text{on } \Gamma \\ y \mapsto w_{ij}(y) \qquad [0,1]^N - \text{periodic.} \end{cases} \tag{2.19}$$

We now give the expression of the shape derivatives of the effective tensor entries $A_{ijkl}(\Omega)$

Theorem 2.3.2. *Let $k \geq 2$, and Ω an open, bounded domain of class C^k. The function $A^*_{ijkl}(\Omega)$ defined by (2.2) is two times shape-differentiable with respect to Ω, and for $\theta \in \mathbb{W}^{2,\infty}(\mathbb{R}^N, \mathbb{R}^N)$, we have*

$$(A^*_{ijkl})'(\Omega; \theta) = \int_\Gamma (\theta \cdot n) A\epsilon(\phi_{ij}) : \epsilon(\phi_{kl}), \tag{2.20}$$

Proof of Theorem 2.3.2. A straightforward computation using Hadamard's formulas gives

$$(A^*_{ijkl})'(\Omega; \theta) = \int_\Omega A\epsilon(\phi'_{ij}) : \epsilon(\phi_{kl}) + \int_\Omega A\epsilon(\phi_{ij}) : \epsilon(\phi'_{kl}) + \int_\Gamma (\theta \cdot n) A\epsilon(\phi_{ij}) : \epsilon(\phi_{kl}),$$

then taking ϕ'_{ij} and ϕ'_{kl} as a test function in the variational formulation of problem (2.19) and integrating by parts, we immediately see that

$$\int_\Omega A\epsilon(\phi'_{ij}) : \epsilon(\phi_{kl}) = \int_\Omega A\epsilon(\phi_{ij}) : \epsilon(\phi'_{kl}) = 0,$$

which concludes the proof. □

Remark 2.3.1. *Throughout the proof, we have been freely interchanging the order of classical and shape derivatives, mainly it is why we are able to write* $\epsilon(\phi_{ij})'_{(\theta)} = \epsilon(\phi'_{ij_{(\theta)}})$. *This is a classical result and a detailed proof can be found in [24]*

2.3.3 Shape derivatives of the objectives

Here we state the main result on the differentiability of both the least-squares matching $J(\Omega)$, and the robust matching $\mathcal{J}_2(\Omega, \delta)$ functionals, and we compute their corresponding shape derivatives.

Theorem 2.3.3. *Let* $k \geq 2$, *then for all* Ω *of class* C^k, *and* $\theta, \xi \in \mathbb{W}^{k,\infty}(\mathbb{R}^N, \mathbb{R}^N)$:

i. The Least-squares matching $J(\Omega)$ *from* (2.3) *is shape differentiable for all* $\Omega \in \mathcal{A}_\varepsilon(Y)$, *and its shape derivative reads*

$$J'(\Omega; \theta) = \int_\Gamma (\theta \cdot n) k(\Omega)$$

where

$$k(\Omega) = \sum_{1 \leq i,j,k,l \leq N} (A^*_{ijkl}(\Omega) - G_{ijkl}) A\epsilon(\phi_{ij}) : \epsilon(\phi_{kl}). \tag{2.21}$$

ii. The robust matching $\mathcal{J}(2, \delta) = J(\Omega) + \delta \int_\Gamma |k(\Omega)|^2$ *is well defined. It is shape differentiable for all* $\Omega \in \mathcal{A}_\varepsilon(Y)$, *and its shape derivative is given by*

$$\mathcal{J}'_2(\Omega, \delta; \theta) = \int_\Gamma (\theta \cdot n) \left[k(\Omega) + \delta \left(\sum_{1 \leq i,j \leq N} A\epsilon(\phi_{ij}) : \epsilon(p_{ij}) + \partial_n(k(\Omega)^2) + \mathcal{H} k(\Omega) \right) \right]. \tag{2.22}$$

where $\mathcal{H}$ *is the main curvature to the boundary* Γ, *and* p_{ij} *are the adjoint states*

solutions to the following problem :

$$\int_\Omega A\epsilon(p_{ij}) : \epsilon(\psi) + 2 \sum_{1\leq k,l\leq N} \int_\Omega A\epsilon(\phi_{kl}) : \epsilon(\psi) \int_\Gamma k(\Omega) A\epsilon(\phi_{ij}) : \epsilon(\phi_{kl}) = 0 \qquad (2.23)$$

for all $\psi \in \mathbb{H}^1_\#(Y)$. .

Proof.

i. With the help of Theorem 2.3.1 and the chain rule, we immediately see that $J(\Omega)$ is shape-differentiable and we have

$$J'(\Omega;\theta) = \sum_{1\leq i,j,k,l\leq N} \Big(A^*_{ijkl}(\Omega) - G_{ijkl}\Big)(A^*_{ijkl})'(\Omega;\theta).$$

Pluging in the expression of the shape derivative ${A^*_{ijkl}}'(\Omega,\theta)$ of the effective tensor entries from (2.20) and rearanging the sums yields the desired result.

ii. The shape differentiability is an immediate result of Theorem 2.3.1. The difficulty lies in differentiating the second term corresponding to the norm of the shape gradient

$$L(\Omega) = \int_\Gamma k(\Omega)^2,$$

To this end, we use the formal method of Céa for fast differentiation, which allows to obtain a formula that is free from the shape derivatives of the state functions $\phi'_{ij} = w'_{ij}$. We thus introduce the Lagrangian :

$$\mathcal{L}(\Omega, w_{11}, p_{11}, \ldots, w_{ij}, p_{ij}) = \int_\Gamma k(\Omega)^2 + \sum_{1\leq i,j\leq N} \int_\Omega A\epsilon(\phi_{ij}) : \epsilon(p_{ij}) \qquad (2.24)$$

for all $p_{ij} \in \mathbb{H}^1_\#(Y)$. Which consists of the robust term to be differentiated $L(\Omega)$ and the variational formulations for the problems of the different state functions ϕ_{ij}. Then following the steps in [21], differentiating $\mathcal{L}$ with respect to p_{ij} gives the equation for the state function ϕ_{ij} for all $\phi \in \mathbb{H}^1_\#(Y)$:

$$\partial_{p_{ij}}\mathcal{L}(\Omega, w_{11}, p_{11}, \ldots, w_{ij}, p_{ij}; \phi) = \int_\Omega A\epsilon(\phi_{ij}) : \epsilon(\psi) = 0. \qquad (2.25)$$

Similarly differentiating with respect to w_ij, we find the equation to be satisfied by

the adjoint state p_{ij} for all $\psi \in \mathbb{H}^1_{\#}(Y)$:

$$\begin{aligned}\partial_{w_{ij}}\mathcal{L}(\Omega, w_{11}, p_{11}, \dots, w_{ij}, p_{ij}; \psi) &= 2\sum_{1\le k,l\le N}\int_\Omega A\epsilon(\phi_{kl}) : \epsilon(\psi)\int_\Gamma k(\Omega)A\epsilon(\phi_{ij}) : \epsilon(\phi_{kl}) \\ &\quad + \int_\Omega A\epsilon(p_{ij}) : \epsilon(\psi) \\ &= 0.\end{aligned}$$

Given the shape differentiability of the state functions w_{ij}, and the adjoint states p_{ij} (the proof follows the same lines as the shape differentiability of the state functions), we have using the chaine rule :

$$\begin{aligned}L'(\Omega;\theta) &= \mathcal{L}'(\Omega, w_{11}, p_{11}, \dots, w_{ij}, p_{ij}; \theta) \\ &= \partial_\Omega\mathcal{L}(\Omega, w_{11}, p_{11}, \dots, w_{ij}, p_{ij}; \theta) + \sum_{1\le i,j\le N}\partial_{w_{ij}}\mathcal{L}(\Omega, w_{11}, p_{11}, \dots, w_{ij}, p_{ij}; w'_{ij}) \\ &\quad + \sum_{1\le i,j\le N}\partial_{p_{ij}}\mathcal{L}(\Omega, w_{11}, p_{11}, \dots, w_{ij}, p_{ij}; p'_{ij}) \\ &= \partial_\Omega\mathcal{L}(\Omega, w_{11}, p_{11}, \dots, w_{ij}, p_{ij}; \theta) \\ &= \int_\Gamma(\theta\cdot n)\left[\sum_{1\le i,j\le N}A\epsilon(\phi_{ij}) : \epsilon(p_{ij}) + \partial_n(k(\Omega)^2) + \mathcal{H}k(\Omega)^2\right]\end{aligned}$$

which concludes the proof.

□

2.4 Existence results

Our first result states the well posedness of the problem.

Theorem 2.4.1. *Let $\mathcal{A}_\varepsilon(Y)$ be defined as in (2.9), and consider the robust matching functional $\mathcal{J}_2(\Omega)$ as defined in (2.6). Then, for any $\delta > 0$, there exists $\Omega^* \in \mathcal{A}_\varepsilon(Y)$ a solution of problem $(\mathcal{P})$:*

$$\mathcal{J}_2(\Omega^*, \delta) = \min\{\mathcal{J}_2(\Omega, \delta); \Omega \in \mathcal{A}_\varepsilon(Y)\}, \tag{2.26}$$

Thanks to our choice of admissible domains $\mathcal{A}_\varepsilon(Y)$, the following corollary is an immediate consequence of the theorem.

Corollary 2.4.1.1. *Let $\mathcal{A}_\varepsilon(Y)$ be defined as in Theorem 2.4.1, and for all $\Omega \in \mathcal{A}_\varepsilon(Y)$, we consider the Lebesgue measure $|\Omega|$. Then, for any $\delta > 0$, there exists $\Omega^* \in \mathcal{A}_\varepsilon(Y)$ a solution of*

$$|\Omega^*| = \min\{|\Omega|;\, \Omega \in \mathcal{A}_\varepsilon(Y);\, \mathbf{A}^*(\Omega) = \mathbf{G}\}, \tag{2.27}$$

for a given elastic tensor $\mathbf{G}$, such that for all symmetric matrix ξ we have:

$$0 \leq \boldsymbol{G}(y)\xi : \xi \leq \boldsymbol{H}(y)\xi : \xi,$$

where $\mathbf{H}$ is an upper bound of $\mathbf{A}^*$

The main challenge to establishing the existence of a minimizer for shape optimization problems is working with the right topology, that would make the functional J continuous, and, maintain the compactness of our set of admissible domains $\mathcal{A}_\varepsilon(Y)$. Here, following the approach in [50], we work with the Hausdorff topology which provides compactness and it is the ε-cone property that gives us the continuity of our functional, by enforcing some regularity on the domains.

Before proving the main statements, we need in a first step to prove continuity of the solutions of the cell problem.

Theorem 2.4.2 (Continuity of the state function)**.** *Let $(\Omega_n)_n$ be a sequence of open sets in the class $\mathcal{A}_\varepsilon(Y)$ converging in the sense of Hausdorff to some open subset Ω of Y. Let w_n, w be the solutions of the cell problem* (2.1) *respectively on Ω_n, Ω, and let $\hat{w}_n = P_{\Omega_n}(w_n)$ be the extension of w_n to Y according to Proposition 2.2.1. Then $\hat{w}_n$ converges strongly in $\mathbb{H}^1_\#(Y)$ to w^* in $\mathbb{H}^1_\#(Y)$ such that $w^*_{|\Omega} = w$*

Proof. Using w_n as a test function in the variational formulation of the cell problem (2.1), we get

$$\int_{\Omega_n} A\epsilon(w_n) : \epsilon(w_n) + \int_{\Omega_n} Ae_{ij} : \epsilon(w_n) = 0, \tag{2.28}$$

by coerciveness of the bilinear form $a(w_n, w_n) = \int_{\Omega_n} A\epsilon(w_n) : \epsilon(w_n)$, and Korn's lemma for periodic functions, there exists $C_k > 0$, independent of w_n such that

$$\|w_n\|_{\mathbb{H}^1(\Omega_n)} \leq C_k \|\epsilon(w_n)\|_{\mathbb{L}^2(\Omega_n)} \leq a(w_n, w_n)^{\frac{1}{2}}.$$

The extension property stated in Proposition 2.2.1, gives that the sequence $\hat{w}_n$ is bounded in $\mathbb{H}^1(Y)$.

Up to a subsequence, it may be assumed that $\hat{w}_n$ converges weakly in $\mathbb{H}^1(Y)$ and strongly in $\mathbb{L}^2(Y)$ to a function $w^* \in \mathbb{H}^1(Y)$. Let us check that $w^*_{|\Omega}$ satisfies the variational equation in Ω. Introducing the characteristic function $\mathcal{X}_{\Omega_n}$ and $\mathcal{X}_\Omega$, this may also be written

$$\int_Y \mathcal{X}_{\Omega_n} A\epsilon(\hat{w}_n) : \epsilon(v) + \int_Y \mathcal{X}_{\Omega n} A e_{ij} : \epsilon(v) = 0, \qquad \forall v \in \mathbb{H}^1_\#(Y). \tag{2.29}$$

Since by assumption $\mathcal{X}_n$ converges to $\mathcal{X}$ in $\mathbb{L}^p(Y)$, $p \in [1, \infty[$ and almost everywhere, we have

$$\mathcal{X}_{\Omega_n} A e_{ij} : \epsilon(v) \longrightarrow \mathcal{X}_\Omega A e_{ij} : \epsilon(v) \qquad \text{in } \mathbb{L}^1(Y).$$

Using the weak convergence in $\mathbb{H}^1(Y)$ of $\hat{w}_n$, one may pass to the limit in (2.29) and obtain:

$$\int_\Omega A\epsilon(w^*) : \epsilon(v) + \int_\Omega A e_{ij} : \epsilon(v) = 0 \qquad \forall v \in \mathbb{H}^1_\#(Y).$$

This is also valid for all $v \in \mathbb{H}^1_\#(\Omega)$ thanks to the extension property, hence $w^*_{|\Omega} = w$. Since the limit is the same for any subsequence of $(\hat{w}_n)_n$, it follows that the whole sequence $\hat{w}_n$ has the same property. The strong convergence in $\mathbb{H}^1_\#(Y)$ of $\hat{w}_n$ is obtained by going back to the variational formulation and taking $v = \hat{w}_n$ as a test function, which gives

$$\int_Y A\epsilon(\hat{w}_n) : \epsilon(\hat{w}_n) + \int_Y A e_{ij} : \epsilon(\hat{w}_n) = 0.$$

We then have that , $a(\hat{w}_n, \hat{w}_n) \longrightarrow a(w^*, w^*)$, and Korn's Inequality gives

$$\|\hat{w}_n - w^*\|_{\mathbb{H}^1(Y)} \leq C\|\epsilon(\hat{w}_n - w^*)\|_{\mathbb{L}^2(Y)} \leq C^* |a(\hat{w}_n - w^*, \hat{w}_n - w^*)|^{\frac{1}{2}} \longrightarrow 0$$

where C and C^* are independent of w_n, w. This concludes the proof.

□

We are now in position to prove the existence result Theorem 2.4.1.

Proof. We deduce from the continuity of the state (Theorem 2.4.2) that the functional $\psi : \Omega \in \mathcal{A}_\varepsilon(Y) \longrightarrow A^*(\Omega)$ is continuous. We also have by the expression of the kernel of

the shape gradient (Theorem 2.3.3) that

$$\mathcal{J}_2(\Omega,\delta) = J(\Omega) + \delta \int_\Gamma \Big| \sum_{1\le i,j,k,l\le N} \Big(A^*_{ijkl}(\Omega) - G_{ijkl}\Big)\Big(A\epsilon(\phi_{ij}) : \epsilon(\phi_{kl})\Big)\Big|^2.$$

Where $\phi_{ij} \in \mathbb{H}^1(Y)$ are defined in (2.18). Thus $\mathcal{J}_2(\Omega,\delta)$ is continuous on $\mathcal{A}_\varepsilon(Y)$ which is compact for the Hausdorff topology. Thus $\mathcal{J}_2(\Omega,\delta)$ reaches its minimum in $\mathcal{A}_\varepsilon(Y)$. □

We conclude this section with the proof of Corollary 2.4.1.1.

Proof of Corollary 2.4.1.1. Let $(\Omega_n)_n \in \mathcal{A}_\varepsilon(Y)$ be a sequence of sets converging to Ω in the sense of Hausdorff. Then, Proposition 2.2.2 infers that $\mathcal{X}_{\Omega_n} \overset{L^1(Y)}{\longrightarrow} \mathcal{X}_\Omega$. Thus, the Lebesgue measure $|\Omega|$ is continuous on the set of admissible domains $\mathcal{A}_\varepsilon(Y)$ endowed with Hausdorff metric.

On the other hand, the functional $\psi : \Omega \in \mathcal{A}_\varepsilon(Y) \longrightarrow \mathbf{A}^*(\Omega)$ is continuous by Theorem 2.4.2. Therefore, the set

$$\mathcal{M} = \{\Omega \in \mathcal{A}_\varepsilon(Y); \mathbf{A}^*(\Omega) = \mathbf{G}\} = \psi^{-1}(\mathbf{G})$$

is non-empty by Theorem 2.4.1, and is closed in $\mathcal{A}_\varepsilon(Y)$ as the inverse image of a closed set by a continuous function. Since $\mathcal{A}_\varepsilon(Y)$ is compact, $\mathcal{M}$ is compact. Thus the Lebesgue measure $|\Omega|$ has a minimum on the compact set $\mathcal{M}$ and problem (2.27) has a solution. □

2.5 Numerical results

For our simulations, we consider a square mesh with unit volume in which a domain Ω is filled with an isotropic material with Young's modulus $E = 1$, Poisson's ratio $\nu = 0.3$, and a density of material $\theta_A = 0.4$. We are looking to match a general tensor $\boldsymbol{G}$ such that

$$0 \le \boldsymbol{G} \le \boldsymbol{H},$$

where $\mathbf{H} = [H_{ijkl}]_{i,j,k,l=1}^N$ is the upper bound of Hashin-Shtrikman :

$$H_{ijkl} = \kappa_H \delta_{ij}\delta_{kl} + \mu_H(\delta_{ik}\delta_{jl} + \delta_{il}\delta_{jk} + \delta_{ij}\delta_{kl}),$$

and κ_H, and μ_H are defined in Proposition 2.5.1.

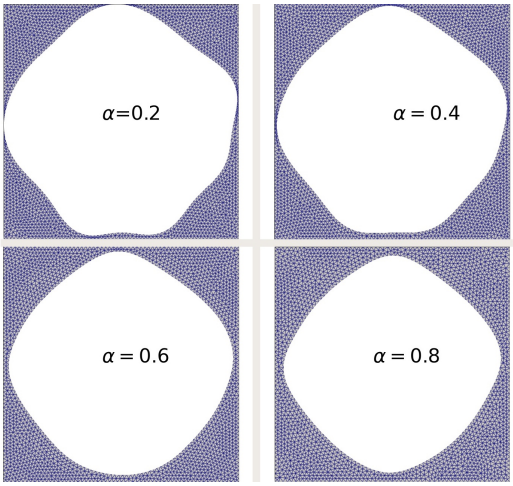

Figure 2.1 – The optimal shapes for the Least-squares matching $J(\Omega)$ for different values of α. From left to right : $\alpha = 0.2, 0.4, 0.6, 0.8$.

Proposition 2.5.1 (Hashin-Shtrikman upper bound, [4])**.** *let A be an elastic tensor with bulk modulus κ and shear modulus μ. Let A^* be the effective elasticity tensor obtained through the homogenization of A, , and an empty inclusion B, in proportions θ and $(1-\theta)$, that we assume to be isotropic, that is, for every symmetric matrix ξ,*

$$A^*\xi = 2\mu_*\xi + \Big(\kappa_* - \frac{2\mu_*}{N}\Big)(tr\xi)I.$$

Then the bulk modulus κ_* and the shear modulus μ_* satisfy

$$\kappa_* \leq \kappa_H = \frac{\theta\kappa\mu}{(1-\theta)(\kappa+2\mu)} \tag{2.30}$$

$$\mu_* \leq \mu_H = \frac{\theta\kappa\mu}{\kappa+(1-\theta)(\kappa+2\mu)} \tag{2.31}$$

All computations are performed within the FreeFem++ environment [49] and both the Least-squares matching $J(\Omega)$ and the (p,δ) robust-matching functional $\mathcal{J}_p(\Omega,\delta)$ is minimized using either a steepest-descent algorithm, or an augmented Lagrangian algorithm (see [59]). For an effective implementation of these techniques in FreeFem++ we refer the reader to ([31],[30],[3]).

We start by looking into the optimal shapes for matching an elastic tensor $\mathbf{G} = \alpha\mathbf{H}$, where $0 < \alpha < 1$. The results are given in Figure 2.1.

As expected, since the upper bound $\mathbf{H}$ is computed for a density matter of 0.4, we see

a volume expansion the lower α gets. Intuitively, as α gets lower and lower, the algorithm needs to fill the domain Ω with more air, to distance itself from the upper bound. More importantly, the optimal shapes for the matching of interior tensors are easy to compute and are not unique due to the simplicity of the problem. Thus in what follows, we try to raise the difficulty by focusing on the upper bound of Haschin-Shtrikman.

2.5.1 Illustration of the non uniqueness of optimal shapes

We first want to provide numerical evidence for answering the following natural question : are we able to match the upper bound of Hashin-Shtrikman? and if so, is the optimal shape unique? It is known (see the book of Allaire [5]) that the Haschin-Shtrikman bounds can be attained by a sequential laminate of rank p, where $p = 3$ in 2-D, and $p = 6$ in 3-D. Numerical results for the scalar case have been done in [28] and for different initial shapes they ended up with different optimal shapes. Here, we investigate numerically whether or not these bounds are attainable for other (matrix) composites, and if not, how close can we get to these bounds. As an example we start from three different inclusions ω_1 corresponding to a disc of radius $r = 0.3$ and two random inclusion ω_2 and ω_3 parametrized by :

$$\partial\omega_2 = \left\{ \begin{pmatrix} 0.1 + 0.5\cos(\theta) + 0.1\cos(4\theta) \\ 0.5\sin(\theta) + 0.1\cos(4\theta) \end{pmatrix}, \quad \theta \in [0, 2\pi] \right\}$$

and,

$$\partial\omega_3 = \left\{ \begin{pmatrix} 0.1 + 0.5\cos(\theta) + 0.1\cos(3\theta) \\ 0.5\sin(\theta) + 0.1\cos(4\theta) \end{pmatrix}, \quad \theta \in [0, 2\pi] \right\}.$$

And, we perform a gradient descent of 400 iterations using the shape derivative $J'(\Omega, \theta)$ given in (2.21) in hope of matching the upper Hashin-Shtrikman bound $\mathbf{H}$. The optimal shapes and numerical results are given in Figure 2.2.

		ω_1	ω_2	ω_3
$J(\Omega)$	initial	$8.71e-03$	$9.53e-03$	$1.3e-02$
	final	$8.18e-05$	$1.90e-05$	$5.17e-08$
$\|J'(\Omega,\theta)\|$	initial	$9.04e-02$	$2.89e-01$	$4.10e-01$
	final	$3.84e-02$	$5.91e-03$	$1.02e-03$
$\text{Vol}(\Omega)$	initial	0.4	0.4	0.4
	final	0.61	0.55	0.50

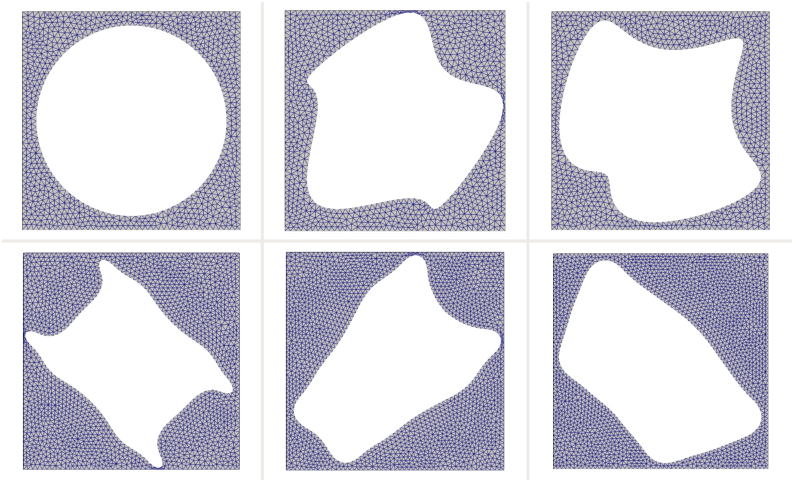

Figure 2.2 – The initial (top), and optimal (bottom) shapes for the Least-squares matching $J(\Omega)$ of the upper Hashin-Shtrikman bound for a mixture of air and material density $\theta = 0.4$.

As we can see in Figure 2.2 and the values table within, starting from different inclusions we are able to drastically decrease the matching up to $e-08$. All the shapes obtained enjoy a certain degree of "natural" symmetry due to the elasticity tensor A. This seems to be the only thing they have in common, since these shapes have different volumes, and different gradient norms $\|J'(\Omega,\theta)\|$.

Thus it makes sense to seek-out the most robust of all shapes (i.e the shape with a minimal gradient norm $\|J'(\Omega,\theta)\|$), which shall be examined below. One should also notice that despite having multiple "solutions" to minimize $J(\Omega) = \|A^*(\Omega) - \mathbf{H}\|_F^2$, that none of these solution satisfy the density matter constraint for which the upper bound was computed (i.e $\text{Vol}(\Omega) = 0.4$). Before moving on to robustness, we would like to test how much the density matter constraint and the diagonal symmetry of the shapes influences the matching criterion $J(\Omega)$, for this we compute $J(\Omega)$ and the norm of the shape derivative $\|J'(\Omega,\theta)\|$ for the same inclusion ω_3, but with different volumes and different orientations, the results are given below :

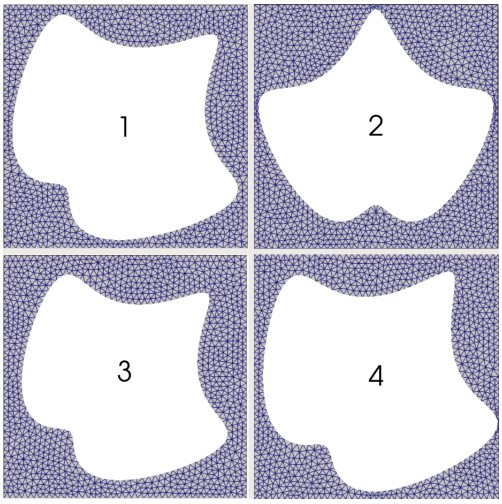

	1	2	3	4
$J(\Omega)$	0.014	0.013	0.009	0.016
$\|J'(\Omega,\theta)\|$	0.41	0.64	0.23	0.5
$\mathrm{Vol}(\Omega)$	0.4	0.5	0.5	0.4

Figure 2.3 – The inclusion ω_3 with different orientations and different volumes and the corresponding computed quantities.

We can see from Figure 2.3 that the optimal shapes seem to be ultimately defined by symmetry and closeness to the volume constraint. Indeed, changing the orientation to the left between the inclusions 2 and 3 while fixing the volume, has a strong effect on the matching functional J and the norm of the shape gradient. Similarly, fixing the volume and slightly changing the orientation between 1 and 4 slightly causes the matching and norm of the shape gradient increase. This confirms our intuition, and thus, our initial guesses for the rest of this section shall satisfy both the diagonal symmetry constraint and the density matter constraint.

2.5.2 Robust optimal shapes

Here for our numerical simulations, and for the sake of comparison, we consider the inclusion ω_3 illustrated in Figure 2.3, which is close to a critical point of the matching objective $J(\Omega)$. We first start by testing the shape derivative of the robust term $L(\Omega) = \int_\Gamma k(\Omega)^2$. To this end we perform a gradient descent of 100 iterations, and we compare $L'(\Omega;\theta)$ which is supposed to describe the change in the norm of the shape derivative $\|J'(\Omega;\theta)\|_{\mathbb{L}_2}$, with the shape derivative $J'(\Omega;\theta)$ which describes the change in the matching functional. The final results and convergence graphs are given below, and they show that in the neighborhood of a critical shape, minimizing the norm of the shape derivative does not necessary lie in the same direction of the shape derivative J'. One can see from the resulting final shapes of Figure 2.5, that the initial guess ω_3 is indeed in the vicinity of

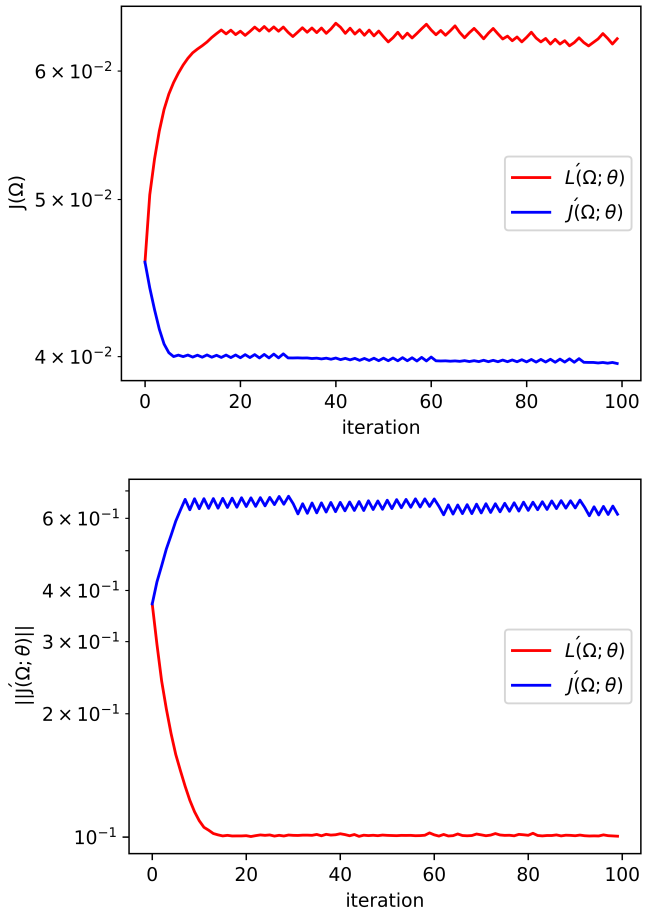

Figure 2.4 – Convergence results for both the matching objective $J(\Omega)$ (top) and the norm of the shape derivative $\|J'(\Omega;\theta)\|$ (bottom) using different shape gradients.

a critical shape for the objective $J(\Omega)$, despite using a line search, it becomes difficult to decrease both objectives after a couple of iterations, and only the final shape for minimizing the norm of the shape derivative is different from the initial guess.

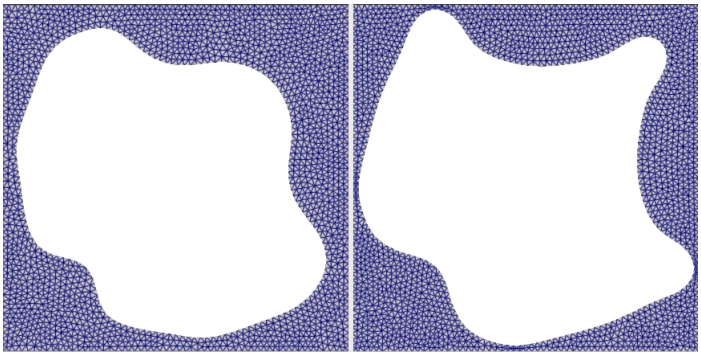

Figure 2.5 – Final shapes using the gradient of the matching objective J' (right), and the gradient of the robust term L' (left).

We now look at the robust functional $\mathcal{J}_2(\Omega, \delta) = J(\Omega) + \delta \|k(\Omega)\|_2^2$. We perform a gradient descent of 100 iterations using the shape derivative $\mathcal{J}_2'(\Omega, \delta; \theta)$ given in (2.22) for different values of the deformation magnitude δ. The final shapes and convergence results are given in the figures below. One can see in Figure 2.4 that, as δ gets bigger we are able to reach lower values for the norm of the shape derivative $\|J'(\Omega; \theta)\|$. This translates in the shapes having lesser and lesser details on the boundary, as shown in Figure 2.6. Taking $\delta = 0.06$, leads to oscillations along the optimization process, this can be intuitively explained by the algorithm getting conflicted between the minimization of the norm of the shape derivative or minimizing the matching, which have opposite directions based on Figures 2.4 and 2.7.

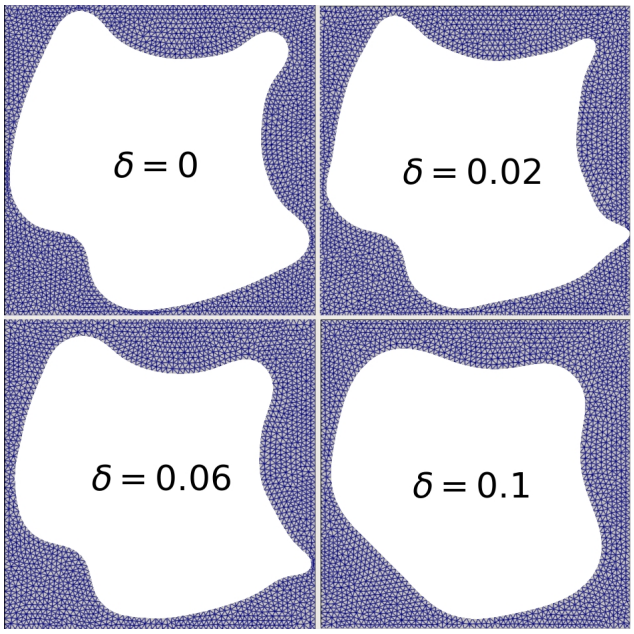

Figure 2.6 – The final shapes for minimizing the robust functional $\mathcal{J}_2(\Omega, \delta)$ using different values of δ.

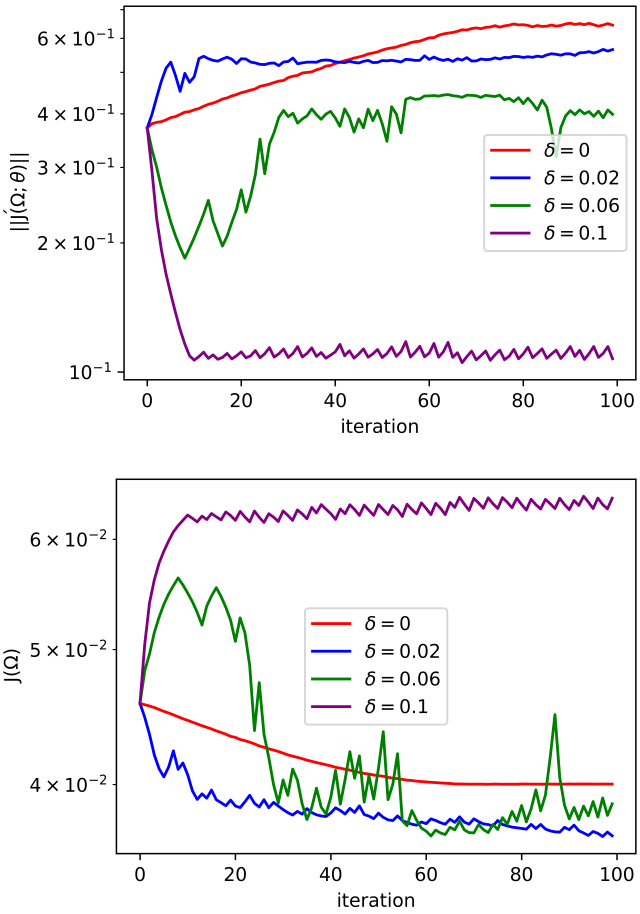

Figure 2.7 – Convergence results for both the matching objective $J(\Omega)$ (bottom) and the norm of the shape derivative $\|J'(\Omega;\theta)\|$ (top) using different shape gradients.

2.5.3 Volume constraint

Here we address the volume constraint, we investigate how close can we match the upper Hachin-Shtrikman bound $\boldsymbol{H}$ with minimal volume V. We start from a circular inclusion and seek to minimize the following augmented lagrangians

$$\mathcal{L}(\Omega) = V(\Omega) + \lambda(J(\Omega) - J_{target}) + \frac{\mu}{2}(J(\Omega) - J_{target})^2$$

Where $V(\Omega)$ is the volume of Ω, and λ, $\mu > 0$. To this end, we perform a gradient descent of 100 iterations using the shape derivatives of the above augmented lagrangian, which is easily deduced from Theorem 2.3.3 and the shape derivative of the volume given by

$$V'(\Omega; \theta) = \int_{\partial\omega} (\theta \cdot n).$$

Figure 2.9 shows the computed optimal shapes for minimizing the Least-squares matching $J(\Omega)$, and for minimizing the volume $V(\Omega)$. Convergence results are shown in Figure 2.8, and It shows clearly the antagonistic relation between the matching of the desired effective material properties and the density matter used to obtain it, this is no surprise and is coherent with the optimal shapes computed in Figure 2.2, we were only able to match the upper bound of Hashin-Shtrikman computed for a density matter $V = 0.4$ by adding more material (final volume $V = 0.5$).

2.5.4 Summary

Our numerical tests show that the inverse Homogenization problem of light-weight elastic microstructures has infinite solutions, the reason is due to the simple nature of the problem and ultimately makes the matching of a desired effective material properties a question of density matter constraint (volume of the optimal inclusions) and of symmetry of these inclusions. For this same reason, the question of finding shapes with minimal volume does not seem practical and the results show that increasing the volume (up to certain limits) will result for an easier and better matching of the upper bound which is reasonable. Finally if there is no hope in finding optimal structures with minimal volume, if one is interested in finding robust structures that will not lose performance despite geometrical uncertainties, the minimisation of the worst-case scenario, or Its variants

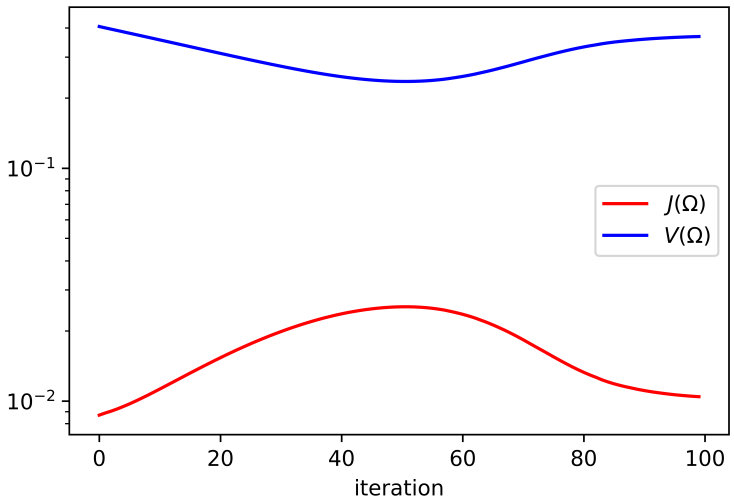

Figure 2.8 – Convergence results for the matching $J(\Omega)$ and the volume $V(\Omega)$.

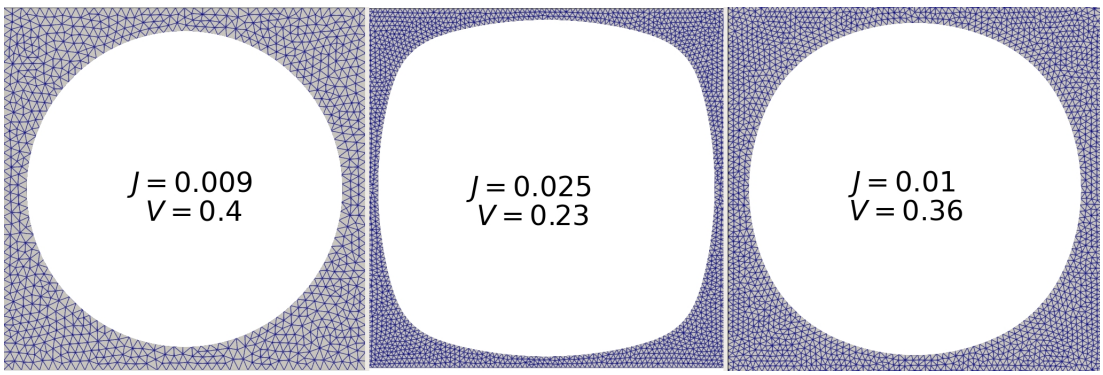

Figure 2.9 – The initial domain (left), the domain with minimal volume (middle) and the final domain (right) with the computed values of the matching objective $J(\Omega)$ and volume $V(\Omega)$

used in this work, does allow to obtain structures that are less sensitive to geometric perturbations, even in the vicinity of optimal solutions. One can then alternate between the minimization of an objective and the norm of Its shape derivative or use the robust penalization of the norm.

Chapter 3

Inverse homogenization of piezomaterials

3.1 Introduction

A piezoelectric material is a material capable of producing electric energy upon application of stress. Since their discovery in 1880, piezoelctric materials have been at the center of industrial and technological innovations. The piezoelctric effect Perhaps the first practical application of piezoelectric materials was the invention of the sonar during world war I. Since then they have been widely used for sensors (longitudinal, transversal and shear Detection of pressure variations in the form of sound), energy harvesting (some crystals like quartz, can generate potential differences of thousands of volts), and actuators (the mechanical response of a piezoelectric material can change better-than-µm precision, making them the most important tool for positioning objects with extreme accuracy). Piezo-composite materials are new promising materials that are composed of a piezo-electric material and a polymer, they can be combined in multiple ways to provide excellent tailorable properties. In particular the model of a polymer matrix and piezoelectric rod is most useful (see Figure 3.1). This type of piezo-composite, among many advantages, has a good matching to water and human tissue and is used in the medical field for ultrasonic medical diagnostic and bioengineering. The design of a piezo-composite starts at the level of the microstructure (cell), if we consider the model of a polymer matrix periodically filled with piezoelectric rods, then the global effective properties of the composite can be estimated at the cell level through the theory of homogenization. The homogenization of piezoelectric composite have been extensively studied in the works of Miara, Mekchour et al. [54, 40, 41]. In [56] The authors give the cell problems to solve in order to characterize the so-called corrector functions, which are then used to compute the global effective properties of the different tensors used in piezoelectricity (the elastic, dielectric and piezoelectric coupling tensors). The authors produce numerical results for

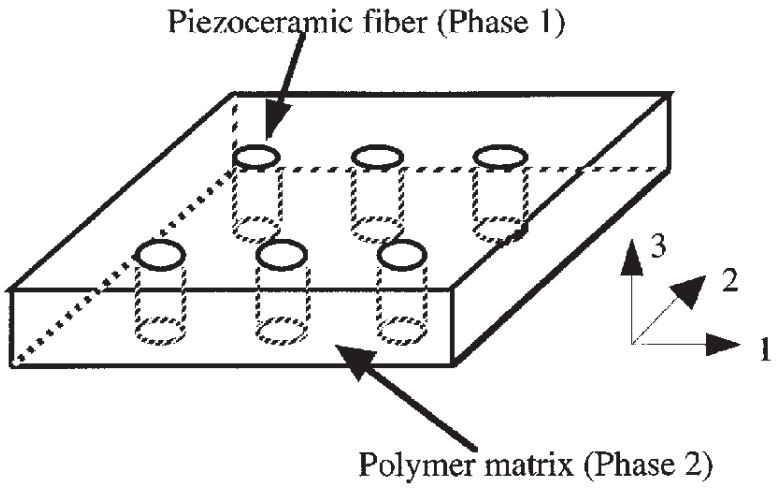

Figure 3.1 – A polymer matrix-piezo-electric rod composite

the design of bone materials, and the computed homogenized entries are up-to a scaling parameter very close to numerical experiments. In this work we look at the inverse problem through a shape optimization approach. That is, we want to design a piezo-composite with certain desired properties, and we search for the optimal design of the micro structure that will yield matching, global effective piezoelectric properties. To this end, we study the sensitivity with respect to the shape of the piezoelectric inclusion, we then use the knowledge of the shape derivatives of the effective tensor entries to compute optimal matching shapes. In Section 3.2 we recall the piezoelectric model and present the inverse homogenization problem. Section 3.3 gives the existence of optimal inclusions for the matching criterion inside a class of admissible inclusions, namely inclusions with a smooth geometric boundary. In Section 3.4 we give the shape derivatives for the different effective tensors that we then use to compute the shape derivative of the matching criterion. Finally, section **??** is dedicated to numerical simulations.

3.2 The problem

Due to the nature of the problem, and the different order tensors used to model it, we abstain from using conventional notation for matrix-vector operations and we shall use the more general double contraction operator ":" between two tensors of different orders. For example, the double contraction of a third order tensor $\boldsymbol{T} = a \otimes b \otimes c$ and a second

order tensor : $\boldsymbol{S} = d \otimes e$ is the first order tensor

$$\boldsymbol{R} = \boldsymbol{T} : \boldsymbol{S} = (c \cdot e)(b \cdot d)a$$

where a, b, c, d, e are first order tensors (vectors).

3.2.1 The piezoelectric model

The properties of a piezoelectric material are described by three tensors : the fourth order elasticity tensor $\mathbf{A} = [A_{ijkl}]_{i,j,k,l=1}^{N}$, the second-order dielectric tensor $\mathbf{D} = [d_{ij}]_{i,j=1}^{N}$, and the third order piezoelectric coupling tensor $\mathbf{G} = [g_{kij}]_{k,i,j=1}^{N}$. We assume that :

— $\mathbf{A}$ is positive definite and satisfies both minor and major symmetries

$$\Big(A_{ijkl} = A_{jikl} = A_{klij}\Big).$$

— $\mathbf{D}$ is positive definite and symmetric $d_{ij} = d_{ji}$.

— $\mathbf{G}$ satisfies the following symmetry $g_{kij} = g_{kji}$.

.

The electromechanical behaviour of this material is given by the elastic displacement $\mathbf{u}$, and the electric potential φ, which both are related to the stress tensor $\sigma = [\sigma_{ij}]_{i,j=1}^{N}$ and to the electric displacement vector $\mathbf{E} = [E_i]_{i=1}^{N}$ by the constitutive laws as follows :

$$\begin{cases} \boldsymbol{\sigma}(u, \varphi) & = \boldsymbol{A} : \varepsilon(u) - \boldsymbol{G} : \nabla\varphi, \\ \mathbf{E}(u, \varphi) & = \boldsymbol{G} : \varepsilon(u) + \boldsymbol{D} : \nabla\varphi \end{cases}$$

where $\epsilon(u) = \frac{1}{2}\Big(\nabla u + {}^t\nabla u\Big)$ is the linearized strain tensor. The equilibrium equations related to mechanical forces f and to electric volume charges q, being applied in a domain W, read as

$$\begin{cases} -div(\boldsymbol{\sigma}(u, \varphi)) & = f & \text{in } W \\ -div(\mathbf{E}(u, \varphi) & = q & \text{in } W. \end{cases}$$

3.2.2 The inverse homogenization problem

Homogenization is concerned with the situation where the different tensors describing the properties of the piezomaterial are no longer constant throughout the domain Ω. In

what follows, and for the sake of generality, we assume there is a periodic distribution of two piezoelectric phases. The periodicity size is denoted $\epsilon > 0$. Let $Y = [0,1]^N$ be the rescaled unit periodic cell, we define the periodic sobolev space $\mathbb{H}^1_{\#}(Y)$ as in Lemma 3.3.1, and we consider a subdomain Ω of Y, with a smooth boundary $\Gamma = \partial\Omega$. Throughout the paper, the domain Ω will represent (up to the scaling) the part occupied by the phase 2, while $\Omega^c = Y \setminus \overline{\Omega}$ will represent the domain occupied by the phase 1, i.e.

$$Y = \Omega \cup \Omega^c \cup \Gamma \qquad \text{with} \quad \overline{\Omega} \subset Y.$$

Thus, for all $x \in W$, we have $y = \frac{x}{\epsilon} \in Y$ and we define the oscillating elastic, dielectric and piezoelectric coupling tensors given by :

$$\begin{aligned}
\mathbf{A}(y) &= \mathbf{A}_1(y) + \Big(\mathbf{A}_2(y) - \mathbf{A}_1(y)\Big)\mathbb{1}_\Omega(y),\\
\mathbf{D}(y) &= \mathbf{D}_1(y) + \Big(\mathbf{D}_2(y) - \mathbf{D}_1(y)\Big)\mathbb{1}_\Omega(y),\\
\mathbf{G}(y) &= \mathbf{G}_1(y) + \Big(\mathbf{G}_2(y) - \mathbf{G}_1(y)\Big)\mathbb{1}_\Omega(y).
\end{aligned}$$

When $\epsilon \to 0$, the medium can be considered homogeneous, with effective constant elastic, dielectric and piezoelectric coupling tensors $\mathbf{A}^*$, $\mathbf{D}^*$, and $\mathbf{G}^*$.

To compute these homogenized tensors, one needs so-called correctors

$$(\chi^{ij}, \pi^{ij}) \in [\mathbb{H}^1_{\#}(Y)]^N \times \mathbb{H}^1_{\#}(Y),\ i,j = 1,\dots,N,$$

and

$$(w^k, \eta^k) \in [\mathbb{H}^1_{\#}(Y)]^N \times \mathbb{H}^1_{\#}(Y)\,, k = 1,\dots,N,$$

corresponding to the local displacements and electric potentials in the cell Y. These correctors have been defined by Miara et al in [55] and the references therein, to which we refer the interested reader for more details. The correctors are defined as solutions to the following cell problems

$$\begin{cases} -div\Big(\boldsymbol{\sigma}(\chi_{rs} + \Pi^{rs}, \pi_{rs})\Big) &= 0 \qquad \text{in } Y\\ -div\Big(\boldsymbol{E}(\chi_{rs} + \Pi^{rs}, \pi_{rs})\Big) &= 0 \qquad \text{in } Y, \end{cases} \qquad \begin{cases} -div\Big(\boldsymbol{\sigma}(w_k, \eta_k + \Pi^k)\Big) &= 0 \qquad \text{in } Y\\ -div\Big(\boldsymbol{E}(w_k, \eta_k + \Pi^k)\Big) &= 0 \qquad \text{in } Y, \end{cases}$$

where the vectorial function $\Pi^{rs} = (\Pi^{rs}_i)$, and the scalar one Π^k, are defined as

$$\Pi^{rs}_i = y_s\delta_{ir} \qquad \text{and} \qquad \Pi^k = y_k.$$

On the interface $\Gamma = \partial\Omega$ we have to impose the transmission condition for fields of mechanical displacements and stresses, namely

$$\begin{cases} [\boldsymbol{\sigma}(\chi_{rs} + \Pi^{rs}, \pi_{rs}) : n] &= 0 \qquad \text{on } \Gamma \\ [\chi_{rs} + \Pi^{rs}] &= 0 \qquad \text{on } \Gamma, \end{cases}$$

and also for the electrical field,

$$\begin{cases} [\boldsymbol{E}(\chi_{rs}, \pi_{rs}) : n] &= 0 \qquad \text{on } \Gamma \\ [\pi_{rs}] &= 0 \qquad \text{on } \Gamma. \end{cases}$$

With n the normal vector to the boundary Γ, oriented from the interior of Ω, to the exterior Ω^c. And where we denote the jump of a function $\boldsymbol{f}$ through the interface Γ by

$$[\boldsymbol{f}(y)] = \boldsymbol{f}^+(y) - \boldsymbol{f}^-(y) = \lim_{t \to 0^+} \boldsymbol{f}(y + tn(y)) - \lim_{t \to 0^-} \boldsymbol{f}(y + tn(y)).$$

Remark 3.2.1.

— *In case one considers an insulated elastic material for the phase* 2*, then one only specifies a free Neumann condition for the electric field on the interface* Γ*, i.e.*

$$\boldsymbol{E_1}(\chi_{rs}, \pi_{rs}) : n = 0 \qquad \text{on } \Gamma$$

— *In case the phase* 2 *is taken as the void, i.e. the case of a periodically perforated piezoelectric material, one prescribes free Neumann conditions, on both the electric field and the mechanical stress. Namely :*

$$\begin{cases} \boldsymbol{\sigma_1}(\chi_{rs}, \pi_{rs}) : n = 0 \qquad \text{on } \Gamma \\ \boldsymbol{E_1}(\chi_{rs}, \pi_{rs}) : n = 0 \qquad \text{on } \Gamma \end{cases}$$

Thus the correctors $(\chi^{ij}, \pi^{ij}), (w^k, \eta^k) \in [\mathbb{H}^1_\#(Y)]^N \times \mathbb{H}^1_\#(Y)$ are solutions to the fol-

lowing problems :

$$\begin{cases} -div\Big(\boldsymbol{\sigma}(\chi_{rs}+\Pi^{rs},\pi_{rs})\Big) &= 0 \qquad \text{in } Y \\ -div\Big(\boldsymbol{E}(\chi_{rs}+\Pi^{rs},\pi_{rs})\Big) &= 0 \qquad \text{in } Y \\ [\boldsymbol{\sigma}(\chi_{rs},\pi_{rs}):n] &= 0 \qquad \text{on } \Gamma \\ [\boldsymbol{E}(\chi_{rs},\pi_{rs}):n] &= 0 \qquad \text{on } \Gamma \\ [\chi_{rs}] &= 0 \qquad \text{on } \Gamma \\ [\pi_{rs}] &= 0 \qquad \text{on } \Gamma \\ y \mapsto \chi_{rs}(y) & \qquad [0,1]^N - \text{periodic} \\ y \mapsto \pi_{rs}(y) & \qquad [0,1]^N - \text{periodic} \end{cases} \tag{3.1}$$

$$\begin{cases} -div\Big(\boldsymbol{\sigma}(w_k,\eta_k+\Pi^{k})\Big) &= 0 \qquad \text{in } Y \\ -div\Big(\boldsymbol{E}(w_k,\eta_k+\Pi^{k})\Big) &= 0 \qquad \text{in } Y \\ [\boldsymbol{\sigma}(w_k,\eta_k):n] &= 0 \qquad \text{on } \Gamma \\ [\boldsymbol{E}(w_k,\eta_k):n] &= 0 \qquad \text{on } \Gamma \\ [w_k] &= 0 \qquad \text{on } \Gamma \\ [\eta_k] &= 0 \qquad \text{on } \Gamma \\ y \mapsto w_k(y) & \qquad [0,1]^N - \text{periodic} \\ y \mapsto \eta_k(y) & \qquad [0,1]^N - \text{periodic} \end{cases} \tag{3.2}$$

Having solved the local problems, the following formulas for $\mathbf{A}^*$, $\mathbf{D}^*$, and $\mathbf{G}^*$ can be evaluated :

$$A^*_{ijkl}(\Omega) = \frac{1}{|Y|}\Big[\int_Y \Big(A : \varepsilon(\chi_{ij}+\Pi^{ij})\Big) : \varepsilon(\chi_{kl}+\Pi^{kl}) + \int_Y \Big(D : \nabla\pi_{ij}\Big) : \nabla\Pi^{kl}\Big], \tag{3.3}$$

$$D^*_{kl}(\Omega) = \frac{1}{|Y|}\Big[\int_Y \Big(A : \varepsilon(w_k)\Big) : \varepsilon(w_l) + \int_Y \Big(D : \nabla(\eta_k+\Pi^{k})\Big) : \nabla(\eta_l+\Pi^{l})\Big], \tag{3.4}$$

$$G^*_{kij}(\Omega) = \frac{1}{|Y|}\Big[\int_Y \Big(G : \varepsilon(\chi_{ij}+\Pi^{ij})\Big) : \nabla\Pi^{k} + \int_Y \Big(D : \nabla\pi_{ij}\Big) : \nabla\Pi^{k}\Big]. \tag{3.5}$$

Of course, these effective tensors are bounded for real applications, one can see for example [15] and the references therein, where the well known Voigt-Reuss and Haschin-Schtrikman bounds are derived for periodic piezoelectric composites.

The problem of finding periodic composites with prescribed effective properties has been vastly examined in the literature for the purely elastic case (see for example [68, 47, 11]). To our best knowledge, the question of tayloring piezoelectric composites was not yet considered. In this paper, we are interested in the simple question of finding optimal cell designs to match desired piezoelectric properties within the admissible properties as defined by the bounds.

To make things explicit, and for the sake of reducing the heavy use of tensors, we use Voigt notation, to write in matrix form, the elasticity tensor $\boldsymbol{A}$ as $[A_{ij}]_{i,j=1}^{2N}$. We transform the dielectric matrix $\boldsymbol{D}$ into the row vector (d_i), and we define the piezoelectric property matrix $\boldsymbol{P}$ as :

$$\boldsymbol{P} = \begin{cases} [p_{ij}]_{\substack{i=1,\dots,2N+1 \\ j=1,\dots,2N}} \\ \\ p_{ij} = \begin{cases} A_{ij} & 1 \leq i \leq 2N \\ dj & i = 2N+1. \end{cases} \end{cases} \tag{3.6}$$

Accordingly, we define $\boldsymbol{P}^*(\Omega)$ the corresponding effective matrix. We then follow the approach in [28], we choose the Frobenius norm on matrices to make precise the notion of closeness between matrices and we define the objective

$$J(\Omega) = \frac{1}{2}\|\boldsymbol{P}^*(\Omega) - \boldsymbol{P}\|_F^2 = \frac{1}{2}\sum_{\substack{i=3N+1 \\ i,j=1}}^{\substack{j=2*N}} \left(p_{ij}^* - p_{ij}\right)^2 \tag{3.7}$$

as a least square matching of the desired properties. This allows us to state our shape optimisation problem $\mathcal{P}$ as :

Problem 2. *Given a class of admissible domains $\mathcal{A}(Y)$, find an inclusion $\Omega^* \in \mathcal{A}(Y)$ such that*

$$J(\Omega^*) = \min\{J(\Omega); \Omega \in \mathcal{A}(Y)\}. \tag{3.8}$$

3.3 Existence results

For the rest of our analysis, we will need some useful analysis tools, namely, Poincaré's inequality and Korn's lemma for periodic functions that we recall here.

Lemma 3.3.1 (Korn and Poincaré's inequalities for periodic functions)**.** *Let W be an unbounded domain with a 1-periodic structure, set $Y =]0,1[^N$ and let $W \cap Y$ be a domain with a Lipschitz boundary. Then for any*

$$v \in \mathbb{H}^1_{\#}(W) = \left\{ v \in \mathbb{H}^1(W),\ v \text{ is } Y\text{-periodic}, \int_{W\cap Y} v dx = 0 \right\}$$

the following inequalities hold with constants C_k, and C_p independent of v :

— *Korn's inequality :*

$$\|v\|_{\mathbb{H}^1(W\cap Y)} \leq C_k \|\epsilon(v)\|_{\mathbb{L}^2(W\cap Y)} \tag{3.9}$$

— *Poincaré's inequality :*

$$\|v\|_{\mathbb{L}^2(W)} \leq C_p \|\nabla v\|_{\mathbb{L}^2(W)}. \tag{3.10}$$

We will also be using some different shape optimization tools and notions that have been recalled in chapter 2, to which we refer the interested reader who is unfamiliar with shape optimisation.

Our first result gives the existence of an optimal inclusion in the class of domains satisfying a uniform ϵ-cone property.

Theorem 3.3.1. *Let $\mathcal{A}_\varepsilon(Y) = \{\Omega \subset Y, \Omega \text{ open with the } \varepsilon\text{-cone property}\}$, and consider the matching functional $J(\Omega)$ as defined in (3.8). Then, there exists $\Omega^* \in \mathcal{A}_\varepsilon(Y)$ a solution of problem $(\mathcal{P})$:*

$$J(\Omega^*) = \min\{J(\Omega); \Omega \in \mathcal{A}_\varepsilon(Y)\}, \tag{3.11}$$

Thanks to our choice of admissible domains $\mathcal{A}_\varepsilon(Y)$, the following corollary is an immediate consequence of the theorem.

Corollary 3.3.1.1. *Let $\mathcal{A}_\varepsilon(Y)$ be defined as in Theorem 3.3.1 and let $\mathbf{P}$ be a given piezoelectric matrix that is such that the matching set*

$$\mathcal{M} = \{\Omega;\ \Omega \in \mathcal{A}_\varepsilon(Y);\ \mathbf{P}^*(\Omega) = \mathbf{P}\}$$

is not empty. Then, there exists $\Omega^* \in \mathcal{A}_\varepsilon(Y)$ minimizing the volume of the inclusion that

is a solution of

$$|\Omega^*| = \min\{|\Omega|;\, \Omega \in \mathcal{A}_\varepsilon(Y);\, \mathbf{P}^*(\Omega) = \mathbf{P}\}, \tag{3.12}$$

.

Proving the existence of a minimiser boils down to proving the continuity of the objective $J(\Omega)$, and the compactness of the set of admissible domains $\mathcal{A}_\varepsilon(Y)$ for a given topology. The latter is easily given by the Hausdorff topology which is naturally compact for our choice admissible domains, the former is dependent on the continuity of the corrector functions that we state in the following theorem.

Theorem 3.3.2 (Continuity of the corrector functions)**.** *Let $(\Omega_n)_n$ be a sequence of open sets in $\mathcal{A}_\varepsilon(Y)$ converging in the sense of Hausdorff to some open subset Ω of Y. Let (χ_n, π_n), (w_n, η_n), respectively (χ, π), (w, η), be the solutions of of the cell problems* (3.1) *and* (3.2) *respectively on Ω_n, Ω. Then (χ_n, π_n), (w_n, η_n) converge strongly in $\mathbb{H}^1_\#(Y)$ to (χ, π), (w, η), in $\mathbb{H}^1_\#(Y)$.*

Proof of Theorem 3.3.2. Since the two problems (3.1) and (3.2) are similar we give the proof for the couple of solutions (χ_n, π_n). The key to proove convergence in $\mathbb{H}^1_\#(Y)$ to (χ, π) is the coerciveness of the elastic and dielectric tensors and the boundedness of the materials properties. In fact, by coerciveness of the bilinear forms

$$a(\chi_n, \chi_n) = \int_Y \Big(A : \varepsilon(\chi_n)\Big) : \varepsilon(\chi_n), \tag{3.13}$$

and

$$b(\pi_n, \pi_n) = \int_Y \Big(D : \nabla\pi_n\Big) : \nabla\pi_n, \tag{3.14}$$

there exists, $C_1, C_2 > 0$ such that

$$\|\varepsilon(\chi_n)\|^2_{\mathbb{L}^2(Y)} \leq C_1 a(\chi_n, \chi_n)$$
$$\|\nabla\pi_n\|^2_{\mathbb{L}^2(Y)} \leq C_2 b(\pi_n, \pi_n).$$

Using Korn and Poincaré's inequalities for periodic functions, one immediately sees that

there exists $C_k, C_p > 0$ independent of χ_n, π_n such that :

$$\|\chi_n\|_{\mathbb{H}^1_\#(Y)} \leq C_k$$
$$\|\pi_n\|_{\mathbb{H}^1_\#(Y)} \leq C_p$$

Thus, the sequence (χ_n, π_n) is bounded in $\mathbb{H}^1_\#(Y)$, up to a subsequence it may be assumed that it converges weakly in $\mathbb{H}^1_\#(Y)$, and strongly in $\mathbb{L}^2(Y)$ to a couple of functions (χ, π). It is easy to check that (χ, π) satisfy the variational equational of problem (3.1). The strong convergence in $\mathbb{H}^1_\#(Y)$ is deduced by taking $(v, \psi) = (\chi_n - \chi, \pi_n - \pi)$ in the variational formulation of (3.1), and once again applying korn and poincaré's inequalities. We get the existence of C_k, C'_k, C_p, $C'_p > 0$ idnependent of χ_n, π_n, χ, π such that

$$\|\chi_n - \chi\|^2_{\mathbb{H}^1_\#(Y)} \leq C_k \|\varepsilon(\chi_n - \chi)\|^2_{\mathbb{L}^2(Y)} \leq C'_k a(\chi_n - \chi, \chi_n - \chi) \overset{n\to\infty}{\longrightarrow} 0$$
$$\|\pi_n - \pi\|^2_{\mathbb{H}^1_\#(Y)} \leq C_p \|\nabla(\pi_n - \pi)\|^2_{\mathbb{L}^2(Y)} \leq C'_p a(\pi_n - \pi, \pi_n - \pi) \overset{n\to\infty}{\longrightarrow} 0.$$

This concludes the proof. □

Remark 3.3.1. *In case the phase 2 is taken as the void, i.e, the case of a periodacially perforated piezoelectric material, one would have to adapt the proof and prove the continuity of the bounded extensions of the couples (χ_n, π_n), such a bounded extension is guaranteed with our choice of admissible domains, see [23]. The proof then is an easy adaptation of the proof of Theorem 2.4.2.*

We are now in position to prove the existence result Theorem 3.3.1.

Proof of Theorem 3.3.1.
We deduce from the continuity of the state (Theorem 3.3.2) that the functional $J(\Omega)$ is continuous on $\mathcal{A}_\varepsilon(Y)$, which is compact for the Hausdorff topology. Thus $J(\Omega)$ reaches its minimum on $\mathcal{A}_\varepsilon(Y)$. □

We conclude this section with the proof of Corollary 3.3.1.1.

Proof of Corollary 3.3.1.1.
Let $(\Omega_n)_n \in \mathcal{A}_\varepsilon(Y)$ be a sequence of sets converging to Ω in the sense of Hausdorff. Then $\mathcal{X}_{\Omega_n} \overset{L^1(Y)}{\longrightarrow} \mathcal{X}_\Omega$, see [50, p 59]. Thus, the Lebesgue measure $|\Omega|$ is continuous on the set of admissible domains $\mathcal{A}_\varepsilon(Y)$ endowed with the Hausdorff metric.

On the other hand, the functional $\psi : \Omega \in \mathcal{A}_\varepsilon(Y) \longrightarrow \mathbf{P}^*(\Omega)$ is continuous by Theorem 3.3.2. Therefore, the matching set

$$\mathcal{M} = \{\Omega \in \mathcal{A}_\varepsilon(Y); \mathbf{P}^*(\Omega) = \mathbf{P}\} = \psi^{-1}(\mathbf{P})$$

is closed in $\mathcal{A}_\varepsilon(Y)$ as the inverse image of a closed set by a continuous function. Since $\mathcal{A}_\varepsilon(Y)$ is compact, $\mathcal{M}$ is compact. Thus the Lebesgue measure $|\Omega|$ has a minimum on the compact set $\mathcal{M}$ and problem (3.12) has a solution. □

3.4 Shape differentiation of the effective tensor entries

3.4.1 Shape differentiability of the state functions

We introduce a vector field $\theta : \mathbb{R}^N \to \mathbb{R}^N$ that vanishes on the boundary ∂Y of the reference cell but whose action may deform the interior surface Γ. We consider the perturbation of the identity $I + \theta$, where $\theta \in \mathbb{W}^{1,\infty}(\mathbb{R}^N, \mathbb{R}^N)$ and is close to 0 in the norm of this space, so that $I + \theta$ is a bi-Lipschitz homeomorphism. We denote by :

— $\Omega_\theta = (I + \theta)(\Omega)$, and $Y_\theta = \Omega_\theta \cup \Omega_\theta^c \cup \Gamma_\theta$

— $\boldsymbol{A}(\theta) = A((I + \theta) \circ (y))$, likewise for $\boldsymbol{D}(\theta)$ and $\boldsymbol{G}(\theta)$

— $(\chi_\theta, \pi_\theta) = (\chi_{ij\theta}, \pi_{ij\theta})$ $\Big($respectively $(w_\theta, \eta_\theta) = (w_{k\theta}, \eta_{k\theta})\Big) \in [\mathbb{H}^1_\#(Y_\theta)]^N \times \mathbb{H}^1_\#(Y_\theta)$ the solutions to the cell problem (3.1) (respectively (3.2)) in Y_θ.

— $\tilde{\varphi} = \varphi \circ (I + \theta)$, for a general function φ.

The first result states the shape differentiability of the solutions of these problems. The proof relies on the Implicit Function Theorem following the lines presented in [50, Chapter 5].

Theorem 3.4.1. *Assume Ω is open, bounded and of class C^3. Then the mappings, $\theta \mapsto (\tilde{\chi}_\theta, \tilde{\pi}_\theta)$, and $\theta \mapsto (\tilde{w}_\theta, \tilde{\eta}_\theta)$ are of class C^2 in the variational space $[\mathbb{H}^1_\#(Y)]^N \times \mathbb{H}^1_\#(Y)$.*

Before giving the proof, we need to make some simplifications concerning the form of the variational formulations of problems (3.1) and (3.2). Since both problems are similar,

consider the variational formulation of problem (3.1) for example :
Find $(\chi_{ij}, \pi_{ij}) \in [\mathbb{H}^1_{\#}(Y)]^N \times \mathbb{H}^1_{\#}(Y)$, $i, j = 1, \dots, N$ such that :

$$\begin{cases} a(\chi_{ij} + \Pi^{ij}, v) - c(v, \pi_{ij}) &= 0 \qquad \forall v \in [\mathbb{H}^1_{\#}(Y)]^N \\ c(\chi_{ij} + \Pi^{ij}, \psi) + b(\pi_{ij}, \psi) &= 0 \qquad \forall \psi \in \mathbb{H}^1_{\#}(Y). \end{cases} \tag{3.15}$$

where the bilinear forms $a(u, v), b(\phi, \psi)$ are defined in (3.13), (3.14) for all $u, v \in [\mathbb{H}^1_{\#}(Y)]^N$ and $\phi, \psi \in \mathbb{H}^1_{\#}(Y)$. The bilinear form $c(u, \psi)$ is given by

$$c(u, \psi) = \int_Y \Big(G : \varepsilon(u) \Big) : \nabla \psi. \tag{3.16}$$

Due to the symmetry assumptions on the elastic and piezoelectric tensors $\boldsymbol{A}$ and $\boldsymbol{G}$, one can easily check that the bilinear forms $a(u, v), c(u, \psi)$ rewrite as :

$$\begin{aligned} a(u, v) &= \int_Y \Big(A : \nabla u \Big) : \nabla v \\ c(u, \psi) &= \int_Y \Big(G : \nabla u \Big) : \nabla \psi \end{aligned}$$

where we replaced the symmetrized stress tensor $\varepsilon(u)$ by ∇u.

Proof of Theorem 3.4.1.
To avoid heavy notations, we drop the indexing components. The variational formulation of problem (3.1) in Y_θ can be written as :

$$\begin{aligned} &\int_Y \Big(\tilde{A}_\theta : \nabla \tilde{\chi}_\theta \Big) : \nabla v + \int_Y \Big(\tilde{D}_\theta : \nabla \tilde{\pi}_\theta \Big) : \nabla \psi + \int_Y \Big(\tilde{G}_\theta : \nabla \tilde{\chi}_\theta \Big) : \nabla \psi \\ &\quad - \int_Y \Big(\tilde{G}_\theta : \nabla v \Big) : \nabla \pi_\theta + \int_Y \Big(S^A_\theta : e_{ij}) : \nabla v + \int_Y \Big(S^G_\theta : e_{ij} \Big) : \nabla \psi = 0 \end{aligned} \tag{3.17}$$

with

$$\begin{cases} \tilde{A}_\theta &= (I + D\theta)^{-1\ T} (I + D\theta)^{-1} A(\theta)\, det(I + D\theta), \\ \tilde{D}_\theta &= (I + D\theta)^{-1\ T} (I + D\theta)^{-1} D(\theta)\, det(I + D\theta), \\ \tilde{G}_\theta &= (I + D\theta)^{-1\ T} (I + D\theta)^{-1} G(\theta)\, det(I + D\theta), \\ S^A_\theta &= {}^T(I + D\theta)^{-1} A(\theta)\, det(I + D\theta), \\ S^G_\theta &= {}^T(I + D\theta)^{-1} G(\theta)\, det(I + D\theta). \end{cases} \tag{3.18}$$

We define two operators Q_θ, S_θ from $[\mathbb{H}^1_\#(Y)]^N \times \mathbb{H}^1_\#(Y)$ to its dual $[\mathbb{H}^1_\#(Y)']^N \times \mathbb{H}^1_\#(Y)'$ by the expressions : for all (χ,π), $(v,\psi) \in [\mathbb{H}^1_\#(Y)]^N \times \mathbb{H}^1_\#(Y)$, $Q_\theta(\chi,\pi)$ is the bilinear form defined by

$$\langle Q_\theta(\chi,\pi),(v,\psi)\rangle = \int_Y \Big(\tilde{A}_\theta : \nabla\tilde{\chi}_\theta\Big) : \nabla v + \int_Y \Big(\tilde{D}_\theta : \nabla\tilde{\pi}_\theta\Big) : \nabla\psi + \int_Y \Big(\tilde{G}_\theta : \nabla\tilde{\chi}_\theta\Big) : \nabla\psi - \int_Y \Big(\tilde{G}_\theta : \nabla v\Big) : \nabla\pi_\theta;$$

and S_θ is the bilinear form defined by

$$\langle S_\theta,(v,\psi)\rangle = \int_Y \Big(S^A_\theta : e_{ij}) : \nabla v + \int_Y \Big(S^G_\theta : e_{ij}\Big) : \nabla\psi.$$

Consider now the mapping F defined as

$$\begin{array}{rccc} F: & \mathbb{W}^{1,\infty}(\mathbb{R}^N,\mathbb{R}^N) \times [\mathbb{H}^1_\#(Y)]^N \times \mathbb{H}^1_\#(Y) & \to & [\mathbb{H}^1_\#(Y)']^N \times \mathbb{H}^1_\#(Y)' \\ & (\theta,\chi,\pi) & \mapsto & Q_\theta(\chi,\pi) + S_\theta. \end{array}$$

so that the functions $(\tilde{\chi}_\theta,\tilde{\pi}_\theta)$ satisfy the relation $F(\theta,\tilde{\chi}_\theta,\tilde{\pi}_\theta) = 0$ in $[\mathbb{H}^1_\#(Y)']^N \times \mathbb{H}^1_\#(Y)'$. We shall apply the Implicit Function Theorem around $\theta = 0$.

First, we check that F is of class C^2 for θ small enough. Indeed :

— $\theta \mapsto det(I + D\theta) \in \mathbb{L}^\infty(Y)$ is of class C^∞ since $\theta \mapsto I + D\theta \in \mathbb{L}^\infty(\mathbb{R}^N,\mathcal{M}_N)$ is linear and continuous and therefore C^∞.

— The mapping $M \mapsto det(M)$ is multilinear and therefore differentiable since the dimension of $\mathcal{M}_N$ is finite.

— Similarly $\theta \mapsto (I + D\theta)^{-1} = \sum_{j\geq 0}(-1)^j(D\theta)^j \in \mathbb{L}^\infty(\mathbb{R}^N,\mathcal{M}_d)$ is also C^∞.

Since F is bilinear with respect to the arguments (χ,π), its partial derivative with respect to (χ,π) is simply

$$\Big(D_{(\chi,\pi)}F(0,\chi,\pi).(h_1,h_2)\Big)(v,\psi) = \langle Q_0(\chi,h_2) + Q_0(h_1,\pi),(v,\psi)\rangle.$$

One can check using korn and Poincaré's inequalities that there exist $\alpha > 0$ such that

$$\alpha\Big(\|\chi\|_{\mathbb{H}^1(Y)} + \|\pi\|_{\mathbb{H}^1(Y)}\Big) \leq \ell((\chi,\pi),(\chi,\pi)) = \langle Q_0(\chi,\pi),(\chi,\pi)\rangle.$$

Thus, ℓ is coercive, and by the Lax-Milgram Theorem, $D_(\chi,\pi)F(0,\chi,\pi)$ is an isomorphism. The Implicit Function Theorem can be applied and provides that there exists a

C^3 map φ on a neighborhood of 0, such that $F(\theta, \varphi(\theta)) = 0$ and $\varphi(0) = (\chi, \pi)$. This proves the C^3 regularity of $\theta \mapsto (\tilde{\chi}_\theta, \tilde{\pi}_\theta)$ and the C^2 regularity of $\theta \mapsto (\chi_\theta, \pi_\theta)$. □

Due to the advection term, the shape derivative do not exists in the usual Sobolev space since it has to jump on the interface. This difficulty emphasized in [2] has generated a rather large literature ([2, 63]). Two nice answers are now known to deal with these jumps, the differention of a min-max as introduced by Delfour and Zolesio (see [32, 19]), or the use of an adapted functional space the so called broken Sobolev spaces (see [34, 33])

Corollary 3.4.1.1. *Assume Ω is open, bounded and of class C^3. Then the mappings, $\theta \mapsto (\chi_\theta, \pi_\theta)$, and $\theta \mapsto (w_\theta, \eta_\theta)$ are of class C^2, furthermore the shape derivatives $(\chi'_\theta, \pi'_\theta)$ belong to the variational space $\mathbb{V}^N \times \mathbb{V}$ and satisfie :*

$$\begin{cases} -div\Big(\boldsymbol{\sigma}(\chi'_\theta, \pi'_\theta)\Big) & = 0 \qquad in\ \Omega \cup \Omega^c \\ -div\Big(\boldsymbol{E}(\chi'_\theta, \pi'_\theta)\Big) & = 0 \qquad in\ \Omega \cup \Omega^c \\ [\chi'_\theta] & = -(\theta \cdot n)[\partial_n \chi] \qquad on\ \Gamma \\ [\pi'_\theta] & = -(\theta \cdot n)[\partial_n \pi] \qquad on\ \Gamma \\ [\boldsymbol{\sigma}(\chi'_\theta, \pi'_\theta) : n] & = [\boldsymbol{\sigma}(\chi_\theta, \pi_\theta)] : \nabla_\Gamma(\theta \cdot n) - (\theta \cdot n)[D(\boldsymbol{\sigma}(\chi_\theta, \pi_\theta) : n) : n] \qquad on\ \Gamma \\ [\boldsymbol{E}(\chi'_\theta, \pi'_\theta) : n] & = [\boldsymbol{E}(\chi_\theta, \pi_\theta)] : \nabla_\Gamma(\theta \cdot n) - (\theta \cdot n)[D(\boldsymbol{E}(\chi_\theta, \pi_\theta) : n) : n] \qquad on\ \Gamma \end{cases} \tag{3.19}$$

where $\mathbb{V}$ is the broken Sobolev space :

$$\mathbb{V} = \Big\{ v \in \mathbb{L}^2_\#(Y);\ v_\Omega = v_{|\Omega} \in \mathbb{H}^1(\Omega)\ and\ v_c = v_{|\Omega^c} \in \mathbb{H}^1(\Omega^c) \Big\}, \tag{3.20}$$

and

$$\mathbb{L}^2_\#(Y) = \Big\{ v \in \mathbb{L}^2(Y),\ v\ is\ Y\text{-}periodic,\ \int_{W \cap Y} v dx = 0 \Big\}.$$

Proof of Corollary 3.4.1.1. Theorem 3.4.1 establishes the existence of the material derivatives $(\dot{\chi}_\theta, \dot{\pi}_\theta)$, i.e. the derivatives of the mapping $\theta \mapsto (\tilde{\chi}_\theta, \tilde{\pi}_\theta)$ in the variational space $[\mathbb{H}^1_\#(Y)]^N \times \mathbb{H}^1_\#(Y)$. The shape derivatives $(\chi'_\theta, \pi'_\theta)$,i.e. the derivatives of the mapping

$\theta \mapsto (\chi_\theta, \pi_\theta)$, are then given by

$$\chi'_\theta = \dot{\chi}_\theta - \theta \cdot \nabla \chi$$
$$\pi'_\theta = \dot{\pi}_\theta - \theta \cdot \nabla \pi.$$

— The equation satisfied inside the domain $\Omega \cup \Omega^c$ is easily obtained in the weak sense, by differentiating the weak formulation (3.15).

— Differentiating the Dirichlet jump conditions on the interface $\Gamma = \partial\Omega$ for χ, and π, we have that

$$[\chi'_\theta + \theta \cdot \nabla \chi] = 0 \Longrightarrow [\chi'_\theta] = -(\theta \cdot n)[\partial_n \chi]$$
$$[\pi'_\theta + \theta \cdot \nabla \pi] = 0 \Longrightarrow [\pi'_\theta] = -(\theta \cdot n)[\partial_n \pi]$$

One can see that the jump of the shape derivatives doesn't vanish, which means they are discontinuous across the interface Γ and thus cannot belong to $[\mathbb{H}^1_\#(Y)]^N \times \mathbb{H}^1_\#(Y)$. As a result the shape derivatives $(\chi'_\theta, \pi'_\theta)$ only exist in the variational space $\mathbb{V}^N \times \mathbb{V}$.

— Finally, differentiating the Neumann jump condition we have :

$$[\boldsymbol{\sigma}(\chi'_\theta, \pi'_\theta) : n + \boldsymbol{\sigma}(\chi, \pi) : n' + \theta.D(\boldsymbol{\sigma}(\chi_\theta, \pi_\theta) : n)] = 0,$$

The shape derivative of the normal to the boundary is given by :

$$n'_\theta = -\nabla_\Gamma(\theta \cdot n),$$

thus, we get :

$$[\boldsymbol{\sigma}(\chi'_\theta, \pi'_\theta) : n] = [\boldsymbol{\sigma}(\chi_\theta, \pi_\theta)] : \nabla_\Gamma(\theta \cdot n) - (\theta \cdot n)[D(\boldsymbol{\sigma}(\chi_\theta, \pi_\theta) : n) : n],$$

and we have a similar equation for $[\boldsymbol{E}(\chi'_\theta, \pi'_\theta)]$, which concludes the proof.

□

3.4.2 Shape sensitivity of the property tensors

In this section we compute the shape derivatives of the effective tensors entries, that we rewrite in a convenient way as

$$\begin{aligned} A^*_{ijkl}(\Omega) &= \int_Y \Big(A : \nabla\phi_{ij}\Big) : \nabla\phi_{kl} + \int_Y \Big(D : \nabla\pi_{ij}\Big) : \nabla\pi_{kl} \\ D^*_{kl}(\Omega) &= \int_Y \Big(A : \nabla w_k\Big) : \nabla w_l + \int_Y \Big(D : \nabla\varphi_k\Big) : \nabla\varphi_l \end{aligned} \tag{3.21}$$

where $\phi_{ij} = \chi_{ij} + \Pi^{ij}$, and $\varphi_k = \eta_k + \Pi^k$. We denote by $\phi'_{ij} = \chi'_{ij}$ and $\varphi'_k = \eta'_k$ the respective shape derivatives in the direction θ. Due to the shape derivatives being discontinuous across the interface, when differentiating, we want to consider these functions inside, and outside of Ω separately, so we introduce the set Θ that might designate either Ω, or Ω^c. Most importantly, recall that the variational formulations of the cell problems for all $(v, \psi) \in [\mathbb{H}^1_\#(Y)]^N \times \mathbb{H}^1_\#(Y)$ writes:

$$\begin{cases} \displaystyle\int_Y \Big(A : \nabla\phi_{ij}\Big) : \nabla v - \int_Y \Big(G : \nabla v\Big) : \nabla\pi_{ij} & = 0 \\ \displaystyle\int_Y \Big(G : \nabla\phi_{ij}\Big) : \nabla\psi + \int_Y \Big(D : \nabla\pi_{ij}\Big) : \nabla\psi & = 0 \end{cases} \tag{3.22}$$

$$\begin{cases} \displaystyle\int_Y \Big(A : \nabla w_k\Big) : \nabla v - \int_Y \Big(G : \nabla v\Big) : \nabla\varphi_k & = 0 \\ \displaystyle\int_Y \Big(G : \nabla\varphi_k\Big) : \nabla\psi + \int_Y \Big(D : \nabla\varphi_k\Big) : \nabla\psi & = 0 \end{cases} \tag{3.23}$$

We have the following theorem for the shape derivatives of the effectives tensors :

Theorem 3.4.2. *Let $k \geq 1$, and Ω an open, bounded domain of class C^k. The functions $A^*_{ijkl}(\Omega)$ and $D^*_{kl}(\Omega)$ defined by* (3.21) *are shape-differentiable with respect to Ω, and for $\theta \in \mathbb{W}^{1,\infty}(\mathbb{R}^N, \mathbb{R}^N)$, we have :*

$$\begin{aligned} A^*_{ijkl}{}'(\Omega,\theta) = &\int_\Gamma (\theta\cdot n)\Big[\Big(A : \nabla\phi_{ij}\Big) : \nabla\phi_{kl}\Big] - \int_\Gamma (\theta\cdot n)\Big[\Big(D : \nabla\pi_{ij}\Big) : \nabla\pi_{kl}\Big] \\ &- \int_\Gamma (\theta\cdot n)\Big[\Big(G : \nabla\phi_{ij}\Big) : \nabla\pi_{kl}\Big] - \int_\Gamma (\theta\cdot n)\Big[\Big(G : \nabla\phi_{kl}\Big) : \nabla\pi_{ij}\Big] \end{aligned} \tag{3.24}$$

and

$$
\begin{aligned}
D_{kl}^{*}{}'(\Omega,\theta) = &\int_{\Gamma}(\theta\cdot n)\Big[\Big(D:\nabla\varphi_k\Big):\nabla\varphi_l\Big] - \int_{\Gamma}(\theta\cdot n)\Big[\Big(A:\nabla w_k\Big):\nabla w_l\Big] \\
&- \int_{\Gamma}(\theta\cdot n)\Big[\Big(G:\nabla w_k\Big):\nabla\varphi_l\Big] - \int_{\Gamma}(\theta\cdot n)\Big[\Big(G:\nabla w_l\Big):\nabla\varphi_k\Big]
\end{aligned}
\tag{3.25}
$$

where the brackets denote the jump across the boundary Γ.

Proof.
Using Hadamard's boundary differentiation formulas we have :

$$
\begin{aligned}
A_{ijkl}^{*}{}'(\Omega) = &\int_Y \Big(A:\nabla\phi_{ij}^{'}\Big):\nabla\phi_{kl} + \int_Y \Big(A:\nabla\phi_{ij}\Big):\nabla\phi_{kl}^{'} + \int_\Gamma \operatorname{div}\Big(\Big(\Big(A:\nabla\phi_{ij}\Big):\nabla\phi_{kl}\Big)\theta\Big) \\
&+ \int_Y \Big(D:\nabla\pi_{ij}^{'}\Big):\nabla\pi_{kl} + \int_Y \Big(D:\nabla\pi_{ij}\Big):\nabla\pi_{kl}^{'} + \int_\Gamma \operatorname{div}\Big(\Big(\Big(D:\nabla\pi_{ij}\Big):\nabla\pi_{kl}\Big)\theta\Big)
\end{aligned}
\tag{3.26}
$$

since the shape derivatives ϕ'_{ij} and π'_{ij} are discontinuous across the boundary Γ, we need to make sure equation (3.26) make sense, and thus we seek to get rid of the shape derivatives by finding an equivalent formula on the boundary for these integrals.

The variational equations (3.22) are a priori only valid for functions in $[\mathbb{H}^1_{\#}(Y)]^N \times \mathbb{H}^1_{\#}(Y)$, however, due to the zero jump condition on the boundary Γ, and following the arguments in [58] one can easily check that it is valid for functions $(v,\psi) \in \mathbb{V}^N \times \mathbb{V}$, where $\mathbb{V}$ is the broken sobolev space defined earlier above. Thus, we can take $v = \phi'_{ij}, \phi'_{kl}$ and $\psi = \pi'_{ij}, \pi'_{kl}$ in equations (3.22) that we plug back into equation (3.26) to get

$$
\begin{aligned}
A_{ijkl}^{*}{}'(\Omega) = &\int_Y \Big(G:\nabla\phi_{ij}^{'}\Big):\nabla\pi_{kl} + \int_Y \Big(G:\nabla\phi_{kl}^{'}\Big):\nabla\pi_{ij} - \int_Y \Big(G:\nabla\phi_{ij}\Big):\nabla\pi_{kl}^{'} \\
&- \int_Y \Big(G:\nabla\phi_{kl}\Big):\nabla\pi_{ij}^{'} + \int_\Gamma \operatorname{div}\Big(\Big(\Big(A:\nabla\phi_{ij}\Big):\nabla\phi_{kl}\Big)\theta\Big) \\
&+ \int_\Gamma \operatorname{div}\Big(\Big(\Big(D:\nabla\pi_{ij}\Big):\nabla\pi_{kl}\Big)\theta\Big)
\end{aligned}
\tag{3.27}
$$

It is now easier to find a formula for the terms containing shape derivatives of the state functions. One has to notice that due to the symmetry of the dielectric tensor $\boldsymbol{D}$, taking $\psi = \pi_{ij}$ and $\psi = \pi_{kl}$ in (3.22) we have the following equations :

$$
\begin{cases}
\int_Y \Big(D:\nabla\pi_{ij}\Big):\nabla\pi_{kl} &= -\int_Y \Big(G:\nabla\phi_{ij}\Big):\nabla\pi_{kl} \\
\int_Y \Big(D:\nabla\pi_{ij}\Big):\nabla\pi_{kl} &= -\int_Y \Big(G:\nabla\phi_{kl}\Big):\nabla\pi_{ij},
\end{cases}
\tag{3.28}
$$

that we differentiate using Hadamard's formula and sum to get :

$$\begin{aligned}
&\int_Y \Big(G : \nabla\phi'_{ij}\Big) : \nabla\pi_{kl} + \int_Y \Big(G : \nabla\phi'_{kl}\Big) : \nabla\pi_{ij} - \int_Y \Big(G : \nabla\phi_{ij}\Big) : \nabla\pi'_{kl} - \int_Y \Big(G : \nabla\phi_{kl}\Big) : \nabla\pi'_{ij} \\
&\quad + 2\int_\Gamma \operatorname{div}\Big(\Big(\Big(D : \nabla\pi_{ij}\Big) : \nabla\pi_{kl}\Big)\theta\Big) + \int_\Gamma \operatorname{div}\Big(\Big(\Big(G : \nabla\phi_{ij}\Big) : \nabla\pi_{kl}\Big)\theta\Big) \\
&\qquad + \int_\Gamma \operatorname{div}\Big(\Big(\Big(G : \nabla\phi_{kl}\Big) : \nabla\pi_{ij}\Big)\theta\Big) = 0
\end{aligned} \tag{3.29}$$

Finally, plugging back equation (3.29) in (3.27) and applying the the divergence theorem we find the desired formula (3.24).

The proof of formula (3.25) for the shape derivative of the effective dielectrique tensor $D^*_{kl}(\Omega)$ follows the same steps where we use the symmetry of the elastic tensor A to get a similar expression to (3.28), that we differentiate to find a formula for terms containing the shape derivatives.

□

Part II

Optimal ship hulls

Chapter 4

Introduction

The earliest historical evidence of boats is found in Egypt, dating back to 4000 BCE. Historical representations (see Figure 4.1) show that the design of the ship was simply determined by its function : a fighting ship requires speed and the ability to quickly manoeuvre in any direction which resulted in a long and narrow design for warships. In contrast, trading vessels were built to carry as much goods as possible, and thus had a round design. The fact that these designs are easily identifiable on ancient artifacts

Figure 4.1 – Left: a long and narrow Vikings warship : The Gokstad [1](9^{th} century). Right: the sculpture of a round trading phoenician ship (13^{th} century BCE).

shows how slow the evolution of ship design was during this 6000 years period. Indeed, for thousands of years, ship builders relied only on experience for their designs. It was not until the mid-19^{th} century and the advent of of steam power that ship designers started to rely on theory for a more rigorous approach which resulted in what we call today the field of ship hydrodynamics.

Today, ships are no longer determined by their basic functions : war, trading or transportation, but the fact that they use different powering settings brings in the cost variable, be it financial (ultimately fuel cost), or environmental cost (greenhouse gas emissions). For example, a large modern container vessel with a capacity of 7750 container has a

1. Photo by B.C. TØrrisen.

fuel consumption of 217 tons per day, which gives a fuel bill of $3,353,952$\$ for a 28-day transport, and produces between 11 and 42 grams of CO_2 per tonne-kilometer (transport of one tonne over a distance of 1 Kilometer). To minimize the cost, a ship must be designed to both fulfill its basic function and move efficiently through the water with a minimal external force. Theoretically, this boils down to minimizing the ship's resistance R_T defined as the force required to tow the ship in calm water at constant velocity V.

Needless to say, the evolution of ship design during the last 150 years is producing better efficient ships, and industries are investing even more in research as the demand for large efficient carriers is rising due to the growth of international shipping, and recently ocean wind-farms.

Perhaps the most famous hull design for minimizing the ship's resistance is the bulbous bow, a protruding bulb at the front of the ship, just beneath the waterline. Its effect can be explained using the concept of destructive interference of waves : the wave created by the bulb will work to cancel the wave created by the bow of the ship, thereby reducing the wave resistance R_w, which is a form of drag and defined as the energy required to push the water out of the way of the hull.

Despite being optimal for minimizing the wave-making resistance, it is by no means universal for all types of ships. Indeed, adding a bulb increases the wetted surface of the ship, which increases the viscous resistance of the ship. The viscous resistance R_v is defined as the net force opposing the ship's motion due to the pressure distribution of water acting over the entire wetted surface of the hull. At low speeds, for example, the wave-making resistance is low and the viscous resistance makes up to 85% of the total ship's resistance, thus adding a bulb to minimize the wave-making resistance will increase the total ship's resistance. Intuitively, minimizing the viscous resistance ultimately comes down to minimizing the wetted area of the hull and making it as smooth as possible : a spherical design has the least wetted surface for a given volume of the hull, but it will create a lot of waves at the surface.

In the absence of revolutionary new ideas, the design of optimal ships seems to be a tradeoff between round and spherical hulls to minimize the viscous part R_v, and long, bulbous hulls to minimize the wave-making resistance R_w. Finding new ideas comes down to a better understanding of the underlying physical models used to describe the resistance of ships, and while the viscous resistance R_v is ultimately a function of the geometry of the hull and the viscosity of the water, the modeling of the wave-making resistance is more complex.

The theory of ship waves has been studied for centuries and perhaps the first mathematical discoveries date back to Sir Isaac Newton, who determined in 1687 that the ship's resistance should be a quadratic function of its velocity V. In 1871 Sir William Froude, in one of the most discoveries of naval engineering and ship design, gave a separation of the total ship's resistance R_T into viscous resistance R_v and wave resistance R_w. He also normalized the notion of a ship's velocity by introducing the Froude number, a non-dimensional measure for the velocity of a ship.

In 1898, the mathematician J.H. Michell obtained a formula for the wave making resistance in an extraordinary paper [57] that only depends on the velocity of the ship and the (supposedly thin) shape of the hull. This formula reads

$$R_{Michell}(u,\alpha) = \frac{4\rho g\alpha}{\pi}\int_1^\infty |T(u,\lambda)|^2 \frac{\lambda^2}{\sqrt{\lambda^2-1}} d\lambda$$

with

$$T(u,\alpha,\lambda) = \int_D \partial_x u(x,z) e^{-i\lambda\alpha x} e^{-\lambda^2\alpha z} dxdz.$$

Here, D is the support of the hull function u (the middle xOz half-plane of the hull), g is the standard gravity, ρ is the density of water and α is the Kelvin wave number, which is related to the ship's velocity by $\alpha = g/V^2$. Michell gave an astonish, specific example for the numerical evaluation of his formula despite the lack of computing power at the time (the first adding machine capable of direct multiplication was released 5 years earlier in 1894). unfortunately it was not enough to attract the interest of his peers in his work who deemed it impractical considering the difficulty of computing the triple integral for a general hull function u. This changed with the works of T. Havelock and C. Wigley, and perhaps the most remarkable achievement of Michell is that his formula has not been improved upon to this day (see the discussion in [74]). It provides a simple formula for determining the wave resistance of a ship without having to solve any PDE. This is only accurate on certain velocity intervals where the wave-making resistance reaches its maximum (see Figure 5.5), and for this reason itt has been receiving fewer attention from researchers. In 2016, J. Dambrine, M. Pierre and G. Rousseaux brought it back to light in a series of papers on optimal ship hulls.

— The first paper [27] uses Michell's formula to construct an optimization criterion for the total ship resistance. More precisely, for a fixed support D, a fixed velocity V, and for various approximations of Michell's kernel, they formulate the optimization problem to be solved for the optimal hull u^* minimizing the total ship resistance

among functions u of H^1 (with volume and zero constraints), they prove that the problem is well-posed and obtain the global $\mathbb{W}^{2,p}$ regularity of u^*. The authors provide interesting numerical results that are very close to real life application. In particular, the famous bulbous bow was obtained for moderate Froude numbers, which is indeed the range where the wave-making resistance reaches its maximum and is interesting to have a bulbous bow.

— The second paper [26] deals with the shape optimization of the support of the hull D, for the true Michell's kernel. i.e. the optimality variable is the domain D, and for a fixed velocity V, the authors formulate the shape optimization problem to solve for an optimal domain D^*, on which an optimal hull u^* is computed. The authors prove the existence of an optimal domain and the Hölder regularity of the optimal hull u^*. Numerical examples are given where the authors reproduce the bulbous bow on an optimal domain D^* which leads to a further decrease of the total ship resistance than the previous case of a fixed support.

— The last paper [25] adresses the dependency of the optimal hull on the speed V. The authors proove that the optimal hulls are continuously dependent on the velocity V, they show by means of Γ-convergence (see [17]) that the contribution of Michell's wave resistance vanishes for high Froude numbers. The authors provide a numerical study of the optimal hulls on various velocity intervals showing different profiles of the hulls.

In spite of the limitations of Michell's formula for the wave resistance, it remains a powerful tool for theoretical and numerical purposes. The regularity and continuity results obtained for Michell's resistance are out of reach when considering the full 3D incompressible Navier-Stokes equations, and the numerical approach proposed in the works of J. Dambrine, M. Pierre and G. Rousseaux are much faster than CFD algorithms (computational fluid dynamics). It is clear the next step in studying Michell's wave resistance is to consider varying speeds, the continuous dependency result in [26] indicates that on a given range of speed, a slight change in the shape of the hull can have big changes in the computed total ship resistance. Thus, the question of finding robust optimal hulls, that are optimal for a given speed range arises naturally.

The first interest of this part is to the robust optimal design of ship hulls with respect to the velocity. A natural way of dealing with this is to look for hulls that are optimal on average on a given speed range. Mathematically, if we assume that the Kelvin wave number is a random variable $\nu : \Omega \mapsto \mathbb{R}$ on a complete probability space $(\Omega, \mathcal{A}, \mathbb{P})$ with

a probability distribution $\mathbb{P}_\nu$, we look for optimal hulls that minimize the expectation of the total ship's resistance which is given by the functional

$$\begin{aligned}\mathcal{J}(u) &= \mathbb{E}\Big[R_{total}(u,\nu)\Big] \\ &= \mathbb{E}\Big[R_v(u,\nu) + R_{Michell}(u,\nu)\Big].\end{aligned}$$

We start by searching optimal hulls which minimize the expectation on a fixed domain (support of the hull): this is studied in chapter 7. We give an existence result for an optimal hull minimizing the expectation of the total resistance, and a regularity result for the expectation of Michell's kernel $H\nu$ which belongs to $\mathbb{L}^q(D\times D)$ for all $1 \leq q < \frac{5}{4}$, This kernel consists of a quadruple integral (2 for the domain, 1 for the wave contributions, and one for the speed range) and is computationally heavy to approximate. Numerical results are given to compute these optimal hulls u_D^* on different fixed supports for a given speed range, and to compare it to other hulls, namely a standard type of hulls called a Wigley hull, and an optimal hull $\bar{u}_D$ computed for a specific fixed speed V chosen as the average speed on our speed range. Numerical results show that the optimal hulls for minimizing the expectation will perform better on most of the speed range, despite the global computed expectation for u_D^* and $\bar{u}_D$ being close.

Chapter 9 is then dedicated to the case of a variable domain. We search the optimal support of an optimal hull which minimizes the expectation of the total resistance. An existence result for an optimal domain contained in a bounding box is given. Note that without bounding box, an optimal domain does not always exist, this is demonstrated by [25, Theorem 3.5] and by numerical results where steepest descent algorithms are unable to converge for area Froude numbers $Fr_a \in [1,2]$.

We then compute these optimal domains for different Froude number intervals and with two different descent algorithms : an Augmented Lagrangian algorithm, which is a fast first order descent method, and Newton's method which is a second order descent algorithm and the second main contribution of this work. Recall that the expectation of the total resistance is computed by numerical integration of a kernel that is very expensive to compute leading to a quadruple integral, and keep in mind that a first order descent algorithm for shape optimization takes on average between 100 and 200 iterations to converge. This makes it very costly to produce numerical results for multiple speed intervals and different probability intervals. For this reason, we were forced to limit ourselves to a uniform distribution of the speeds and distributions that are a function of a

uniform law, but if one wants to integrate numerically a random probability distribution through Monte-Carlo methods for example, then the global computation time can be estimated in weeks. The use of a first order method poses an issue, since :

— Usually, first order methods employ a line search, and this might end-up increasing the computation time in the stochastic case. We thus need an algorithm with a constant descent step t, and Newton's method allows to converge with a constant step $t = 1$ (if one is not too far from a critical shape).

— The preservation of the constraint is another issue, first order algorithms are known to oscillate when handling constraints since the descent direction for the objective to be minimized does not necessarily lie in the same direction of the constraint. This can be problematic for our applications since we are working with the area Froude number as a non-dimensional measure for the speed of the ship, thus the descent algorithm must preserve the area constraint along the optimization process, and this is better handled by second order methods.

To our knowledge, Newton's method for shape optimization has been first implemented by Novruzi and Roche in [61]. Since then Harbrecht is perhaps the most published mathematician on the matter [44, 35, 45], and recently this was studied extensively by Vie in [77]. All of the resulting literature agrees that despite its challenging difficulty, Newton's method provides faster and more accurate convergence results. Here we attempt to alleviate this difficulty. Our main contribution is a new discretization of Newton's method based on normal deformation vectors, this results in a diagonal Hessian matrix that is easy to build and invert and most importantly, does not require to solve any problem for the shape derivatives of the state function or adjoint problems. Our discretization is derived and tested in chapter 8. The rate of convergence has been tested through a theoretical result for a purely geometric functional and is indeed quadratic. We then test the algorithm for both geometric and PDE-dependent functional and we compare it to the Augmented Lagrangian algorithm for the shape optimization of the total resistance. The results show that Newton's algorithm is faster, stable after convergence and provides a better preservation of the constraint throughout the optimization process.

Chapter 5

Michell's wave resistance formula

5.1 The formula

The total resistance of water to the motion of a ship is the force required to tow the ship in calm water a constant velocity. A traditional and simplified approach (see, e.g., [14]) uses the decomposition

$$R_{total} = R_{wave} + R_{viscous}. \tag{5.1.1}$$

The wave resistance reflects the energy to push the water out of the way of the hull. This energy goes into creating the wave.

In 1898, Michell [57] gave a formula for the wave resistance, valid for any shape of the hull (and for a constant speed and in an infinite domain). Experiments starting with Wigley in the 1920's showed a reasonable good agreement between theory and experiment (see the review by Gotman [42] and references therein).

Consider a ship moving with constant velocity U on the surface of an unbounded fluid. We assume that the coordinates xyz are fixed to the ship: the xy-plane is the water surface and z is vertically **downward**. The immerged half hull surface is represented by a continuous nonnegative function (see Figure 5.1)

$$y = f(x, z) \geq 0, \quad (x, z) \in \overline{D}.$$

The set $\overline{D}$ on which f is defined is split into three parts: its interior D (an open subset of the upper half-plane with a Lipschitz boundary), in which $f(x, z) > 0$, its boundary Γ_N at the surface $z = 0$ and its boundary Γ_0 under the surface, on which $f(x, z) = 0$ (see Figure 5.2).

It is assumed that the fluid is incompressible, inviscid and that the flow is irrotational. The motion has lasted long enough so that a steady state has been reached.

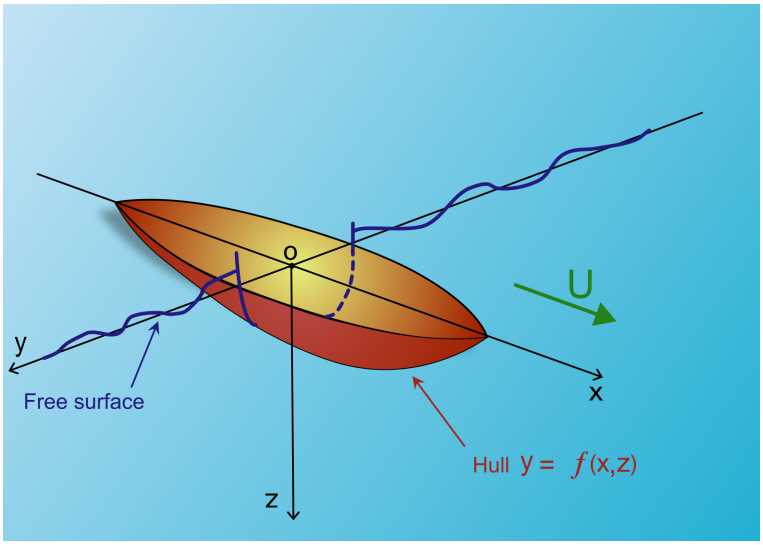

Figure 5.1 – The immerged hull: half of it is represented by a positive function $y = f(x, z)$. The other half hull is obtained by symmetry.

Michell's formula [57] reads

$$R_{Michell} = \frac{4\rho g^2}{\pi U^2} \int_1^\infty (I_1(\lambda)^2 + I_2(\lambda)^2) \frac{\lambda^2}{\sqrt{\lambda^2 - 1}} d\lambda, \tag{5.1.2}$$

with

$$I_1(\lambda) = \int_D \frac{\partial f(x,z)}{\partial x} \exp\left(-\frac{\lambda^2 g z}{U^2}\right) \cos\left(\frac{\lambda g x}{U^2}\right) dxdz, \tag{5.1.3}$$

$$I_2(\lambda) = \int_D \frac{\partial f(x,z)}{\partial x} \exp\left(-\frac{\lambda^2 g z}{U^2}\right) \sin\left(\frac{\lambda g x}{U^2}\right) dxdz. \tag{5.1.4}$$

In this formula, U (in $\mathrm{m} \cdot \mathrm{s}^{-1}$) is the speed of the ship, ρ (in $\mathrm{kg} \cdot \mathrm{m}^{-3}$) is the (constant) density of the fluid and g (in $\mathrm{m} \cdot \mathrm{s}^{-2}$) is the standard gravity. The variables x, z and $f(x, z)$ are expressed in meters. Consequently, the integrals $I_1(\lambda)$ and $I_2(\lambda)$ are in m^2 and $R_{Michell}$ (in Newton) has the dimension of a force.

The integration parameter λ has no dimension: it can be interpreted as $\lambda = 1/\cos\theta$, where θ is the angle between the ship's path and the direction of wave propagation [14, p. 310], [75]. For $\theta = 0$ ($\lambda = 1$), waves follow the ship with their crests aligned perpendicular to the ship's course (transverse waves) and for $\theta = \pm\pi/2$ ($\lambda = +\infty$), waves have crests parallel to the ship's path.

We stress that Michell's approach is a linear theory in which the ship is assumed to be "thin", which means that the angles made by the hull surface with the longitudinal

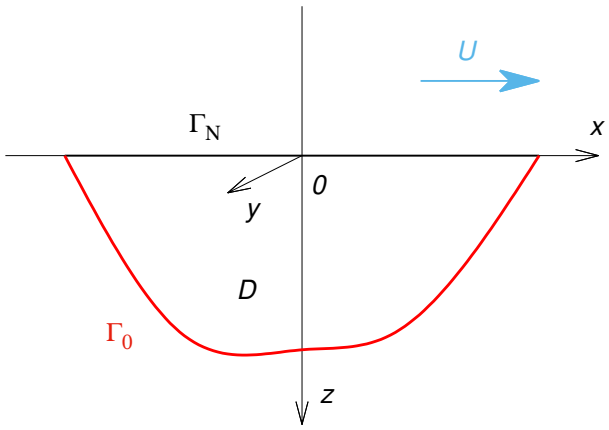

Figure 5.2 – The domain of parameters (x, z)

plane of symmetry are small, i.e.

$$0 \leq f \ll 1, \quad \left|\frac{\partial f}{\partial x}\right| \ll 1 \quad \text{and} \quad \left|\frac{\partial f}{\partial x}\right| \ll 1 \quad \text{in } D. \tag{5.1.5}$$

In our approach, we do not assume the conditions (5.1.5) *a priori*, but we will recover them partly by penalizing these constraints thanks to the viscous resistance.

5.2 The example of a Wigley hull

For a Wigley hull with length L, draft T and beam B, the domain of definition of the hull function is $D = (-L/2, L/2) \times (0, T)$ (see Figure 5.3) and the half hull function reads

$$f(x, z) = (B/2)S(z)(1 - 4x^2/L^2)$$

with

$$S(z) = \begin{cases} 1 - (z/T)^2 & \text{(parabolic cross section)}, \\ 1 - z/T & \text{(triangular cross section)}, \\ 1 & \text{(rectangular cross section)}. \end{cases}$$

The three different Wigley hulls are represented in Figure 5.4. The condition $f = 0$ is satisfied on Γ_0 for the parabolic and for the triangular cross sections, but not for the rectangular one.

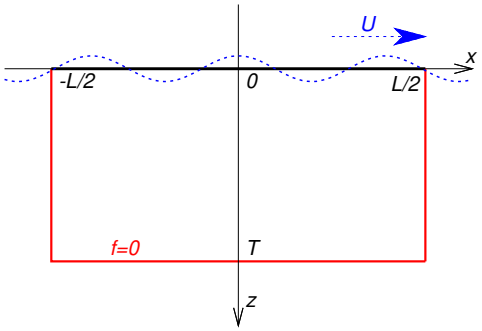

Figure 5.3 – The rectangular domain of parameters (x, z) of a Wigley hull

Wigley hulls are historically important because it is possible to compute exactly the integrals $\mathcal{I}$ and $\mathcal{J}$ in (5.1.3)-(5.1.4), so that only the integral with respect to λ in (5.1.2) remains to be computed by numerical integration. Typical values for a Wigley hull are $L/B = 10$ and $T/B = 1.5$ (see, e.g., [42] ad [51, p. 308]).

Figure 5.5 shows in dashed line the wave resistance coefficient obtained by Michell's formula for a parabolic Wigley model and for various Froude numbers. The (length) Froude number is a dimensionless speed defined by

$$Fr_L = \frac{U}{\sqrt{gL}}$$

and the wave coefficient is a normalized version of the wave resistance; it has no dimension and it is defined by

$$C_W = \frac{2}{\rho U^2 |D|} R_{Michell},$$

where $|D|$ is the area of D ($|D| = TL$ for a Wigely hull) and $R_{Michell}$ is computed by (5.1.2). The curve of C_W has humps and hollows, which is a well-known yet surprising consequence of Michell's formula [42]. Figure 5.5 also shows in solid line the range of experimental data obtained for the same parabolic Wigley hull in different towing tanks. The theoretical and experimental date are in good agreement, although it is difficult to obtain experimentally the wave resistance because an experiment provides the total resistance in formula (5.1.1).

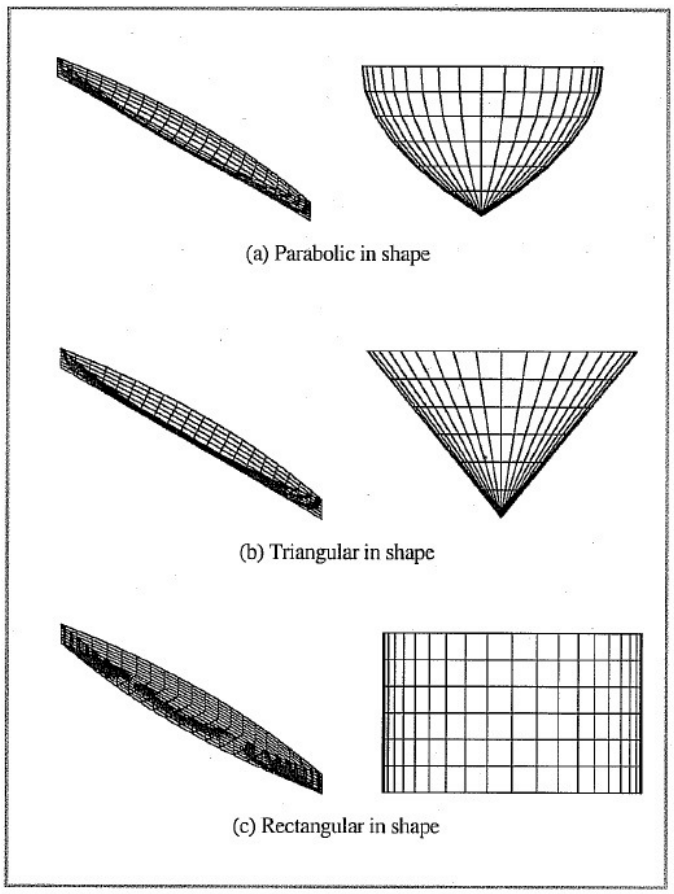

Figure 5.4 – Wigley hulls with different cross sections [73]

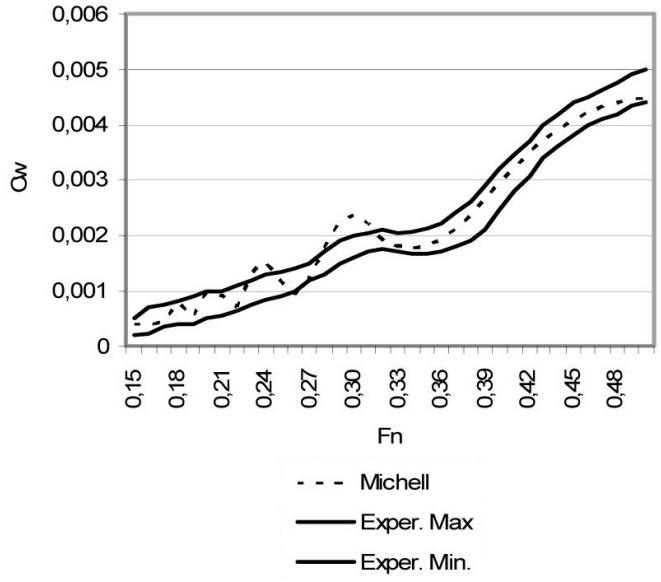

Figure 5.5 – A comparison between Michell's coefficient of wave resistance and experimental data of the parabolic Wigley model [10]

Chapter 6

THE FORMAL OPTIMAL DESIGN PROBLEM

6.1 The viscous resistance and the total resistance

In formula (5.1.1), a traditionnal approach is to express the viscous resistance as (see, e.g., [14])

$$R_{viscous} = \frac{1}{2}\,\rho U^2\, C_F\, A\,. \tag{6.1.1}$$

The viscous resistance $R_{viscous}$ accounts for the effects of viscosity which are not present in Michell's model. In (6.1.1), C_F is the viscous drag (or friction) dimensionless coefficient and A (in m^2) is the surface area of the ship's wetted hull. The coefficient C_F is a positive constant. It is sometimes seen as a positive function which depends continuously on U. For instance, the ITTC 1957 model-ship correlation line formula reads [14, Equation (2.18)]

$$C_F = 0.075/[\log_{10}(Re) - 2]^2, \tag{6.1.2}$$

where $Re = UL_{ref}/\nu_{vis}$ is the Reynolds number (L_{ref} is a reference length and ν_{vis} is the kinematic viscosity of water).

Since the graph of f represents the ship's half-hull, A is given by:

$$A = 2\int_D \sqrt{1 + |\nabla f(x,z)|^2}\, dxdz. \tag{6.1.3}$$

For a thin ship, $|\nabla f|$ is uniformly small (see (5.1.5)), and the integral above can be approximated by performing a Taylor expansion of $\sqrt{1+|\nabla f|^2}$ at first order:

$$A = 2\int_D 1 dxdz + \int_D |\nabla f(x,z)|^2\, dxdz + o(||\nabla f||_\infty^2)\,. \tag{6.1.4}$$

A good approximation of the viscous drag for small ∇f reads

$$R_{viscous} = \frac{1}{2}\rho U^2\, C_F\, \left(2|D| + \int_D |\nabla f(x,z)|^2\, dxdz\right)\,, \tag{6.1.5}$$

where $|D|$ is the area of D.

Summing up, the total resistance for a ship hull defined by f reads

$$R_{total} = R_{Michell} + R_{viscous}, \tag{6.1.6}$$

where $R_{Michell}$ is defined by (5.1.2)-(5.1.4) and $R_{viscous}$ is defined by (6.1.5). In this formula, the cruising speed of the ship, U, is constant.

6.2 The formal optimal design problems

The variables g and ρ are known physical constants and we assume for simplicity that the viscous drag coefficient C_F is a given constant. Then the total resistance defined by (6.1.6), (5.1.2) and (6.1.5) depends only on the function $f : \overline{D} \to \mathbb{R}$ and on the speed U, so we write $R_{total}(f, U)$. The half volume of the hull (a positive real number) is given and it is denoted $\mathcal{V}$.

6.2.1 Robust optimization of the hull for a given domain

In [27], we solved the following convex problem by using an appropriate H^1 functional setting:

$$\begin{cases} \text{Find the function } f_D \text{ which minimizes } R_{total}(f, U) \text{ in the set} \\ \left\{ f : \overline{D} \to \mathbb{R},\ f = 0 \text{ on } \Gamma_0,\ f \geq 0 \text{ in } D \text{ and } \int_D f(x,z)dxdz = \mathcal{V} \right\}. \end{cases} \tag{6.2.1}$$

The solution to this problem may be very sensitive to variations of U. In order to have a more robust problem, we assume here that U is a random function with realizations denoted by U_ω and we consider the problem :

$$\begin{cases} \text{Find the function } f_D^\star \text{ which minimizes } \mathbb{E}(R_{total}(f, U)) \text{ in the set} \\ \left\{ f : \overline{D} \to \mathbb{R},\ f = 0 \text{ on } \Gamma_0,\ f \geq 0 \text{ in } D \text{ and } \int_D f(x,z)dxdz = \mathcal{V} \right\}. \end{cases} \tag{6.2.2}$$

It will be interesting to compare $R_{total}(f_D, \mathbb{E}(U))$ with $\mathbb{E}(R_{total}(f, U))$.

More generally, the cost function $R_{total}(f, U)$ can be replaced by

$$J(f, U) = h(U) \times R_{total}(f, U)$$

where $h : (0, +\infty) \to (0, +\infty)$ is a continuous function of U. For instance, we may choose:

— $h(U) = U$, in which case $J(f, U)$ is an energy;

— $h(U) = 1$, in which case $J(f, U)$ is the resistance;

— $h(U) = 1/(\rho c_F U^2)$, in which case $J(f, U)$ is a normalized resistance.

6.2.2 Robust optimization of the domain and of the hull

Next, we consider the domain D as a variable of the problem. The total resistance is written $R_{total}(D, f_D, U)$ where for a given domain D, f_D is the solution to problem (6.2.1). The cost function is $h(U)R_{total}(D, f_D, U)$ where h is chosen as previously (h is a positive continuous function of U). We fix an area $a > 0$.

In [26, 25], we studied the following shape optimization problem: for a given constant speed U,

$$\begin{cases} \text{Find a set } D^\star \text{ which minimizes } R_{total}(D, f_D, U) \\ \text{among all regular open subsets } D \text{ of the lower half-plane} \\ \text{such that } |D| = a. \end{cases} \tag{6.2.3}$$

Here and below, $|D|$ is the area of the domain D. Since U is fixed, $h(U)$ is fixed as well and we may use the cost function $h(U)R_{total}(D, f_D, U)$ in the problem above without changing its solution(s).

Now we assume again that U is a random function and we are interested in the more robust problem:

$$\begin{cases} \text{Find a set } D^\star \text{ which minimizes } \mathbb{E}\left[h(U)R_{total}(D, f_D, U)\right] \\ \text{among all regular open subsets } D \text{ of the lower half-plane} \\ \text{such that } |D| = a. \end{cases} \tag{6.2.4}$$

Chapter 7

Robust optimal hull for a fixed domain

7.1 Functional setting

Let D be a bounded and connected open subset of the upper half plane $\{(x,z) \in \mathbb{R}^2 \ : \ z>0\}$. We assume that D has a Lipschitz boundary ∂D. For sake of simplicity, we also assume throughout section 7 that the part of ∂D which intersects the x-axis, namely $\partial D \cap (\mathbb{R}\times\{0\})$, is a segment of the x-axis (possibly empty). We denote Γ_N the relative interior of this segment and $\Gamma_0 = \partial D \setminus \Gamma_N$.

We work with the Sobolev space

$$H(D) = \left\{ u \in H^1(D) \ : \ u = 0 \text{ on } \Gamma_0 \text{ in the sense of traces} \right\}.$$

Let $u \in H(D)$ (u is the hull function) and $V>0$ (V is the speed of the ship). For Michell's wave resistance, we set

$$\alpha = \frac{g}{V^2} \tag{7.1.1}$$

and (5.1.2) becomes

$$R_{Michell}(u,\alpha) = \frac{4\rho g\alpha}{\pi} \int_1^\infty |S_u(\lambda)|^2 \frac{\lambda^2}{\sqrt{\lambda^2-1}} d\lambda,$$

with (cf. (5.1.3)-(5.1.4))

$$S_u(\lambda,u,\alpha) = \int_D \frac{\partial u}{\partial x}(x,z) e^{-i\lambda\alpha x} e^{-\lambda^2\alpha z} dxdz.$$

The number α is known as the *Kelvin wave number*. The value $1/\alpha$ (in m) is the typical wavelength of the transverse waves. Transverse waves follow the ship with their crests and troughs aligned perpendicular to the ship's course and the wavelength is the distance

between two successive crests. Since the speed V of the ship can be recovered from α through $V = \sqrt{g/\alpha}$, knowing α is equivalent to knowing V. We will use the variable α because it is more convenient.

Integrating S_u by parts with respect to x and taking advantage of the boundary condition $u = 0$ on $\partial\Omega$, we find that

$$R_{Michell}(u,\alpha) = \frac{4\rho g\alpha^3}{\pi}\int_1^\infty |T(u,\alpha,\lambda)|^2 \frac{\lambda^4}{\sqrt{\lambda^2-1}} d\lambda, \tag{7.1.2}$$

where, for all $\lambda > 0$,

$$T(u,\alpha,\lambda) = \int_D u(x,z) e^{-i\lambda\alpha x} e^{-\lambda^2\alpha z} dxdz.$$

The viscous resistance (6.1.5) reads

$$R_{viscous}(u,\alpha) = \frac{\rho g}{2\alpha} C_F \left(2|D| + \int_D |\nabla u(x,z)|^2 \, dxdz\right).$$

The total resistance is

$$R_{total}(u,\alpha) = R_{viscous}(u,\alpha) + R_{Michell}(u,\alpha). \tag{7.1.3}$$

We assume that the Kelvin wave number is a random variable $\nu : \Omega \to \mathbb{R}$ on a complete probability space $(\Omega, \mathcal{A}, \mathbb{P})$. Moreover, we assume that the probability distribution $\mathbb{P}_\nu$ of ν is a measure which has a compact support in $(0, +\infty)$. We recall that the probability distribution of ν is defined for every Lebesgue-measurable set $B \subset \mathbb{R}$ by

$$\mathbb{P}_\nu(B) = \mathbb{P}(\nu \in B) = \mathbb{P}\left(\{w \in \Omega \ : \ \nu(\omega) \in B\}\right).$$

Concerning the Kelvin wave number, ν denotes the random variable, whereas α is a positive real number.

We recall that if $X : \Omega \to \mathbb{R}$ is a random variable which is square integrable with respect to $\mathbb{P}$, its expectation is defined by

$$\mathbb{E}(X) = \int_\Omega X(\omega) d\mathbb{P}(\omega),$$

and its variance by

$$\mathbb{V}(X) = \mathbb{E}\Big[(X - \mathbb{E}(X))^2\Big] = \mathbb{E}(X^2) - \mathbb{E}(X)^2.$$

If $\varphi : (0, +\infty) \to \mathbb{R}$ is a continuous function, then $\varphi(\nu) : \Omega \to \mathbb{R}$ is a random variable and we have the well-known formula,

$$\mathbb{E}[\varphi(\nu)] = \int_\Omega \varphi(\nu(\omega)) d\mathbb{P}(\omega) = \int_{\mathbb{R}} \varphi(s) d\mathbb{P}_\nu(s).$$

In view of (7.1.3), we consider the cost function

$$\mathcal{J}_D(u) = \mathbb{E}\left[h_{\rho,g,C_F}(\nu)\Big(R_{viscous}(u,\nu) + R_{Michell}(u,\nu)\Big)\right], \tag{7.1.4}$$

where $h_{\rho,g,C_F} : (0, +\infty) \to (0, +\infty)$ is a continuous function which may depend on the physical constants ρ, g and on the viscous coefficient C_F. We note that it could be interesting to consider C_F as a random variable as well (possibly dependent on α, as in (6.1.2)), but we assume for simplicity that C_F is constant.

Following [25], we introduce the normalized viscous resistance functional

$$J_0(u) = \int_D |\nabla u|^2 dxdz$$

and the normalized wave resistance functional

$$J_{wave}(u,\alpha) = \frac{8\alpha^4}{\pi} \int_1^\infty |T(u,\alpha,\lambda)|^2 \frac{\lambda^4}{\sqrt{\lambda^2 - 1}} d\lambda, \tag{7.1.5}$$

where T is defined as previously for all $u \in H(D)$, $\alpha > 0$ and $\lambda > 0$ by

$$T(u,\alpha,\lambda) = \int_D u(x,z) e^{-i\lambda\alpha x} e^{-\lambda^2 \alpha z} dxdz. \tag{7.1.6}$$

The cost function (7.1.4) reads

$$\mathcal{J}_D(u) = \mathbb{E}\left[h_{\rho,g,C_F}(\nu) \frac{\rho g}{2\nu} C_F \left(2|D| + J_0(u) + \frac{1}{C_F} J_{wave}(u,\nu)\right)\right].$$

By setting

$$\tilde{h}(\alpha) = h_{\rho,g,C_F}(\alpha) \frac{\rho g}{2\alpha} C_F, \tag{7.1.7}$$

we have

$$\mathcal{J}_D(u) = \mathbb{E}\left[\tilde{h}(\nu)\left(2|D| + J_0(u) + \frac{1}{C_F}J_{wave}(u,\nu)\right)\right]. \tag{7.1.8}$$

We note that $\tilde{h}$ generally depends on the fixed parameters ρ, g and C_F.

Let us $\mathcal{V} > 0$ denote the half-volume of the hull. We consider the set

$$H_{\mathcal{V}}(D) = \left\{u \in H(D) \ : \ \int_D u\,dxdz = \mathcal{V}\right\},$$

which is a closed affine subspace of $H(D)$. Our robust optimization problem reads:

$$\text{Find } u_D^\star \in H_{\mathcal{V}}(D) \text{ such that } \mathcal{J}_D(u_D^\star) = \min\left\{\mathcal{J}_D(u) \ : \ u \in H_{\mathcal{V}}(D)\right\}. \tag{7.1.9}$$

In (7.1.9), the set D is given and the positive parameters ρ, g, C_F and $\mathcal{V}$ are fixed.

7.2 Theoretical results

The following result will prove useful.

Lemma 7.2.1. *Let $q \in (1,+\infty)$ and let $q' = q/(q-1) \in (1,+\infty)$ denote the conjugate exponent of q. Assume that $H \in L^q(D\times D)$. Then for all $u, v \in L^{q'}(D)$, we have*

$$\int_{D\times D} |H(x,z,x',z')u(x,z)v(x',z')|dxdzdx'dz' \leq \|H\|_{L^q(D\times D)}\|u\|_{L^{q'}(D)}\|v\|_{L^{q'}(D)}. \tag{7.2.1}$$

Moreover, for each $u \in L^{q'}(D)$, the function

$$(x,z) \mapsto \int_D H(x,z,x',z')u(x',z')dx'dz' \tag{7.2.2}$$

belongs to $L^q(D)$.

Proof. Estimate (7.2.1) is a consequence of Hölder's inequality. The claim on the function (7.2.2) follows from (7.2.1), Fubini's theorem and a duality argument. □

By formally switching the integrals in the expression (7.1.5)-(7.1.6), we see that Michell's normalized wave resistance can be written

$$J_{wave}(u,\alpha) = \int_{D\times D} k_\alpha(x,z,x',z')u(x,z)u(x',z')dxdzdx'dz' \tag{7.2.3}$$

where

$$k_\alpha(x,z,x',z') = \frac{8\alpha^4}{\pi} K(\alpha(x-x'),\alpha(z+z')) \tag{7.2.4}$$

and

$$K(X,Z) = \int_1^\infty e^{-\lambda^2 Z}\cos(\lambda X)\frac{\lambda^4}{\sqrt{\lambda^2-1}}d\lambda. \tag{7.2.5}$$

This formal calculation was rigorously proved in [26, Appendix A]. It was shown that Michell's kernel belongs to $L^{5/4-\epsilon}(D\times D)$ and that this estimate is optimal if D contains a half-disk centered on the x-axis.

The results from [26, Appendix A] are summarized in the proposition below. We first note that K is defined and continuous on $\mathbb{R}\times(0,+\infty)$, thanks to the exponential term, so that k_α is continuous on $(\mathbb{R}\times(0,+\infty))^2$.

Proposition 7.2.1. *Let $\alpha > 0$. Michell's normalized wave resistance kernel k_α (7.2.4) belongs to $L^q(D\times D)$ for all $1 \le q < 5/4$. For each $q' > 5$ and for each $u \in L^{q'}(D)$, the formulations for $J_{wave}(u)$ given by (7.1.5)-(7.1.6) and (7.2.3)-(7.2.4)-(7.2.5) are equal.*

Let $q \in (1,5/4)$ and let $q' = q/(q-1) \in (5,+\infty)$ be the conjugate exponent of q. Since $H^1(D)$ is continuously imbedded in $L^{q'}(D)$ for all $q' \in [1+\infty)$ [1], Proposition 7.2.1 and Lemma 7.2.1 show that for all $u \in H(D)$, $J_{wave}(u) < +\infty$.

The following result is proved in [25, Lemma 5.2 (ii)].

Lemma 7.2.2. *For each $u \in H(D)$, the map*

$$\alpha \mapsto J_{wave}(u,\alpha)$$

is continuous on $(0,+\infty)$.

Recall that $\mathbb{P}_\nu$ has a compact support in $(0,+\infty)$, so we may assume that its support is included in $[\nu_{min},\nu_{max}]$ with $0 < \nu_{min} \le \nu_{max} < +\infty$. We define the kernel

$$H_\nu(x,z,x',z') = \int_{\nu_{min}}^{\nu_{max}} \tilde{h}(s)k_s(x,z,x',z')d\mathbb{P}_\nu(s),$$

which has finite values for all $(x,z,x',z') \in D\times D$ (since $z+z' > 0$).

Proposition 7.2.2. *The kernel H_ν belongs to $L^q(D\times D)$ for all $1 \le q < 5/4$ and for all $u \in H(D)$, we have*

$$\mathbb{E}\left[\tilde{h}(\nu)J_{wave}(u,\nu)\right] = \int_{D\times D} H_\nu(x,z,x',z')u(x,z)u(x',z')dxdzdx'dz'. \tag{7.2.6}$$

Proof. We choose $q \in (1, 5/4)$ and we denote $q' \in (5, +\infty)$ the conjugate exponent of q. Since the function $t \mapsto t^{q'}$ is convex on $[0, +\infty)$, by Jensen's inequality, we have

$$|H_\nu(x, z, x', z')|^{q'} \leq \int_{\nu_{min}}^{\nu_{max}} \tilde{h}^{q'}(s)|k_s(x, z, x', z')|^{q'} d\mathbb{P}_\nu(s).$$

Thus, by (7.2.4) and Fubini's theorem,

$$\begin{aligned}\int_{D\times D} |H_\nu(x, z, x', z')|^{q'} \, dxdzdx'dz' \\ \leq \int_{\nu_{min}}^{\nu_{max}} \int_{D\times D} \hat{h}(s)|K(s(x - x'), s(z + z'))|^{q'} dxdzdx'dz' d\mathbb{P}_\nu(s),\end{aligned}$$

where $\hat{h} : (0, +\infty) \to (0, +\infty)$ is a continuous function, namely

$$\hat{h}(s) = \tilde{h}^{q'}(s) \left(\frac{8s^4}{\pi}\right)^{q'}.$$

We perform the change of variable $(\tilde{x}, \tilde{z}, \tilde{x}', \tilde{z}') = (sx, sz, sx', sz')$ and we find

$$\begin{aligned}\int_{D\times D} |H_\nu(x, z, x', z')|^{q'} \, dxdzdx'dz' \\ \leq \int_{D\times D} |K(x - x', z + z')|^{q'} dxdzdx'dz' \int_{\nu_{min}}^{\nu_{max}} \frac{1}{s^4} \hat{h}(s) d\mathbb{P}_\nu(s),\end{aligned}$$

In the right handside above, the first integral is finite thanks to Proposition 7.2.1. The second integral is finite since $[\nu_{min}, \nu_{max}]$ is compactly embedded in $(0, +\infty)$. This proves that H_ν belongs to $L^{q'}(D \times D)$. For the computation of

$$\mathbb{E}\left[\tilde{h}(\nu) J_{wave}(u, \nu)\right],$$

we use the expression (7.2.3). The estimates above combined with Hölder's inequality (as in (7.2.1)) show that we may apply Fubini's theorem. This yields (7.2.6). □

We are in position to prove:

Theorem 7.2.1. *Problem* (7.1.9) *has a unique solution* $u_D^\star$ *which is also the unique*

solution of the boundary value problem

$$\begin{cases} -\Delta u(x,z) + \dfrac{1}{C_F \mathbb{E}\left[\tilde{h}(\nu)\right]} \int_{D\times D} H_\nu(x,z,x',z') u(x',z') dx'dz' = C, \quad \forall (x,z) \in D, \\ \int_D u \, dxdz = \mathcal{V}, \\ u = 0 \ \textit{on} \ \Gamma_0, \\ \dfrac{\partial u}{\partial n} = 0 \ \textit{on} \ \Gamma_N. \end{cases} \tag{7.2.7}$$

Proof. The functional T defined by (7.1.6) depends linearly on its first argument u, so that for each $\alpha > 0$, $u \mapsto J_{wave}(u,\alpha)$ is a quadratic and convex functional on $H(D)$. Thus, $u \mapsto \mathbb{E}(\tilde{h}(\nu) J_{wave}(u,\nu))$ defined by (7.1.5) is convex on $H(D)$. On the other hand, the function J_0 is stricly convex on $H(D)$, thanks to the homogeneous Dirichlet boundary condition on Γ_0 and the Poincaré inequality. Thus, $\mathcal{J}_D$ is stricly convex on $H(D)$ and since $H_\mathcal{V}(D)$ is an affine subspace of $H(D)$, problem (7.1.9) has a most one solution in $H_\mathcal{V}(D)$.

Let (u_n) be a minimizing sequence for problem (7.1.9) in $H_\mathcal{V}(D)$. We have

$$\mathcal{J}_D(u_n) = \mathbb{E}\left[\tilde{h}(\nu) 2|D|\right] + \mathbb{E}\left[\tilde{h}(\nu)\right] J_0(u_n) + \frac{1}{C_F} \mathbb{E}\left[\tilde{h}(\nu) J_{wave}(u_n,\nu)\right].$$

Each one of the three terms in the right hand-side is nonnegative so $\mathcal{J}_D(u_n)$ is nonnegative and the sequence (u_n) is bounded in $H^1(D)$ (thanks to the term $J_0(u_n)$ and the Poincaré inequality). Up to a subsequence, (u_n) converges weakly in $H^1(D)$ to some $u_D^\star$, which belongs to $H_\mathcal{V}(D)$ since the latter is a closed convex subset of $H^1(D)$. By lower semi-continuity of J_0,

$$J_0(u_D^\star) \leq \liminf_n J_0(u_n).$$

Now, let $q' \in (5, +\infty)$. The space $H^1(D)$ is compactly embedded in $L^{q'}(D)$ [1] so (u_n) converges strongly to $u_D^\star$ in $L^{q'}(D)$. By Proposition 7.2.2,

$$\mathbb{E}\left[\tilde{h}(\nu) J_{wave}(u_n,\nu)\right] \to \mathbb{E}\left[\tilde{h}(\nu) J_{wave}(u_D^\star,\nu)\right].$$

Thus, $\mathcal{J}_D(u_D^\star) \leq \liminf_n \mathcal{J}_D(u_n)$. since (u_n) is a minimizing sequence, this proves that $u_D^\star$ is a minimizer.

The Euler-Lagrange equation associated to problem (7.1.9) yields the boundary value

problem (7.2.7). The constant C in the first line is the Lagrange multiplier associated to the volume constraint $\int_D u dxdz = \mathcal{V}$. Conversely, each solution to (7.2.7) is a critical point of $\mathcal{J}_D$ on $H_{\mathcal{V}}(D)$ and by convexity, it is a minimizer. This concludes the proof. □

Proposition 7.2.3. *If D is symmetric with respect to z-axis, then $u_D^\star$ is even with respect to x.*

Proof. Since D is symmetric with respect to the z-axis, for all $(x, z) \in D$, we have $(-x, z) \in D$. Let $\check{u} \in H(D)$ be defined by

$$\check{u}(x, z) = u_D^\star(-x, z), \quad \forall (x, z) \in D.$$

Performing the change of variable $x \mapsto -x$ in $T(\check{u}, \alpha, \lambda)$ (see (7.1.6)), we find that

$$T(\check{u}, \alpha, \lambda) = \int_D u_D^\star(x, z) e^{i\lambda\alpha x} e^{-\lambda^2 \alpha z} dxdz.$$

Thus,

$$|T(\check{u}, \alpha, \lambda)| = |T(u_D^\star, \alpha, \lambda)|$$

and consequently, by (7.1.5),

$$J_{wave}(\check{u}, \alpha) = J_{wave}(u_D^\star, \alpha), \quad \forall \alpha > 0.$$

Similarly, we have $J_0(\check{u}) = J_0(u_D^\star)$ and so

$$\mathcal{J}_D(\check{u}) = \mathcal{J}_D(u_D^\star).$$

Since $\check{u}$ belongs to $H_{\mathcal{V}}(D)$, this shows that $\check{u}$ is a solution to problem (7.1.9). By uniqueness of the solution, $\check{u} = u_D^\star$. □

Theorem 7.2.2. *If D is a rectangle, then the solution $u_D^\star$ to problem* (7.1.9) *belongs to $W^{2,5/4-\epsilon}(D)$ for all $\epsilon > 0$ small enough.*

Proof. Let $q \in (1, 5/4)$. Since $u_D^\star$ belongs to $H^1(D)$ which is continuously embedded in $L^{q'}(D)$, we deduce from (7.2.7), Proposition 7.2.2 and Lemma 7.2.1 that $u_D^\star$ solves the PDE

$$-\Delta u_D^\star + f = C \text{ in } D,$$

where f belongs to $L^q(D)$ and C is constant. The domain D is a rectangle and $u_D^\star$ satisfies homogeneous Dirichlet boundary conditions on three sides and homogeneous Neumann

boundary conditions on one side. By elliptic regularity on polygons [43], $u_D^\star$ belongs to $W^{2,q}(D)$. □

7.3 Numerical simulations

In this section, we present numerical results for the optimal hulls obtained by minimizing the expectation of the total resistance (7.1.3). The cost function is

$$\begin{aligned} \mathcal{J}_D(u) &= \mathbb{E}\left(R_{total}(u,\nu)\right) \\ &= \mathbb{E}\left(R_{viscous}(u,\nu) + R_{Michell}(u,\nu)\right). \end{aligned}$$

In other words, we choose $h_{\rho,g,C_F}(\alpha) = 1$ or equivalently (cf. (7.1.7))

$$\tilde{h}(\alpha) = \frac{\rho g}{2\alpha} C_F$$

in the cost function $\mathcal{J}_D$ defined by (7.1.8). For the domain D, we shall limit ourselves to a rectangle or a half ellipse. We recall that the robust optimization problem (7.1.9) reads

$$\text{Find } u_D^\star \in H_{\mathcal{V}}(D) \text{ such that } \mathcal{J}_D(u^\star) = \min\left\{\mathcal{J}_D(u) \ : \ u \in H_{\mathcal{V}}(D)\right\}. \tag{7.3.1}$$

Our purpose is to investigate numerically the optimal hull which solves (7.3.1). We also want to compare this optimal hull with the solution to the following (non robust) optimization problem:

$$\text{Find } \bar{u}_D \in H_{\mathcal{V}}(D) \text{ such that } R_{total}(\bar{u},\alpha) = \min\left\{R_{total}(u,\alpha) \ : \ u \in H_{\mathcal{V}}(D)\right\}, \tag{7.3.2}$$

where the value α is set to $\alpha = \mathbb{E}(\nu)$. We shall also compare the optimal hulls with the Wigley hulls discussed above.

Problem (7.3.2) was investigated numerically in [27]. In Figure 7.1, we have computed the optimal hull $\bar{u}_D$ for different values of α. The domain is a rectangle with length $L = 2.2\,\mathrm{m}$ and draft $T = 0.3\,\mathrm{m}$. The half volume of the hull is $\mathcal{V} = 0.06\,\mathrm{m}^3$. The other parameters are

$$\rho = 1000\,\mathrm{kg}\cdot\mathrm{m}^{-3}, \quad g = 9.81\,\mathrm{m}\cdot\mathrm{s}^{-1} \quad \text{and} \quad C_F = 0.01. \tag{7.3.3}$$

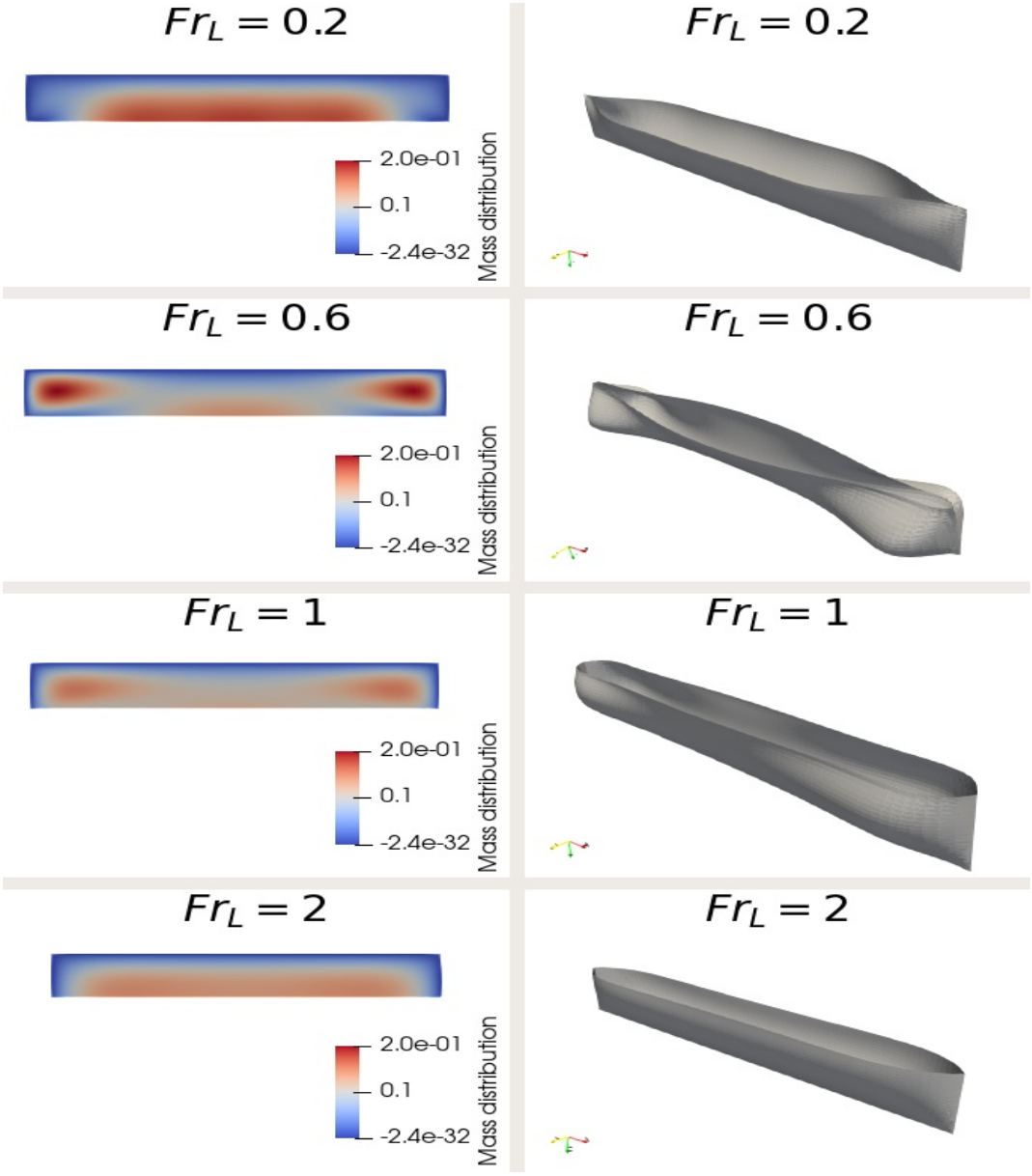

Figure 7.1 – Mass distribution (left) and 3D results (right) of the optimal hull $\bar{u}_D$ from (7.3.2) defined on a fixed rectangular domain for different length Froude numbers.

It is convenient to introduce the length Froude number

$$Fr_L = \frac{V}{\sqrt{gL}} = \frac{1}{\sqrt{\alpha L}}, \tag{7.3.4}$$

which is a dimensionless version of the speed. We recover the results from [27]. Namely, for $Fr_L = 0.6$, the hull has the famous **bulbous bow**, which almost cancels the wave resistance. For large or small Froude numbers ($Fr_L = 2$ or $Fr_L = 0.2$), the influence of Michell's wave resistance is small and the optimal hull mainly minimizes the viscous resistance.

7.3.1 Numerical approximation

The expectation of the water resistance $\mathcal{J}_D(u)$ is given by

$$\begin{aligned}\mathcal{J}_D(u) &= \mathbb{E}[\tilde{h}(\nu)\Big(2|D| + J_0(u) + \frac{1}{C_F} J_{\text{wave}}(u,\nu)\Big)] \\ &= 2\mathbb{E}[\tilde{h}(\nu)]|D| + \mathbb{E}[\tilde{h}(\nu)]J_0(u) + \frac{1}{C_F}\mathbb{E}[\tilde{h}(\nu)J_{\text{wave}}(u,\nu)].\end{aligned}$$

By dropping the constant term, we see that minimizing $\mathcal{J}(u)$ is the same as minimizing

$$\tilde{\mathcal{J}}_D(u) = \int_D |\nabla u|^2 + \frac{1}{C_F \mathbb{E}[\tilde{h}(\nu)]} \int_{D\times D} H_\nu(x,z,x',z')u(x,z)u(x',z')dxdzdx'dz'. \tag{7.3.5}$$

By Theorem 7.2.1, a minimizer u^* of $\tilde{\mathcal{J}}_D(u)$ in $H_\nu(D)$ is a solution to the boundary value problem:

$$\begin{cases} -\Delta u(x,z) + \frac{1}{C_F\mathbb{E}[\tilde{h}(\nu)]} \int_{D\times D} H_\alpha(x,z,x',z')u(x',z')dx'dz' = C, \quad \forall (x,z) \in D, \\ \int_D u\, dxdz = \mathcal{V}, \\ u = 0 \text{ on } \Gamma_0, \\ \dfrac{\partial u}{\partial n} = 0 \text{ on } \Gamma_N. \end{cases} \tag{7.3.6}$$

To solve this problem, we adopt a finite element approach, in the sense that the optimal hull u^* will be sought in a finite dimensional space

$$\mathcal{V}^h \subset H(D) \subset H^1(D).$$

Given a basis of P_1 (continuous and piecewise linear) finite elements $\{\phi_1, \phi_2, \dots, \phi_n\}$, we can write:

$$\text{for all } u \in \mathcal{V}^h, \quad u = \sum_{i=1}^{n} u_i \phi_i. \tag{7.3.7}$$

Then we have the following discretization of $\tilde{\mathcal{J}}_D(u)$

$$\tilde{\mathcal{J}}_D(u) = U^t \Big(M_0 + \frac{1}{C_F \mathbb{E}[\tilde{h}(\nu)]} M_w \Big) U, \tag{7.3.8}$$

where $U = (u_1, \dots, u_n)^t$ is the vector of the coordinates of u and M_0, M_w are matrices approximating J_0 and $\mathbb{E}[\tilde{h}(\nu) J_{wave}(u, \nu)]$. This yields the following discrete optimization problem:

$$u_D^* = \underset{u \in \mathcal{V}_h,\ \int_D u dx dz = \mathcal{V}}{\operatorname{argmin}} \Big\{ U^t \Big(M_0 + \frac{1}{C_F \mathbb{E}[\tilde{h}(\nu)]} M_w \Big) U \Big\}. \tag{7.3.9}$$

Let us give some insight on the numerical computation of these matrices.

Approximation of the viscous resistance

When u is given by (7.3.7), the expression of the viscous resistance J_0 reads

$$\begin{aligned} \int_D |\nabla u|^2 &= \langle \nabla u, \nabla u \rangle_{L^2} \\ &= \langle \sum u_i \nabla \phi_i, \sum u_j \nabla u_j \rangle_{L^2} \\ &= \sum_{i,j=1} u_i u_j \langle \nabla \phi_i, \nabla \phi_j \rangle_{L^2}. \end{aligned}$$

The computation of the stiffness matrix $\langle \nabla \phi_i, \nabla \phi_j \rangle_{L^2}$ is standard, this matrix is non-diagonal, symmetric, and positive definite.

Approximation of the expectation of the wave resistance

Here, before discretizing, it is easier to write:

$$\begin{aligned} \mathbb{E}[\tilde{h}(\nu) J_{\text{wave}}(u, \nu)] &= \mathbb{E}[R_{Michell}(u, \nu)] \\ &= \frac{4\rho g}{\pi} \mathbb{E}\left[\nu^3 \int_1^\infty |T(u, \nu, \lambda)|^2 \frac{\lambda^4}{\sqrt{\lambda^2 - 1}} d\lambda \right] \\ &= \frac{4\rho g}{\pi} \int_{\nu_{\min}}^{\nu_{\max}} \alpha^3 f(\alpha) \int_1^\infty |T(u, \alpha, \lambda)|^2 \frac{\lambda^4}{\sqrt{\lambda^2 - 1}} d\lambda d\alpha \end{aligned}$$

where $T(u,\alpha,\lambda)$ is given by (7.1.6) and f is the probability density function of ν on the interval $[\nu_{min},\nu_{max}] \subset (0,+\infty)$. The approximation of the integral is done as follows:

— for a given α, λ, the integral $T(u,\alpha,\lambda) = \int_D u(x,z)\exp(-i\lambda\alpha x - \lambda^2\alpha z)dxdz$ is computed by exact integration over each triangle of the mesh which approximates the domain D (see Appendix A for details).

— The integration over α is handled by a numerical integration (a Newton-Cotes formula of order 5, known as Boole's rule).

Concerning the density f, we consider two cases:

— A continuous uniform probability distribution for the Kelvin number on $[\nu_{min},\nu_{max}]$, in which case

$$f(\alpha) = \frac{1}{\nu_{max}-\nu_{min}} \text{ on } [\nu_{min},\nu_{max}]; \tag{7.3.10}$$

— A continuous uniform probability distribution for the speed $V = \sqrt{g/\alpha}$, as in (7.3.12).

Let us recall from [27] the main steps for the approximation of $\int_1^\infty |T_u(\alpha,\lambda)|^2 \frac{\lambda^4}{\sqrt{\lambda^2-1}}d\lambda$.

1. First, the infinite integral is approximated by:

$$\int_1^\infty |T(u,\alpha,\lambda)|^2 \frac{\lambda^4}{\sqrt{\lambda^2-1}}d\lambda \approx \int_1^\Lambda |T(u,\alpha,\lambda)|^2 \frac{\lambda^4}{\sqrt{\lambda^2-1}}d\lambda$$

where Λ is a large constant conveniently chosen. We then have:

$$\begin{aligned}\int_1^\Lambda |T(u,\alpha,\lambda)|^2 \frac{\lambda^4}{\sqrt{\lambda^2-1}}d\lambda &= \int_1^2 T_u(\lambda)T_u(\lambda)^t \frac{\lambda^4}{\sqrt{\lambda^2-1}}d\lambda + \int_2^\Lambda T_u(\lambda)T_u(\lambda)^t \frac{\lambda^4}{\sqrt{\lambda^2-1}}d\lambda \\ &= T_u(1)T_u(1)^t \int_1^2 \frac{1}{\sqrt{\lambda^2-1}}d\lambda + \int_2^\Lambda T_u(\lambda)T_u(\lambda)^t \frac{\lambda^4}{\sqrt{\lambda^2-1}}d\lambda \\ &\quad \int_1^2 \frac{\lambda^4 T_u(\lambda)T_u(\lambda)^t - T_u(1)T_u(1)^t}{\sqrt{\lambda^2-1}}d\lambda.\end{aligned}$$

2. The first integral can be computed explicitly [73]:

$$T_u(1)T_u(1)^t \int_1^2 \frac{1}{\sqrt{\lambda^2-1}}d\lambda = \ln(2+\sqrt{3})T_u(1)T_u(1)^t.$$

3. The second integral, which is not singular anymore, is computed with a second order midpoint formula:

$$\int_1^2 \frac{\lambda^4 T_u(\lambda)T_u(\lambda)^t - T_u(1)T_u(1)^t}{\sqrt{\lambda^2-1}}d\lambda \approx \sum_{i=1}^{N_0} \frac{\lambda_{i,0}^4 T_u(\lambda_{i,0})T_u(\lambda_{i,0})^t - T_u(1)T_u(1)^t}{\sqrt{\lambda_{i,0}^2-1}}\delta\lambda_0$$

where $\delta\lambda_0 = \frac{1}{N_0}$ and $\lambda_{i,0} = 1 + (i - \frac{1}{2})\delta\lambda_0$.

4. Finally, the function under the third integral has an exponential decay for most values of z. Therefore the third integral is cut in intervals of exponentially growing lengths (we set $\Lambda = 2^{k_\Lambda}$), therefore:

$$\int_2^\Lambda T_u(\lambda)T_u(\lambda)^t \frac{\lambda^4}{\sqrt{\lambda^2-1}} d\lambda \approx \sum_{k=1}^{k_\Lambda - 1} \int_{2^k}^{2^{k+1}} T_u(\lambda)T_u(\lambda)^t \frac{\lambda^4}{\sqrt{\lambda^2-1}} d\lambda$$

on each interval, the integral is computed with a second order midpoint approximation formula:

$$\int_{2^k}^{2^{k+1}} T_u(\lambda)T_u(\lambda)^t \frac{\lambda^4}{\sqrt{\lambda^2-1}} d\lambda \approx \sum_{i=1}^{N_k} T_u(\lambda_{i,k})T_u(\lambda_{i,k})^t \frac{\lambda_{i,k}^4}{\sqrt{\lambda_{i,k}^2-1}}$$

where $\delta\lambda_k = \frac{2^k}{N_k}$, and $\lambda_{i,k} = 2^k + (i - \frac{1}{2})\delta\lambda_k$.

7.3.2 Numerical results

For all the simulations, we consider a rectangular domain D or a half ellipse D of length $L = 2.2\,\mathrm{m}$ and draft $T = 0.3\,\mathrm{m}$. The half volume of the hull is $\mathcal{V} = 0.06\,\mathrm{m}^3$ and the other parameters are as in (7.3.3). For convenience, we shall consider probability distributions on the Kelvin wave number $\alpha = \frac{g}{V^2}$. We are only going to consider probability distributions with a compact support included in $[\nu_{\min}, \nu_{\max}]$ with $0 < \nu_{\min} < \nu_{\max} < +\infty$. The bounds $\nu_{\min}, \nu_{max}$ are chosen so that the corresponding length Froude numbers are $Fr_{L_{\min}} = 0.2$ and $Fr_{L_{\max}} = 1$. Thus, we have

$$\begin{cases} \nu_{\min} = \frac{1}{Fr_{L_{\max}}^2 L} = 0.45 \\ \nu_{\max} = \frac{1}{Fr_{L_{\min}}^2 L} = 11.36. \end{cases}$$

.

Optimal hulls for different domains

We start our investigation by computing the solutions u_D^* for the discrete problem (7.3.9) for different domains and with different probability distributions. While the volume constraint is enforced on our problem, the constraint of positive solution is not. It is expected that the solutions will be positive throughout the domain. Thus, we compute a

solution for a given range, and we check its positivity numerically. The computed solutions satisfy this condition for most ranges of speed.

The case of a continuous uniform distribution of the Kelvin wave number

Recall that a continuous uniform probability distribution has a probability density function

$$f(\alpha) = \frac{1}{\nu_{\max} - \nu_{\min}} \quad \text{on} \quad [\nu_{min}, \nu_{max}].$$

Figure 7.2 shows the computed optimal solutions for the rectangular domain and for the

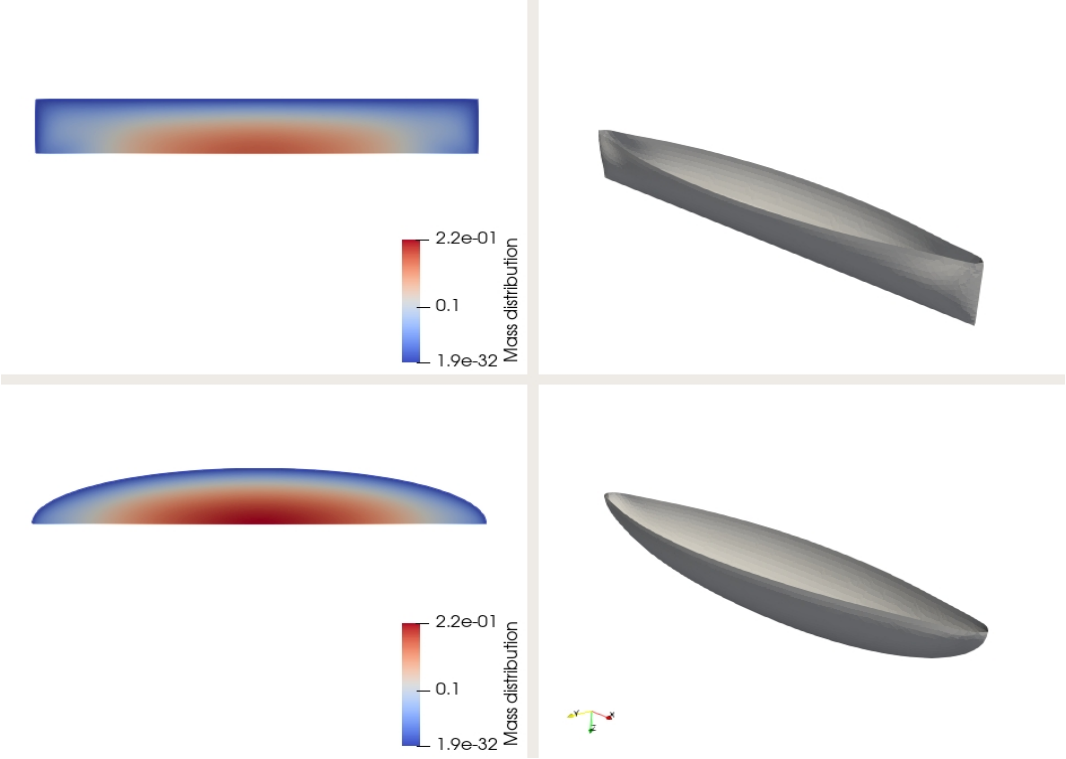

Figure 7.2 – Mass distribution (left), and 3D results (right) of the optimal hulls for minimizing the expectation of the water resistance $\mathcal{J}_D(u)$ with a uniform distribution ν of the Kelvin wave number on a rectangular domain (top), and a half ellipse (bottom).

half ellipse. We note that there is no bulbous bow. In this case, the mean value of α is

$$\mathbb{E}[\nu] = (\nu_{max} + \nu_{min})/2 = 5.90. \tag{7.3.11}$$

This corresponds to a Froude number equal to $Fr_L = 0.277$. Thus, the distribution of Froude numbers is concentrated near 0.2. The robust optimal hull $u_D^\star$ is close to the

hull $\bar{u}_D$ obtained in Figure 7.1 for $Fr_L = 0.2$. We also note that the optimal hulls are symmetric back and front, in agreement with Proposition 7.2.3.

The case of a continuous uniform distribution of the velocity

We consider a uniform distribution of the velocities V on the interval $[V_{\min}, V_{\max}]$, where $[V_{\min}, V_{\max}]$ is computed such that the corresponding length Froude interval is $[0.2, 1]$. That is, we take

$$\begin{cases} V_{\min} &= 0.2\sqrt{gL} = 0.93 \\ V_{\max} &= \sqrt{gL} = 4.64 \end{cases}$$

By an appropriate change of variable, we see that the probability density of $\nu = \frac{g}{V^2}$ is given by

$$f(\alpha) = \frac{\sqrt{g/\alpha}}{2\alpha(V_{\max} - V_{\min})} \quad \text{on} \quad [\nu_{min}, \nu_{max}]. \tag{7.3.12}$$

Figure 7.3 shows the computed optimal hulls. They are not very different from the shapes computed in Figure 7.2 for a uniform distribution of ν. In this new situation, the Froude is uniform over the interval $[0.2; 1.0]$ and the mean value of the Froude number is 0.6. We see that the robust optimal hull $u_D^\star$ has no bulbous bow. This is a striking contrast with the (non robust) optimal hull $\bar{u}_D$ obtained for $Fr_L = 0.6$ in Figure 7.1. This contrast is studied further in the next section.

7.3.3 Comparison between the robust hull and other hulls

Here we seek to compare the performance of the optimal solution u_D^* for minimizing the expectation of the water resistance with other hulls. To this end, we consider a rectangular domain D, and two other hulls:

— $\overline{u}_D$ which is computed on D as the optimal solution minimizing the water resistance for $\alpha = \mathbb{E}[\nu]$ (cf. problem (7.3.2));

— w is a Wigley hull, which is a standard shape of hulls defined in subsection 5.2. We use a Wigley hull defined on D and with a triangular cross section such that $\int_D w(x,z)dxdz = \mathcal{V}$. Since $\int_D w(x,z)dxdz = BLT/6$, we have $B = 6\mathcal{V}/(LT) = 0.5454$

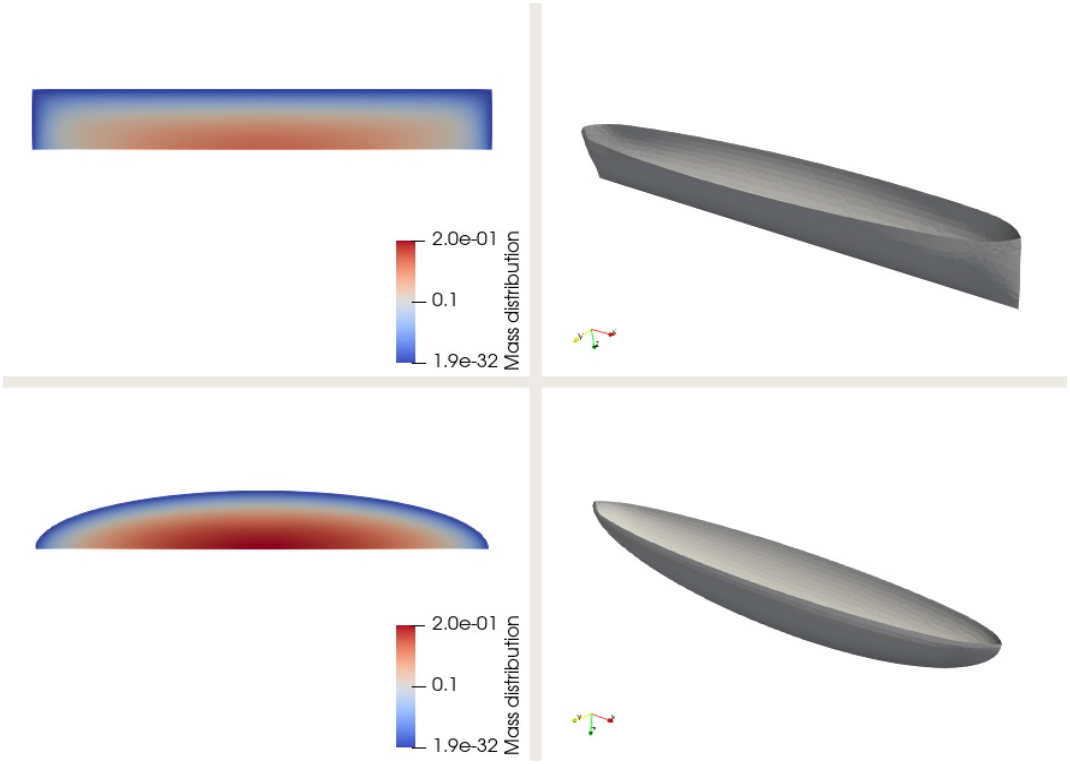

Figure 7.3 – Mass distribution (left), and 3D results (right) of the optimal hulls for minimizing the expectation of the water resistance $\mathcal{J}_D(u)$ with a uniform distribution of velocity on a rectangular domain (top), and an ellipse (bottom).

For each hull, we compute the viscous resistance, the wave resistance and total resistance of the water for different distributions of ν.

The case of a continuous uniform distribution on ν

Figure 7.4 gives the shapes of the computed optimal hulls u_D^* and $\overline{u}_D$. Although the shapes do not seem too different, they perform differently for different length Froude numbers. First, since Fr_L is a decreasing function of α (see (7.3.4)), a uniform law on ν gives more weight to small length Froude numbers (the mean Froude number is 0.277 on the interval $[0.2, 1]$, cf. (7.3.11)).

Figure 7.5 shows that the computed viscous resistance is very similar for both u_D^* and $\overline{u}$. Both hulls are more optimal than the standard Wigley hull w. The main difference lies in the computed Michell wave resistance shown in Figure 7.6 which explains the difference in the computed total water resistance shown in Figure 7.7.

— First, one can see the oscillations of Michell's wave resistance for $Fr_L \in [0.2, 0.35]$.

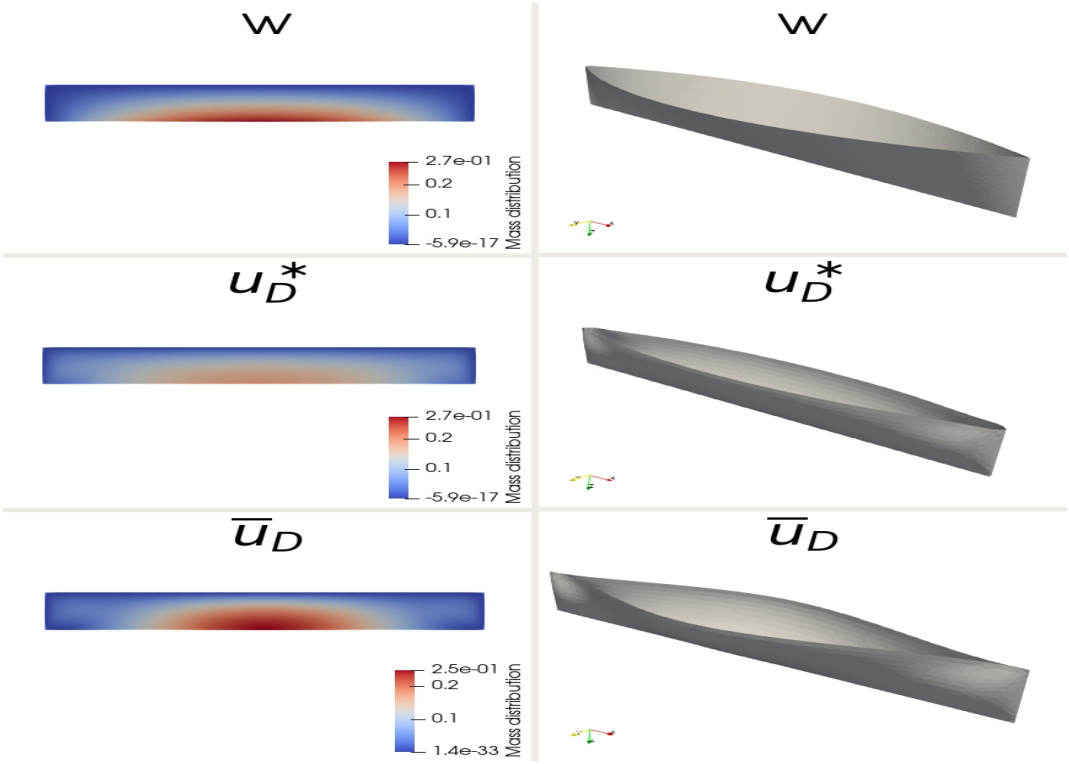

Figure 7.4 – Mass distribution (left), and 3D results (right) of a Wigley hull w, and the optimal hulls u_D^*, optimized for $\mathcal{J}(u)$, and $\overline{u}_D$, optimized for $J(u, \mathbb{E}[\nu])$ for a uniform distribution of ν.

These oscillations are well known for the Wigley hull w (see section 5), they are smoother for u_D^* and seem to vanish for $\overline{u}_D$.

— We see that u_D^* is optimal on the whole interval $[0.35, 1]$ and $\overline{u}_D$ is optimal for small Froude numbers in $[0.2, 0.35]$. This is no surprise, since u_D^* is computed as an optimal hull for $\alpha = \mathbb{E}[\nu]$ which corresponds to $Fr_L = 0.28$.

— The expectation of $u_D^\star$ (equal to 24 N) is much lower than the expectation of $\bar{u}_D$ (36 N). This translates the optimality of $u_D^\star$ over most of the speed interval $[0.2, 1]$, as can be seen in Figure 7.7 which represents the total resistance. The fact that the standard Wigley hull whose expectation is 33 N outperforms $\bar{u}_D$ shows how disastrous it can be to ignore the velocity variations during the optimization process.

Thus, although the optimal hulls possess similar geometries, they have different performances when it comes to Michell's wave resistance. When it comes to minimizing the total water resistance for a given interval of velocities, it is more interesting to look for shapes that minimize the expectation of the total water resistance, despite the lengthy

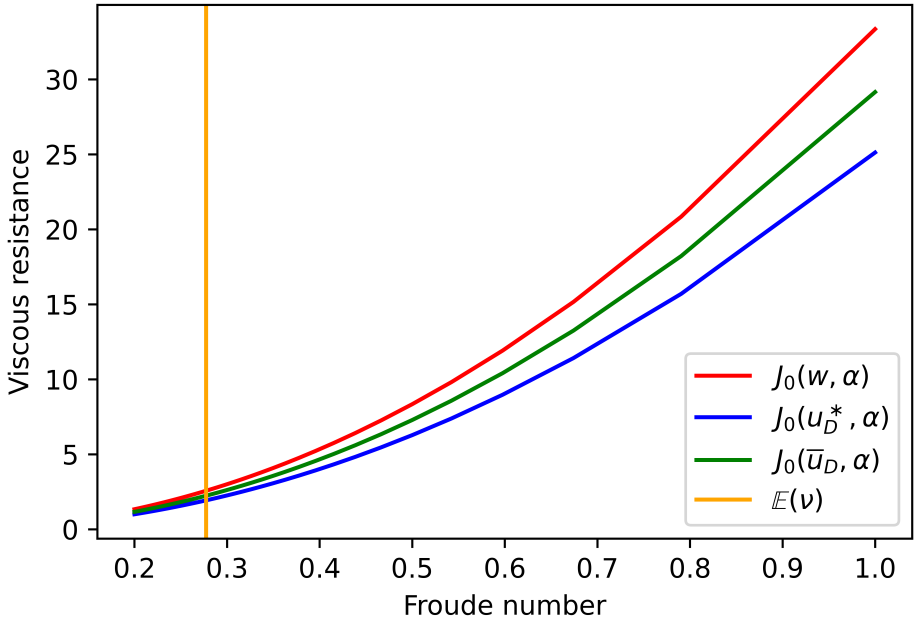

Figure 7.5 – Viscous water resistance $\tilde{h}(\alpha)J_0(u)$ for different hulls with a uniform distribution of ν.

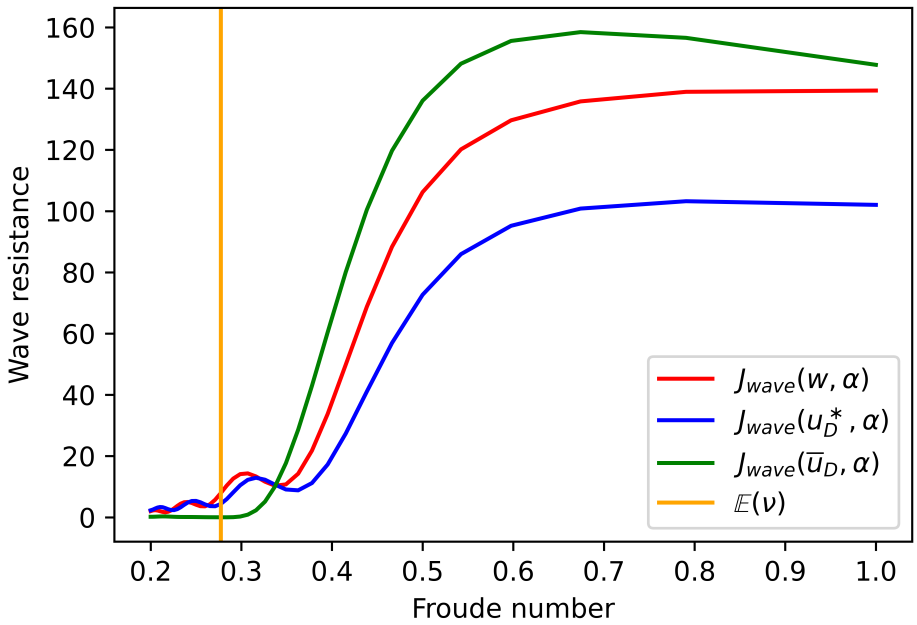

Figure 7.6 – Water wave resistance $\frac{1}{C_F}\tilde{h}(\alpha)J_{\text{wave}}(u, \alpha)$ for different hulls with a uniform distribution of ν.

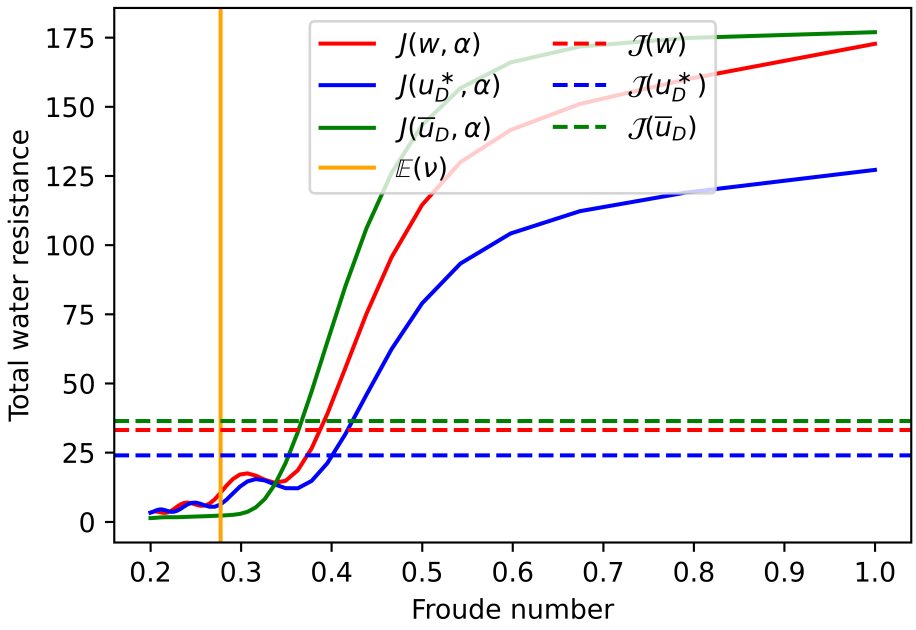

Figure 7.7 – Total water resistance $\tilde{h}(\alpha)J_0(u) + \frac{1}{C_F}\tilde{h}(\alpha)J_{\text{wave}}(u,\alpha)$ for different hulls with a uniform distribution of ν.

calculations it adds to the optimization algorithm.

The case of a continuous uniform distribution on V

Here, the main difference with the previous case is the shape of the optimal hulls. Indeed since the length Froude number is proportional to the velocity V, we have that $\mathbb{E}[V] = 0.6$ is on the center of the Froude interval $[0.2, 1]$. This explains the shapes of the optimal hulls, i.e. we get the bulbous bow regime for $\overline{u}_D$ which is optimal at $Fr_L = 0.6$. In contrast, u_D^* corresponds to an average on the whole interval $[0.2, 1]$ of the optimal shapes given in Figure 7.1. Most importantly, we see that:

— The computed viscous resistance given in Figure 7.9 is very different for $u_D^\star$ and $\bar{u}_D$. This is no surprise, since unlike the previous case, the shapes of the optimal hulls are very different. We see that the bulbous bow obtained for $\overline{u}$ has a worse performance than the standard Wigley hull w. This reflects intuitively the dependance of the viscous resistance on the geometry of the hull. i.e. the smoother is the geometry of the hull, the lower is the viscous resistance going to be.

— The oscillations in Michell's wave resistance shown in Figure 7.10 are spikier for $\overline{u}$ than u_D^*. Unlike the previous case, taking a uniform distribution on the velocity V

doesn't give more weight to small Froude numbers. Thus, we see higher oscillations for $\overline{u}_D$ which doesn't take into account small Froude numbers, contrary to u_D^*.

— Surprisingly, the expectation of the total water resistance is very close for $u_D^\star$ (equal to 83 N) and $\bar{u}_D$ (84 N), but the geometry of the hulls is strikingly different. Both hulls perform much better than the Wigley hull, whose expectation is 128 N.

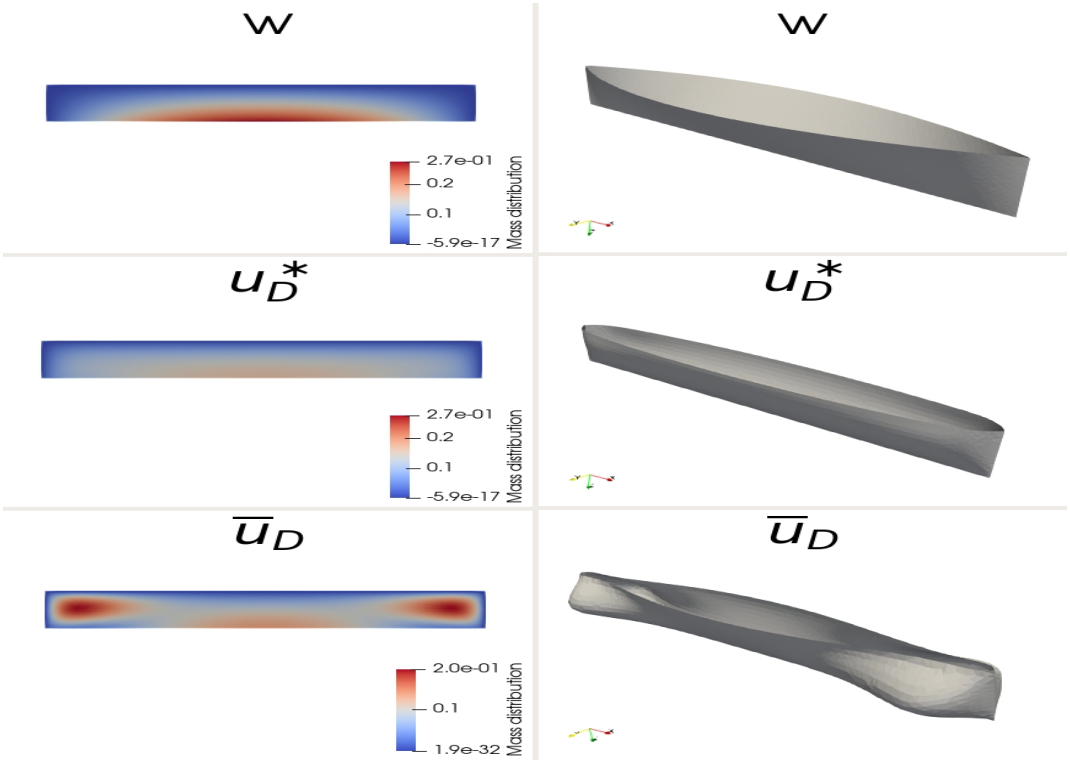

Figure 7.8 – Mass distribution (left), and 3D results (right) of a Wigley hull w,the optimal hull u_D^*, optimized for $\mathcal{J}(u)$ and $\overline{u}$, optimized for $J(u, \mathbb{E}[\nu])$ for a uniform distribution of the velocity V.

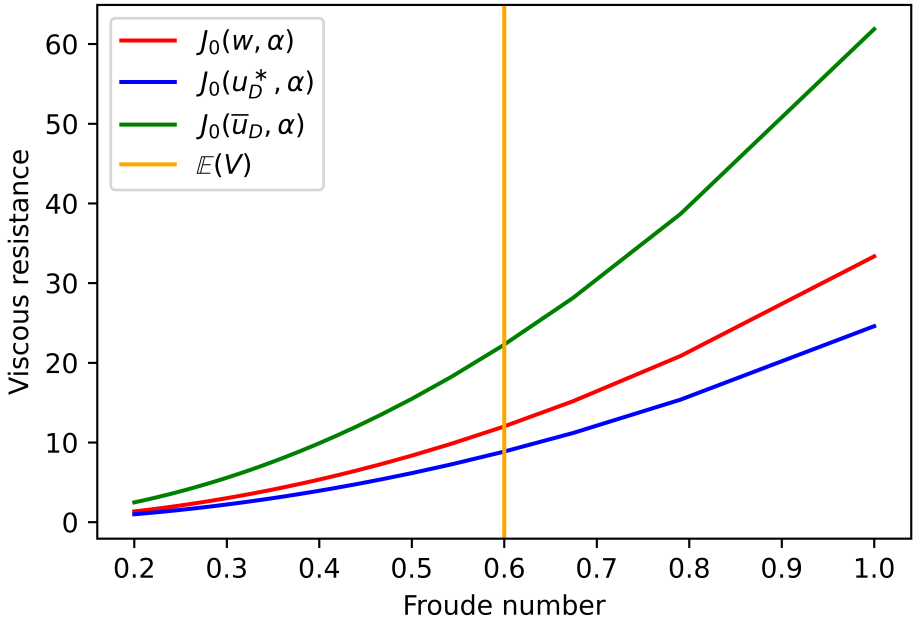

Figure 7.9 – Viscous water resistance $\tilde{h}(\nu)J_0(u)$ for different hulls with a uniform distribution of the velocity V.

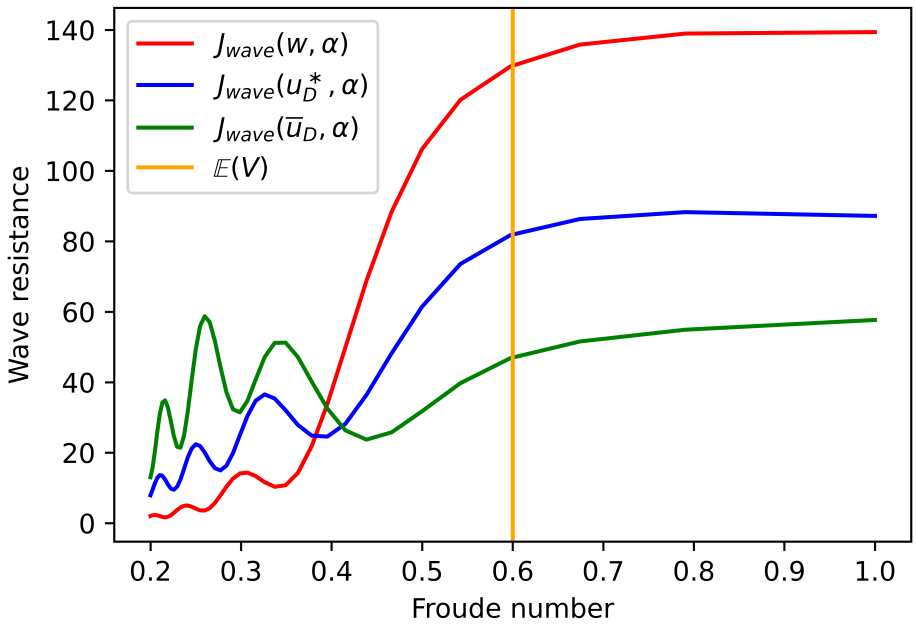

Figure 7.10 – Water wave resistance $\tilde{h}(\alpha)J_0(u)+\frac{1}{C_F}\tilde{h}(\alpha)J_{\text{wave}}(u,\alpha)$ for different hulls with a uniform distribution of the velocity V.

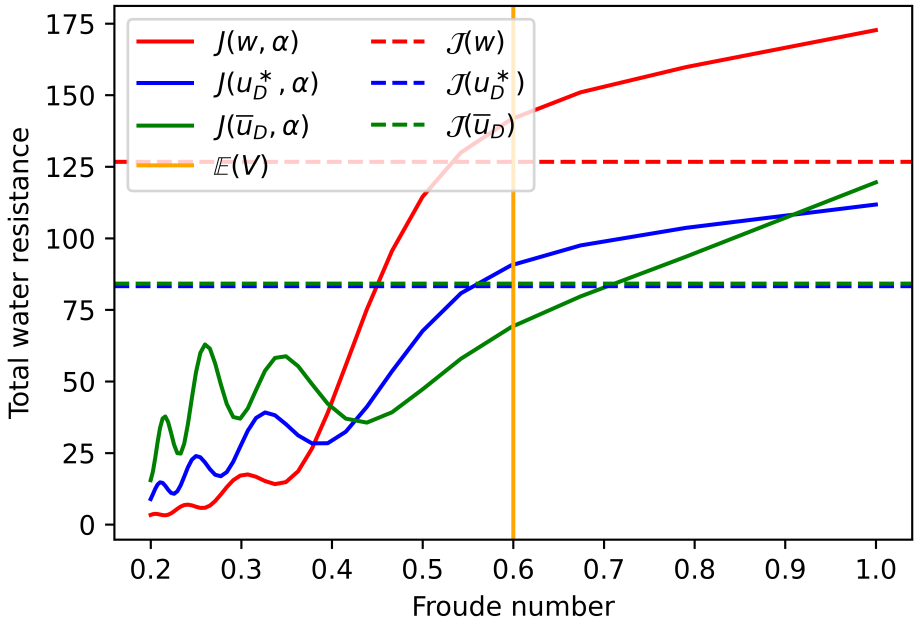

Figure 7.11 – Total water resistance $R_{total}(u, \alpha)$ for different hulls with a uniform distribution of the velocity V.

Chapter 8

Numerical methods for shape optimization: Newton's algorithm

In this section we describe our discretization of Newton's method for shape optimization. Given the complex form of second order shape derivatives, the literature on its numerical implementation is scarce. To our knowledge, this was first discussed in [61] where the authors give a discretization of the second order shape derivative as a full matrix. In order to build such a matrix, one would have to solve nb problems for the local shape derivatives of the state functions of the PDE problem, where nb is the number of degrees of freedom of the mesh approximating the geometry. This difficulty was then mediated in [44], where the author uses a conjugate-gradient method to compute the inverse of the Hessian matrix at every iteration. Recently, Newton's method, and in general second order shape optimization algorithms, have been extensively studied in [77], where the author proposes the idea of differentiating along paths normal to the boundary of the geometry to obtain simpler forms of the resulting discrete Hessian, which is still given by a full matrix.

In this work, we seek a simple implementation of Newton's method in hope of obtaining a super-linear convergent algorithm which would help us drastically reduce the computational time for finding optimal domains for minimizing the expectation of the total water resistance. We also hope that the second order character of the algorithm will provide a better conservation of the constraints throughout the optimization process, and this is crucial to our applications.

For this purpose, instead of differentiating along paths normal to the boundary, we shall build the discrete Hessian matrix only on the boundary of the geometry, and we shall do this in a basis for deformation vectors that is normal to the boundary. The resulting Hessian matrix is much easier to build and invert since:

— The choice of a normal basis for the deformation vectors produces a diagonal Hessian matrix.

— By working with normal deformation vectors we get rid of the tangential term in the expression of the second order shape derivative and the numerical implementation is much easier.
— No problem has to be solved for the local shape derivatives, since these are often very well known on the boundary by differentiating the equations of the boundary conditions.

In what follows we first describe the algorithm in the simple case of purely geometric functionals, before moving on to the general case of PDE-dependent functionals with constraints.

8.1 Case without PDE

Let $f \in \mathcal{C}^2(\mathbb{R}^2;\mathbb{R})$. We consider the minimization problem

$$\inf_{\Omega\in\mathcal{O}_3} E(\Omega) \tag{8.1.1}$$

where

$$E(\Omega) = \int_\Omega f(x)dx$$

is the function to be minimized. For $k \in \mathbb{N}$, $\mathcal{O}_k$ is the set of bounded open sets of $\mathbb{R}^2$ that are of class C^k. The optimal shape Ω^* is explicitly given by the set of negative values of f:

$$\Omega^* = \{x \in \mathbb{R}^d \,|\, f(x) < 0\}. \tag{8.1.2}$$

We seek to compute Ω^* by Newton's method, and we shall follow an optimize-then-discretize approach. Let us first recall from [50] the first and second order shape derivatives of a geometric functional. Since f is smooth, the objective function $E(\Omega)$ is twice shape-differentiable for all $\Omega \in \mathcal{O}_3$ and the shape derivatives are given by:

$$\begin{aligned} E'(\Omega;\xi) &= \int_\Gamma (\xi\cdot n) f, \\ E''(\Omega;\theta,\xi) &= \int_\Gamma (\theta\cdot n)(\xi\cdot n)\Big(\mathcal{H}f + \partial_n f\Big) + \int_\Gamma Z_{\theta,\xi} f, \end{aligned} \tag{8.1.3}$$

where Γ is the boundary of Ω and

$$Z(\theta,\xi) = \theta_\Gamma \cdot D_\Gamma n\, \xi_\Gamma - \theta_\Gamma \cdot \nabla_\Gamma(\xi\cdot n) - \xi_\Gamma \cdot \nabla_\Gamma(\theta\cdot n).$$

We search for a descent direction by solving Newton's equation: find $\theta = (\theta_1, \theta_2) \in C^{2,\infty}(\mathbb{R}^2; \mathbb{R}^2)$ such that

$$\forall \xi \in C^{2,\infty}(\mathbb{R}^2; \mathbb{R}^2), \qquad E''(\Omega; \theta, \xi) = -E'(\Omega; \xi). \tag{8.1.4}$$

This problem has to be properly discretized. We explain our approach which allows to obtain a diagonal hessian matrix when working with $\mathbb{P}_1$ normal Lagrange finite element deformation vectors without solving any adjoint problem, and give some numerical examples.

8.1.1 Discretization of Newton's equation

Let us start by giving the discrete setting of the problem. Given a triangulation mesh $\mathcal{T}_h$ approximating the domain Ω, Γ_h denotes the boundary of the mesh which consists of an ordered n_{be}-tuple of ordered vertices $(\mathbf{x}_1, \mathbf{x}_2, \ldots, \mathbf{x}_{n_{be}})$. We denote by κ the discrete curvature computed following the steps of Section A.3. Let

$$\mathcal{V}_h = \left\{ u \in C(\Omega, \mathbb{R}) \middle| \forall\, T_i \in \mathcal{T}_h,\ u_{|T_i} \in \mathbb{P}_1 \right\}$$

be the Lagrange finite element space of continuous scalar that are piecewise polynomials of degree 1, and let $(\phi_i)_{1 \le i \le N_h}$ be a basis of $\mathcal{V}_h$ such that:

$$\begin{cases} \forall\, 1 \le i, j \le N_h, & \phi_i(a_j) = \delta_{ij} \\ \forall\, u \in \mathcal{V}_h, & u(x) = \sum\limits_{i=1}^{N_h} u(a_j)\phi_i(x) \end{cases}$$

Where N_h is the dimension of $\mathcal{V}_h$ and $(a_j)_{1 \le j \le N_h}$ are the degrees of freedom of $\mathcal{V}_h$, and we set $f_h(x) = \sum\limits_{i=1}^{N_h} f(a_j)\phi_i(x)$. We denote by $n_h(\mathbf{x}_i)$ the discrete normal vector to the boundary at the vertex $\mathbf{x}_i$ which is approximated as the rotate of the tangent at $\mathbf{x}_i$, $\tau_h(\mathbf{x}_i) = \frac{\overrightarrow{\mathbf{x}_{i-1}\mathbf{x}_{i+1}}}{\left\|\overrightarrow{\mathbf{x}_{i-1}\mathbf{x}_{i+1}}\right\|}$ as shown in Figure 8.1.

We search for a descent direction $\theta_h : \mathbb{R}^2 \to \mathbb{R}^2$ defined on the vertices of $\mathcal{T}_h$ as a solution to equation (8.1.4).

— Since (8.1.4) only contains boundary integrals, we will first compute the descent direction θ_h on the boundary vertices $\mathbf{x}_1, \ldots, \mathbf{x}_{n_{be}}$ before extending it to all of the triangulation $\mathcal{T}_h$ through Hilbertian extension techniques (see [7]).

— Another problem is the tangential term $Z_{\theta,\xi}$ in the expression of the second order derivative $E^{''}(\theta,\xi)$. This term contains tangential components like $\theta_\Gamma, \xi_\Gamma$ which can be difficult to compute and a source of geometrical error. To get around this we follow the idea in [60] that any small perturbation θ of a regular domain Ω can be represented by normal deformations. We thus make the assumption that θ_h is normal to the boundary Γ_h at every vertex $\mathbf{x}_i$, that is:

$$\forall i = 1, \dots, n_{be}, \exists \alpha_i \in \mathbb{R} \quad \theta_h(\mathbf{x}_i) = \alpha_i n_h(\mathbf{x}_i). \tag{8.1.5}$$

— When θ is normal to the boundary Γ one can clearly see that $Z_{\theta,\xi} = -\xi_\Gamma \cdot \nabla_\Gamma(\theta \cdot n)$. for all ξ, moreover, the remaining term in the expression of $E^{''}$ only depends on normal components. We make the choice to solve Newton's equation (8.1.4) only for vectors ξ normal to the boundary, this choice, althought restrictive, helps to get rid of the remaining tangential term. we thus take $\xi_h = n_h(\mathbf{x}_i)$ for $i = 1, \dots, n_{be}$ for the discrete problem.

— Another issue is the discretization of the boundary integral on Γ_h. This can be a major source of error and lack of consistency as noted in [77]. Our choice is to first approximate the integral on each boundary vertex. Indeed, since we are working with $\mathbb{P}_1$ Lagrange finite elements, the contribution of each vertex $\mathbf{x}_i$ to the boundary integrals in equation (8.1.4) only depends on its neighboring vertices $\mathbf{x}_{i-1}$ and $\mathbf{x}_{i+1}$, so that we have for a general integrand g:

$$\begin{aligned}\int_{\Gamma_h} g(x)dx &= \sum_{i=1}^{n_{be}} \int_{T_i \cap \Gamma_h} g(x)dx \\ &= \sum_{i=1}^{n_{be}} \int_{\mathbf{x}_{i-1}}^{\mathbf{x}_{i+1}} g(x)dx.\end{aligned}$$

Thus, assuming all boundary edges $\{\mathbf{x}_i, \mathbf{x}_{i+1}\}$ have the same constant size h, then the contribution of each vertex $\mathbf{x}_i$ to the boundary integral can be approximated by:

$$\int_{\Gamma_h} g(x)dx = \sum_{i=1}^{n_{be}} \int_{\mathbf{x}_i - h}^{\mathbf{x}_i + h} g(x)dx \tag{8.1.6}$$

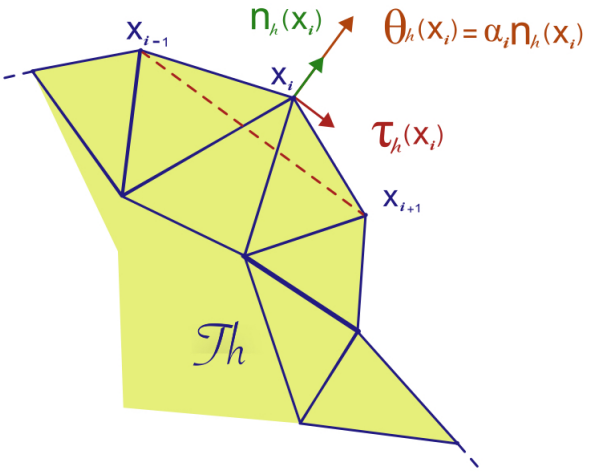

Figure 8.1 – Discrete setting around a vertex $\mathbf{x}_i$

and for each vertex $\mathbf{x}_i$ we have by the fundamental theorem of calculus:

$$\lim_{h\to 0} \frac{1}{2h} \int_{\mathbf{x}_i - h}^{\mathbf{x}_i + h} g(x)dx = g(\mathbf{x}_i) \tag{8.1.7}$$

which means that for a mesh with sufficiently small edge size h, we only need to look for the values of the integrand on each vertex $\mathbf{x}_i$.

Considering all the elements above, we get the following discretization of Newton's equation (8.1.4):

$$\forall i = 1, \dots, n_{be} \quad \lambda_i \Big(\kappa(\mathbf{x}_i) f(\mathbf{x}_i) + \partial_{n_h} f(\mathbf{x}_i) \Big) = f(\mathbf{x}_i). \tag{8.1.8}$$

Finding a descent direction θ through Newton's equation boils down to solving the system of equations (8.1.8) for the values of λ_i at each vertex, and taking:

$$\forall i = 1, \dots, n_{be} \quad \theta(\mathbf{x}_i) = \lambda_i n_h(\mathbf{x}_i). \tag{8.1.9}$$

One can see that the system of equations (8.1.8) can be easily solved, since the left side is given by a diagonal matrix and can be inverted by hand as long as it contains no zero entries.

8.1.2 A simple example

Consider the minimization problem (8.1.1) with

$$f(x,y) = x^2 + y^2 - r^2.$$

One can easily see that the optimal domain for $E(\Omega)$ is the disc of radius r (cf. (8.1.2)). Starting from a domain $\Omega = D_{R_0}$, a disc of radius $R_0 \neq r$, the closest path is normal to the boundary Γ of Ω and thus applying Newton's algorithm (8.1.4) for E we have to solve:

$$\int_\Gamma (\theta \cdot n)(\xi \cdot n)\Big(\mathcal{H} f + \partial_n f\Big) = -\int_\Gamma (\xi \cdot n) f, \quad \forall \xi. \tag{8.1.10}$$

For our choice of f and $\Omega = D_{R_0}$, this reads

$$\int_{\partial D_{R_0}} (\theta \cdot n)(\xi \cdot n)\Big(\frac{1}{R_0}(R_0^2 - r^2) + 2R_0\Big) = -\int_{\partial D_{R_0}} (R_0^2 - r^2)(\xi \cdot n), \quad \forall \xi. \tag{8.1.11}$$

Hence, we deduce that

$$\theta_n = (\theta \cdot n) = -\frac{(R_0^2 - r^2)}{\frac{1}{R_0}(R_0^2 - r^2) + 2R_0}$$

As we would expect, θ_n is constant (independent of (x,y)). Using $\theta = \theta_n n$ to deform the shape, we obtain a new disc of radius

$$R_1 = R_0 + \theta_n = R_0 - \frac{(R_0^2 - r^2)}{\frac{1}{R_0}(R_0^2 - r^2) + 2R_0}.$$

By induction, we obtain a sequence of discs $\Omega_p = D_{R_p}$ of radius R_p such that

$$R_{p+1} = R_p - \frac{(R_p^2 - r^2)}{\frac{1}{R_p}(R_p^2 - r^2) + 2R_p}. \tag{8.1.12}$$

This sequence $(R_p)_{p\in\mathbb{N}}$ converges quadratically to $\Omega_r = D_r$, for all D_{R_0} sufficiently close to D_r. This is confirmed in Table 8.1 where the sequence (R_p) is given for the choices $R_0 = 2$ and $R_0 = 4$.

In comparison, we have tested Newton's algorithm (8.1.10) by the finite element dis-

Table 8.1 – The theoretical radius R_p given by (8.1.12) and the computed radius R_p^h of the minimizing sequence of discs obtained by Newton's algorithm.

Iteration p	Radius R_p			
	Numerical	Theoretical	Numerical	Theoretical
$p = 0$	1.9997	2.00	3.9994	4.00
$p = 1$	1.44204	1.45455	2.68647	2.7234
$p = 2$	1.13669	1.15105	1.85442	1.90104
$p = 3$	1.01764	1.02533	1.35543	1.39613
$p = 4$	0.99962	1.00091	1.09388	1.12276
$p = 5$	0.999731	1.00	1.00872	1.01758
$p = 6$	0.999727	1.00	0.999626	1.00045
$p = 7$	0.999727	1.00	0.99973	1.00

cretization described in Subsection 8.1.1. We stress that a filtering of the boundary mesh was necessary in order to compute correctly the discrete curvature (see Appendix A). At each iteration of Newton's algorithm, we obtained a correct approximation $\Omega_h^{(p)}$ of a disc whose radius R_p^h was computed thanks to the domain's area by the formula $R_p^h = \sqrt{|\Omega_h^{(p)}|/\pi}$. The results are reported in Table 8.1. There is a good agreement beetween the theoretical prediction R_p and its numerical counterpart R_p^h. A quadratic convergence is also observed.

8.1:

8.1.3 Numerical examples

Next, we compute the optimal shapes for problem (8.1.1) and for different functions f_i, namely:

$$
\begin{aligned}
f_1(x,y) &= (x^2+y^2)^5 - 2a^5(x^5 - 10x^3y^2 + 5xy^4) + a^{10} - b^{10} \\
f_2(x,y) &= ((x-0.5)^2+y^2)((x+0.5)^2+y^2) - 0.51^4 \\
f_3(x,y) &= \max(x^2 - 0.6^2, y^2 - 0.6^2),
\end{aligned}
$$

with $a = 0.95$, $b = 0.953$. These functions were inspired by [77].

The initial shape is a unit disc that we successively deform using the discretization (8.1.8), and a constant time step $t = 1$. The results are given in Figures 8.2-8.4.

One can see that the optimal shapes are easily computed after 7 iterations for f_1 and f_2. The convergence rate seems geometric rather than geometric, as illustrated in Figure

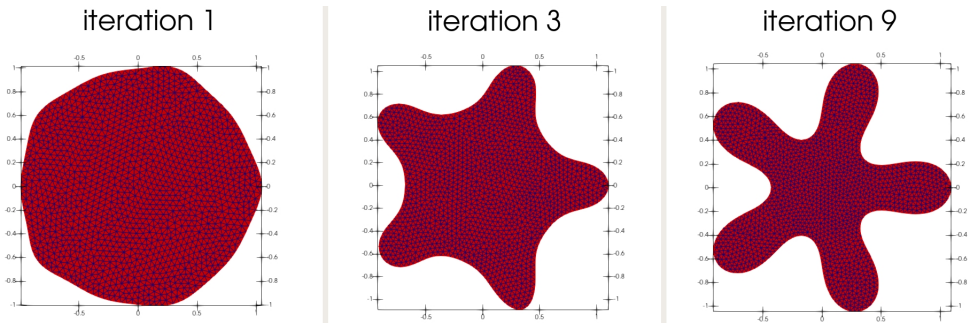

Figure 8.2 – Optimal (right) and intermediate shapes (left and middle) for minimizing $E(\Omega, f_1)$

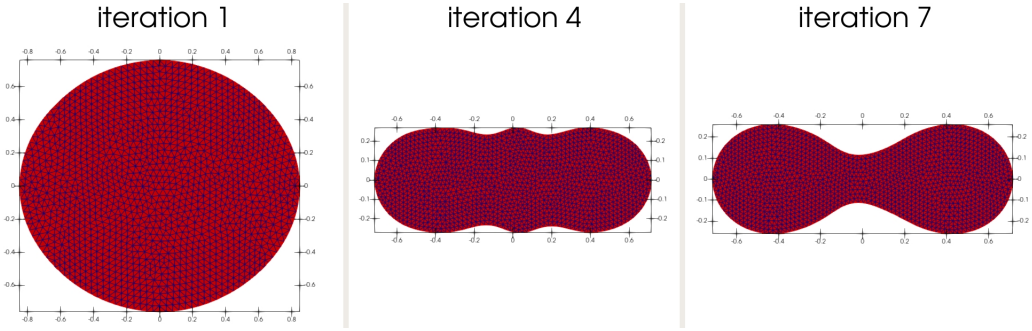

Figure 8.3 – Optimal (right) and intermediate shapes (left and middle) for minimizing $E(\Omega, f_2)$

8.7.

Figure 8.4 helps to illustrate an important issue with the computation of optimal shapes. The discretization (8.1.8) assumes that the optimal shapes are smooth, not only to be able to define the different discrete quantities necessary for the algorithm such as the normals to the boundary n_h, but also the structure of the second order shape derivative adopted in (8.1.3) is only valid for domains Ω that are at least C^3. Thus Newton's algorithm will fail to capture optimal shapes that contain corners or cusps. This is noticed in Figure 8.4 where the set of negative values of the $f_3(x, y)$ is clearly a square, but the algorithm never captures the square but gets stuck oscillating around shapes close to a square.

This oscillation can be seen in Figures 8.5 and 8.6 where we give the $L_\infty(\Omega_h)$ and $L_2(\Omega_h)$ norm of the computed descent directions θ_h. Both $\|\theta_h\|_{L_\infty}$ and $\|\theta_h\|_{L_2}$ converge rapidly for $E(\Omega, f_1)$ and $E(\Omega, f_2)$ after only 7 iterations. In contrast, for $E(\Omega, f_3)$, where the optimal shape is a square, we can see that while the value of the norms is low, it fails to converge and keeps on oscillating.

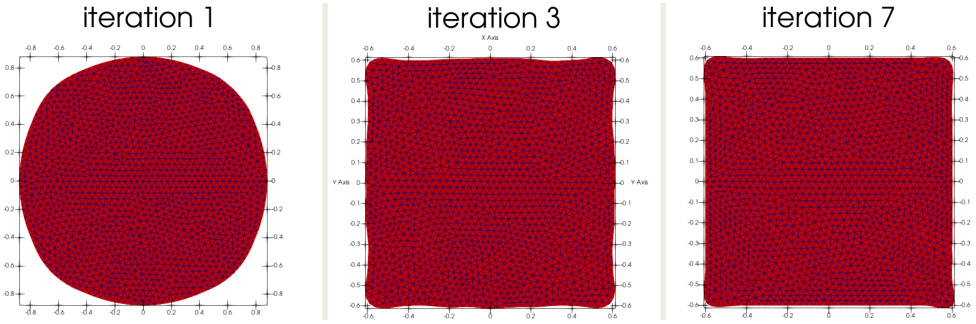

Figure 8.4 – Optimal (right) and intermediate shapes (left and middle) for minimizing $E(\Omega, f_3)$

Moreover, Figures 8.5 and 8.6 shows that both the L_∞ and L_2 norm are constant around the optimal shape, and our experiments suggest that this can be taken as a stopping criterion for Newton's algorithm. This contrasts with first order algorithms where $\|\theta_h\|_{L_\infty}$ or $\|\theta_h\|_{L_2}$ tend to oscillate around critical shapes.

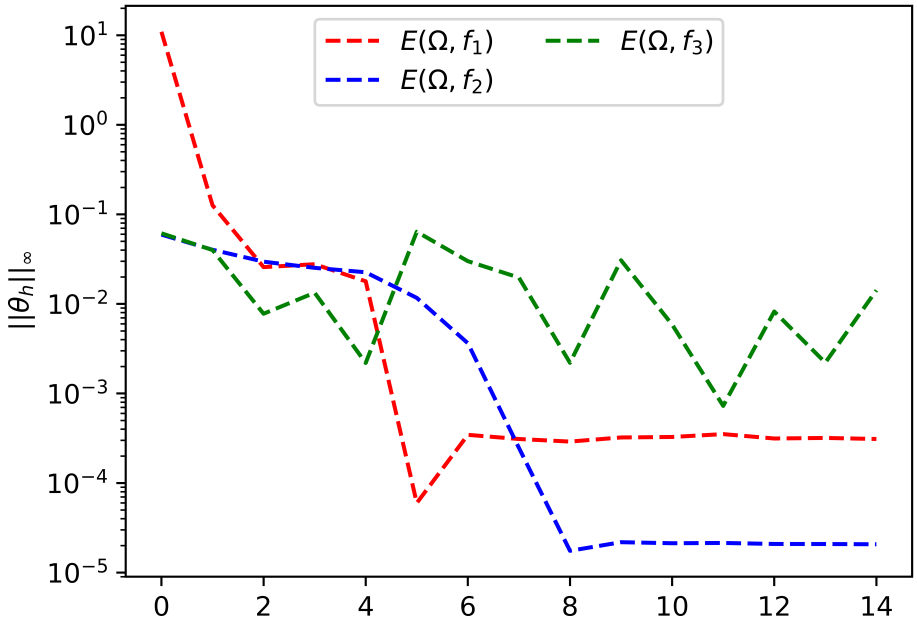

Figure 8.5 – The L_∞ norm of the computed descent direction θ_h at every iteration of the minimization process for the different functionals $E(\Omega, f_i)$

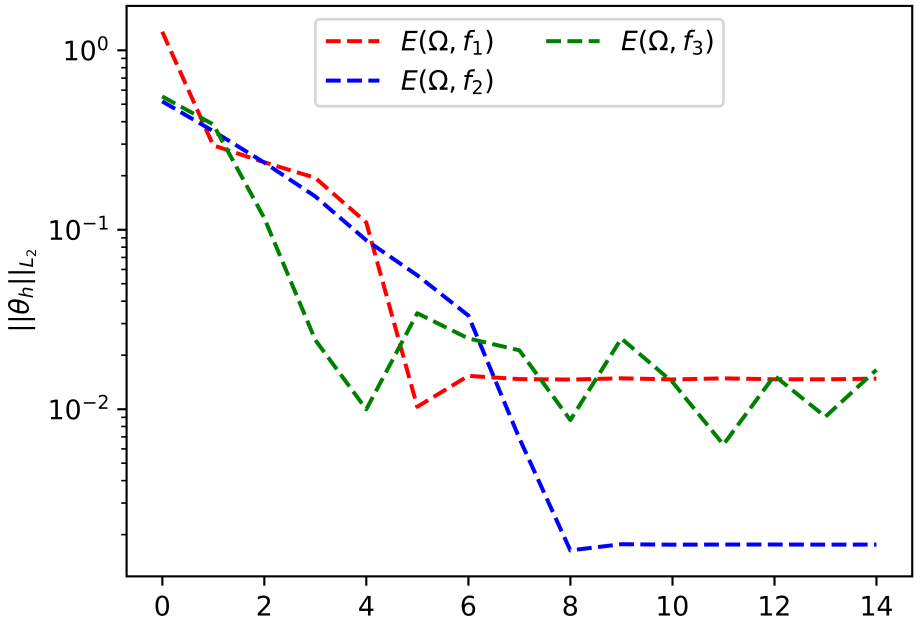

Figure 8.6 – The L_2 norm of the computed descent direction θ_h at every iteration of the minimization process for the different functionals $E(\Omega, f_i)$

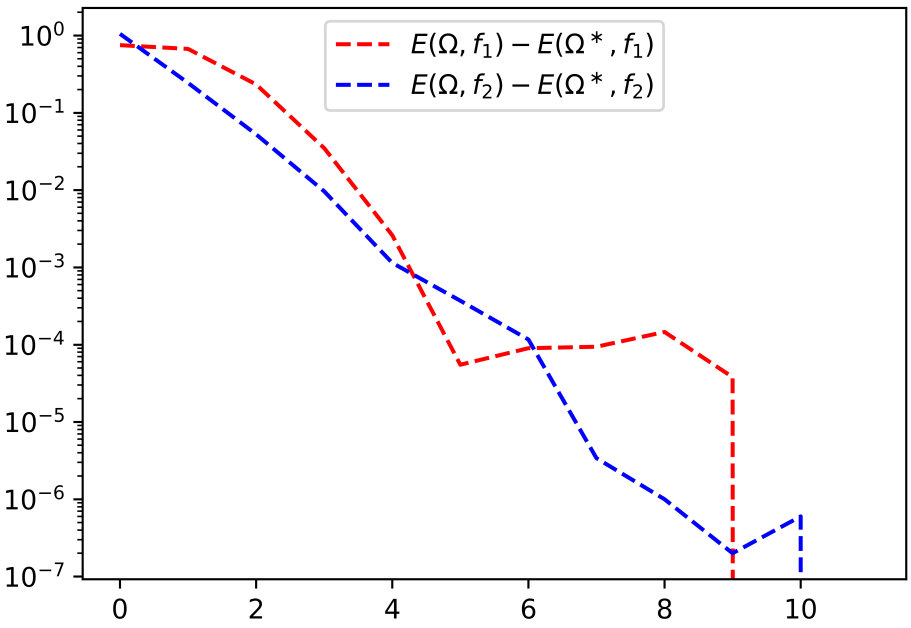

Figure 8.7 – The error to the best shape Ω^* at every iteration of the minimization process for the different functionals $E(\Omega, f_i)$

8.2 The Dirichlet energy

We now look at the general case of functionals that depend on the domain Ω through the solution u of a PDE. We consider the case of the Dirichlet energy (see [76])

$$J(\Omega) = \int_\Omega |\nabla u|^2 \tag{8.2.1}$$

where u is solution to the Dirichlet-Laplace problem

$$\begin{cases} -\Delta u &= 1 \qquad \text{in } \Omega, \\ u &= 0 \qquad \text{on } \Gamma. \end{cases} \tag{8.2.2}$$

Let $\mathcal{A}(\Omega)$ be an appropriate set of admissible domains large enough to contain a ball B_m of measure m. Then it is well known (see for example [18], [64], [76]) that the following shape optimization problem,

$$\max_{\substack{\Omega \in \mathcal{A}(\Omega) \\ |\Omega| = m}} J(\Omega, u) \tag{8.2.3}$$

has a solution which is the ball B_m.

We seek to compute this optimal shape $\Omega^* = B_m$ with our algorithm and to this end we need boundary expressions for the first and second order derivatives J' and J''. These derivatives have been extensively studied in shape optimization literature (see for example [50], [52] and the references therein). Here, we give the calculations for the sake of completeness, and also to rewrite the expressions in a suitable way that can be exploited by our discretization.

8.2.1 Computation of J' and J''

Let us first recall Hadamard's formulas for shape differentiation from [50].

Proposition 8.2.1. *Let Ω be a measurable bounded open set of $\mathbb{R}^d$. Let $f \in \mathbb{W}^{1,1}(\mathbb{R}^d, \mathbb{R}^d)$. The functional $F(\Omega) = \int_\Omega f(x)dx$ is shape-differentiable with*

$$\forall \theta \in W^{1,\infty}(\mathbb{R}^d, \mathbb{R}^d), \qquad F'(\Omega;\theta) = \int_\Omega \operatorname{div}(f\theta). \tag{8.2.4}$$

If, in addition, Ω has a Lipschitz boundary, one can write

$$F'(\Omega;\theta) = \int_{\partial\Omega} (\theta \cdot n) f. \tag{8.2.5}$$

For functionals defined by a boundary integral, we have:

Proposition 8.2.2. *Assume that Ω is a bounded domain of class C^3. Let also $g \in W^{2,1}(\mathbb{R}^d, \mathbb{R}^d)$. Then the functional $G(\Omega) = \int_{\partial\Omega} g(x)dx$ is shape-differentiable with*

$$\forall \theta \in W^{1,\infty}(\mathbb{R}^d, \mathbb{R}^d), \qquad G'(\Omega;\theta) = \int_{\partial\Omega} (\theta \cdot n)\Big(\partial_n g + \mathcal{H} g\Big). \tag{8.2.6}$$

We also need the following important result due to Simon [70] for the computation of the second order shape derivative.

Theorem 8.2.1. *Assume that $E(\Omega)$ is of class C^2. Then $\forall\, (\theta, \xi) \in \mathbb{W}^{2,\infty}(\mathbb{R}^d, \mathbb{R}^d)^2$ the 2^{nd} order derivative reads*

$$E''(\Omega;\theta,\xi) = (E')'(\Omega;\theta,\xi) - E'(\Omega;\theta \cdot \nabla\xi). \tag{8.2.7}$$

Finally, we will be using the following lemma for the tangential components.

Lemma 8.2.1. *Let $\theta, \xi \in C^{1,\infty}(\mathbb{R}^d;\mathbb{R}^d)$, and n the outer unit normal to the boundary Γ. Then*

$$(\xi\cdot\nabla)\theta\cdot n-(\xi\cdot n)\partial_n(\theta\cdot n)=(\xi_\Gamma\cdot\nabla)\theta\cdot n,$$

and

$$(\xi_\Gamma\cdot\nabla)\theta\cdot n=\xi_\Gamma\cdot\nabla_\Gamma(\theta\cdot n)-D_\Gamma n\,\xi_\Gamma\cdot\theta_\Gamma.$$

Proof. The decomposition of ξ in its tangential and normal components gives

$$(\xi\cdot\nabla)\theta\cdot n=(\xi_\Gamma\cdot\nabla)\theta\cdot n+(\xi\cdot n)\Big((n\cdot\nabla)\theta\cdot n\Big).$$

Given that $\|n\|=1$, we have $(n\cdot\nabla)n=0$. Then,

$$(n\cdot\nabla)\theta\cdot n=\nabla(\theta\cdot n)\cdot n-(n\cdot\nabla)n\cdot\theta=\nabla(\theta\cdot n)\cdot n,$$

and

$$(\xi\cdot\nabla)\theta\cdot n=(\xi_\Gamma\cdot\nabla)\theta\cdot n+(\xi\cdot n)\partial_n(\theta\cdot n).$$

On the other hand,

$$\begin{aligned}(\xi_\Gamma\cdot\nabla)\theta\cdot n&=\nabla(\theta\cdot n)\cdot\xi_\Gamma-(\xi_\Gamma\cdot\nabla)n\cdot\theta,\\(\xi_\Gamma\cdot\nabla)n\cdot n&=\nabla(\theta\cdot n)\cdot\xi_\Gamma-D_\Gamma n\theta_\Gamma\cdot\theta_\Gamma.\end{aligned}$$

□

We have the following theorem for the shape derivatives of $J(\Omega)$.

Theorem 8.2.2. *Let $\Omega\in\mathcal{O}_3$. then the Dirichlet energy $J(\Omega)$ defined in* (8.2.1) *is twice shape differentiable, and for all $\theta,\xi\in\mathbb{W}^{2,\infty}(\mathbb{R}^d,\mathbb{R}^d)$ we have*

$$J'(\Omega;\xi)=\int_\Gamma(\xi\cdot n)(\partial_n u)^2 \tag{8.2.8}$$

and

$$J''(\Omega;\theta,\xi) = \int_\Gamma (\theta\cdot n)\nabla u'_\xi\cdot\nabla u + \int_\Gamma (\xi\cdot n)\nabla u'_\theta\cdot\nabla u + \int_\Gamma (\theta\cdot n)(\xi\cdot n)\Big[(\partial_n+\mathcal{H})|\nabla u|^2\Big] + \int_\Gamma Z_{\theta,\xi}|\nabla u|^2 \tag{8.2.9}$$

where

$$Z_{\theta,\xi} = D_\Gamma n\,\theta_\Gamma\cdot\xi_\Gamma - \xi_\Gamma\cdot\nabla_\Gamma(\theta\cdot n) - \theta_\Gamma\cdot\nabla_\Gamma(\xi\cdot n).$$

The function u'_ξ is the shape derivative of the state function u, and is solution to the following problem:

$$\begin{cases} -\Delta u'_\xi &= 0 & \text{in } \Omega,\\ u'_\xi &= -(\xi\cdot n)\partial_n u & \text{on } \Gamma. \end{cases} \tag{8.2.10}$$

Proof of Theorem 8.2.2. The computation of the first order derivative is a straight forward application of Hadamard's formula for domain integrals, we thus have:

$$J'(\Omega;\xi) = 2\int_\Omega \nabla u'_\xi\cdot\nabla u + \int_\Omega \operatorname{div}\left(\xi|\nabla u|^2\right). \tag{8.2.11}$$

Problem (8.2.10) is obtained by differentiating the Dirichlet-Laplace problem (8.2.2) (see [50]). In general, the differentiation on the boundary Γ is obtained by differentiating the transported boundary condition

$$u_t\circ\phi(t) = 0$$

where t denotes the time step, $\phi(t) = (I + t\xi)$ and u_t the solution of (8.2.2) on $\Omega_t = (I + t\xi)(\Omega)$. This gives

$$u'_\xi + \xi\nabla u = 0 \qquad \text{and} \qquad \nabla_\Gamma u = 0.$$

which gives the second equation in (8.2.10). The differentiation in the interior of the domain Ω is easy to obtain in the weak sense, if Ω is open and $v\in C_0^\infty(\Omega)$, for small t, we also have $v\in C_0^\infty(\Omega_t)$ and therefore

$$\int_{\mathbb{R}^d} v = \int_{\Omega_t} v = \int_{\Omega_t}\nabla u_t.\nabla v = \int_{\mathbb{R}^d} -\Delta u_t v.$$

By differentiation, we obtain

$$\int_\Omega -\Delta u' v = 0, \qquad \forall v \in C_0^\infty(\Omega),$$

from which we deduce the first equation in (8.2.10).

Finally, using problem (8.2.10), and an integration by parts in (8.2.8), we find that the first term cancels out and we get

$$J'(\Omega;\xi) = \int_\Omega \mathrm{div}(\xi|\nabla u|^2).$$

Using the divergence theorem gives

$$J'(\Omega;\xi) = \int_\Gamma (\xi\cdot n)|\nabla u|^2. \tag{8.2.12}$$

One then can see that due to the Dirichlet boundary condition, we have that $\nabla_\Gamma u = 0$, thus $|\nabla u|^2 = (\partial_n u)^2$. This, however, only makes the calculations and numerical implementation more complexe. We shall therefore consider the expression (8.2.12) for the rest of the calculations. We now can use Lemma 8.2.1 to compute the second order derivative of J. First differentiating J' in the direction ξ we get:

$$\begin{aligned} J''(\Omega;\xi,\xi) &= \Big(J'(\Omega;\xi)\Big)' - J'(\Omega;(\xi\cdot\nabla)\xi) \\ &= -\int_\Gamma \xi\cdot\nabla_\Gamma(\xi\cdot n)|\nabla u|^2 + 2\int_\Gamma (\xi\cdot n)\nabla u'_\xi\cdot\nabla u + \int_\Gamma (\xi\cdot n)^2\Big[(\partial_n+\mathcal{H})|\nabla u|^2\Big] \\ &\quad + \int_\Gamma (\xi\cdot n)\partial_n(\xi\cdot n)|\nabla u|^2 - \int_\Gamma \Big((\xi\cdot\nabla)\xi\cdot n\Big)|\nabla u|^2. \end{aligned}$$

To bring out the canonical form of the second order derivative, we use Lemma 8.2.1 for the decomposition of ξ in tangential components to rewrite the last integral in the equation above. This gives

$$\begin{aligned} J''(\Omega;\xi,\xi) = 2\int_\Gamma (\xi\cdot n)\nabla u'_\xi\cdot\nabla u + \int_\Gamma (\xi\cdot n)^2\Big[(\partial_n+\mathcal{H})|\nabla u|^2 \\ + \int_\Gamma \Big[D_\Gamma n\,\xi_\Gamma\cdot\xi_\Gamma - 2\xi_\Gamma\cdot\nabla_\Gamma(\xi\cdot n)\Big]|\nabla u|^2 \end{aligned}$$

Finally, we use a polarization formula to get a symmetric form of $J''(\Omega;\theta,\xi)$:

$$J''(\Omega;\theta,\xi) = \frac{1}{2}\Big[J''(\Omega,\theta+\xi,\theta+\xi) - J''(\Omega,\theta,\theta) - J''(\Omega,\xi,\xi)\Big]$$

with

$$\begin{aligned} u'_{\theta+\xi} &= -\Big((\theta+\xi)\cdot n\Big)\partial_n u \\ &= -(\theta\cdot n)\partial_n u - (\xi\cdot n)\partial_n u \\ &= u'_\theta + u'_\xi \quad \text{ on } \Gamma. \end{aligned}$$

This gives the final expression

$$\begin{cases} J''(\Omega;\theta,\xi) & = \int_\Gamma (\theta\cdot n)\nabla u'_\xi\cdot\nabla u + \int_\Gamma (\xi\cdot n)\nabla u'_\theta\cdot\nabla u \\ & \qquad + \int_\Gamma (\theta\cdot n)(\xi\cdot n)\Big[(\partial_n+\mathcal{H})|\nabla u|^2\Big] + \int_\Gamma Z_{\theta,\xi}|\nabla u|^2, \\ Z_{\theta,\xi} & = D_\Gamma n\,\theta_\Gamma\cdot\xi_\Gamma - \xi_\Gamma\cdot\nabla_\Gamma(\theta\cdot n) - \theta_\Gamma\cdot\nabla_\Gamma(\xi\cdot n). \end{cases}$$

□

Remark 8.2.1. *Notice that, a priori the expression of the second order shape derivative J'' given by* (8.2.9) *is problematic for numerical applications since one would have to solve extra problems for the shape derivatives of the state functions u'_θ, u'_ξ at every iteration. To get around this problem, it is common practice in shape optimization to introduce adjoint problems for the shape derivatives, and such formulas for the Dirichlet energy are well known in the literature (see for example [50], [52], and the references therein). In our case, it is easier to keep these derivatives. This is because our discretization only calls for the values of the shape derivatives on the boundary Γ, and we will always have an expression for these quantities, expressions obtained by differentiating the boundary conditions of the state problem. Moreover, these expressions are simplified for normal deformations θ,ξ. This makes the construction of the Hessian matrix according to discretization* (8.1.8) *much more easier, as we shall see next.*

8.2.2 Volume constraint and discretization

Before we proceed to the discrete optimization problem we will need the first and second order shape derivatives of the volume constraint $V(\Omega) = \int_\Omega dx$. The following corollary is easily obtained by taking $f(x,y) = 1$ in the expression of (8.1.3).

Corollary 8.2.2.1. *Let $\Omega \in \mathcal{O}_3$, then the volume functional $V(\Omega)$ is twice shape differ-*

entiable, and for all $\theta, \xi \in \mathbb{W}^{2,\infty}(\mathbb{R}^d, \mathbb{R}^d)$ *we have*

$$V'(\Omega; \xi) = \int_\Gamma (\xi \cdot n), \tag{8.2.13}$$

and

$$V''(\Omega; \theta, \xi) = \int_\Gamma \mathcal{H}(\theta \cdot n)(\xi \cdot n) + \int_\Gamma Z_{\theta,\xi}. \tag{8.2.14}$$

Let us now look at the shape optimization problem (8.2.3). We now have to deal with the volume constraint throughout the optimization process, and to do so we follow the results in [16, chapter 14]. In general, for a given constraint $c(\Omega)$, the right approach is to minimize the objective $J(\Omega)$ while keeping the constraint satisfied, which is called a primal-dual method. To describe this, according to the first-order optimality conditions, we know that when the constraint is qualified at a solution Ω^*, there exists a Lagrange multiplier $\lambda_* \in \mathbb{R}$ such that

$$\begin{cases} J'(\Omega^*; \xi) + \lambda_* c'(\Omega^*, \xi) & = 0, \quad \forall \xi, \\ c(\Omega^*) = 0. \end{cases} \tag{8.2.15}$$

Thus, introducing the Lagrangian

$$L(\Omega_p, \lambda_p) = J(\Omega_p) + \lambda_p c(\Omega_p), \tag{8.2.16}$$

Newton's method defines a step in (Ω, μ) at (Ω_p, λ_p) by linearizing the system (8.2.15). One finds

$$\begin{pmatrix} L_p'' & A_p^T \\ A_p & 0 \end{pmatrix} \begin{pmatrix} \theta_p \\ \mu_p \end{pmatrix} = - \begin{pmatrix} L_p' \\ c_p \end{pmatrix}, \tag{8.2.17}$$

where $L_p'' := L''(\Omega_p; \theta, \xi)$ $L_p' := L'(\Omega_p; \xi)$ are the first and second order shape derivatives of the Lagrangian L and $A_p := c'(\Omega_p; \xi)$ is the shape derivative of the constraint. Given a solution (θ_p, μ_p) to (8.2.17), the Newton method defines the next iterate $(\Omega_{p+1}, \lambda_{p+1})$ by

$$\Omega_{p+1} = (I + \theta_p)(\Omega_p) \qquad \text{and} \qquad \lambda_{p+1} = \lambda_p + \mu_p.$$

We then proceed to build the left hand side of (8.2.17) using our discretization described earlier in Subsection 8.1.1. Once again, taking $\theta_h = \alpha n_h$ and $\xi_h = n_h$, we obtain

that A_p is the row vector with entries

$$\begin{aligned} A_p[i] &= \int_{T_i \cap \Gamma_h} n_h(x) \cdot n_h(x) dx \\ &= \int_{\mathbf{x}_i - h}^{\mathbf{x}_i + h} dx \\ &= 1 \quad \text{(up to a factor } h\text{)}. \end{aligned}$$

The matrix $L_p^{''}$ is the Hessian of the Lagrangian L which is a diagonal matrix of size $n_{be} \times n_{be}$ with diagonal entries given by:

$$L_p^{''}[i,i] = \int_{T_i \cap \Gamma_h} \Big[2\nabla u_n^{h'}(x) \cdot \nabla u^h(x) + (\partial_n + \kappa_h(x)) |\nabla u^h(x)|^2 + \lambda \kappa_h(x) \Big] dx$$

where we used the expressions (8.2.9) and (8.2.14) to compute $L^{''}(\Omega; n_h, n_h)$. Similarly, we have for a small edge size $h \to 0$

$$\begin{aligned} L_p^{''}[i,i] &= \int_{\mathbf{x}_i - h}^{\mathbf{x}_i + h} \Big[2\nabla u_n^{h'}(x) \cdot \nabla u^h(x) + (\partial_n + \kappa_h(x)) |\nabla u^h(x)|^2 + \lambda \kappa_h(x) \Big] dx \\ &= 2\nabla u_n^{h'}(\mathbf{x}_i) \cdot \nabla u^h(\mathbf{x}_i) + (\partial_n + \kappa_h(\mathbf{x}_i)) |\nabla u^h(\mathbf{x}_i)|^2 + \lambda \kappa_h(\mathbf{x}_i). \end{aligned}$$

Going back to the variational formulation (8.2.10), we have that $u'_\theta = (\theta \cdot n) \partial_n u$, in particular this gives

$$u_n{}' = \partial_n u.$$

Thus we can write

$$\begin{aligned} \nabla u_n{}' &= \nabla(\nabla u \cdot n) \\ &= D^2 u \, n + Dn . \nabla u \\ &= D^2 u . n + \partial_n u \, Dn . n \qquad (\nabla_\Gamma u = 0) \\ &= D^2 u . n \qquad (Dn . n = 0 \text{ since } n \text{ is unitary on } \Gamma). \end{aligned}$$

This allows us to rewrite $\nabla u_n^{h'} = D^2 u^h . n$, which should seem problematic at first sight. A priori, u^h is only $\mathbb{P}_1$ and thus $\nabla u^h = (\partial_x u^h, \partial_y u^h)^T$ is only a $\mathbb{P}_0$ function on $\mathcal{T}_h$. i.e. it is constant on each triangle T_i. We thus seek to lift this function as a $\mathbb{P}_1$ function. The easiest way to do so is by interpolation, but our experiments show that the most accurate way to do this is through a least-squares matching of the gradient ∇u^h on the vertices $\mathbf{x}_i$ of Γ. This is described in detail in Appendix A.1. In particular, we define the operator

∇_i^h,

$$\begin{cases} \nabla_i^h : \mathcal{V}_h \Longrightarrow \mathcal{V}_h \times \mathcal{V}_h \\ \varphi_h \mapsto \nabla_i^h \varphi_h = g \approx \nabla \varphi_h(\mathbf{x}_i), \end{cases}$$

where g is the solution to the system $A^T A g = A^T b$, with

$$A = \begin{pmatrix} \mathbf{x}_1^1 - \mathbf{x}_1^i & \mathbf{x}_2^1 - \mathbf{x}_2^i \\ \mathbf{x}_1^2 - \mathbf{x}_1^i & \mathbf{x}_2^2 - \mathbf{x}_2^i \\ \vdots & \vdots \\ \mathbf{x}_1^m - \mathbf{x}_1^i & \mathbf{x}_2^m - \mathbf{x}_2^i \end{pmatrix} \qquad \text{and} \qquad b = \begin{pmatrix} \varphi_h(\mathbf{x}^1) - \varphi_h(\mathbf{x}^i) \\ \varphi_h(\mathbf{x}^2) - \varphi_h(\mathbf{x}^i) \\ \vdots \\ \varphi_h(\mathbf{x}^m) - \varphi_h(\mathbf{x}^i) \end{pmatrix}$$

and m is the number of neighboring vertices of $\mathbf{x}_i$ (see Figure A.1). Not only is this an accurate way of approximating the gradient, but its local character also allows us to cut down on unnecessary computations on the interior of the domain Ω_h. Indeed, $L_p^{''}$ is only defined on the boundary Γ_h, we only need the values of the gradient as a $\mathbb{P}_1$ function on a neighborhood of the boundary vertices $\mathbf{x}_i$. Notice also that this solves the issue of computing the term $\partial_n\big(|\nabla u|^2\big)$, we can compute

$$\partial_n\big(|\nabla u^h|^2\big)(\mathbf{x}_i) = \nabla_i^h\big(|\nabla^h u_h|^2\big).$$

Ultimately, the diagonal entries of the Hessian $L_p^{''}$, and the entries of L_p' read

$$L_p^{''}[i,i] = 2\nabla_i^h\big(\nabla^h u_h\big).n_h(\mathbf{x}_i) \cdot \nabla_i^h u_h + \nabla_i^h\big(|\nabla^h u_h|^2\big) + \kappa_h(\mathbf{x}_i)\big(\lambda + |\nabla_i^h u_h|^2\big) \tag{8.2.18}$$

$$L_p'[i] = \lambda + \big(\nabla_i^h u_h \cdot n_h(\mathbf{x}_i)\big)^2. \tag{8.2.19}$$

8.2.3 Numerical results

In what follows, we test our discretization to compute the optimal shape Ω^* for minimizing the Dirichlet energy (8.2.1) under volume (area, since $d = 2$) contraint $|\Omega| = 0.4$. Recall that the optimal shape in this case is a disc of volume 0.4. Starting from a random guess, we successively compute a descent direction by solving (8.2.17) that we use to move the shape with a constant step $t = 1$. Figure 8.8 shows the starting and optimal shapes, the algorithm converges to a ball. The optimal shape is reached quickly (about 20 iterations), as seen in Figures 8.9 and 8.10. Figure 8.11 shows that the constraint volume is reasonably satisfied during the whole process.

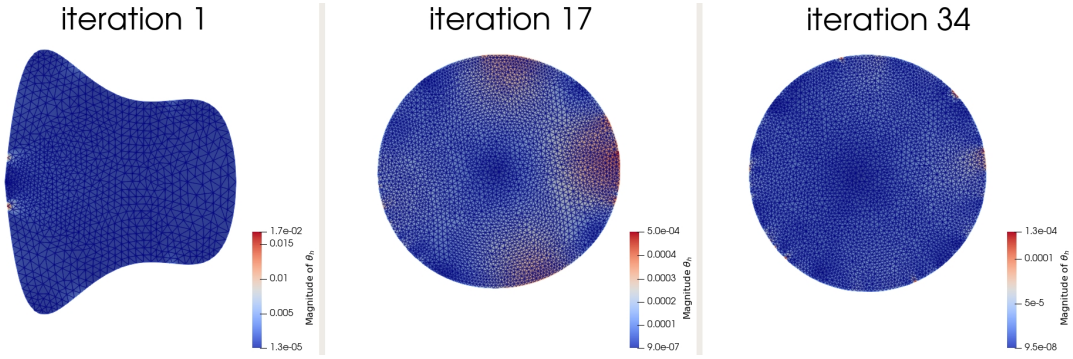

Figure 8.8 – The starting shape (left), the optimal shape Ω^* (middle) and the best shape $\Omega^\times$ (right), with the magnitude of the descent direction θ for the minimization of the Dirichlet energy.

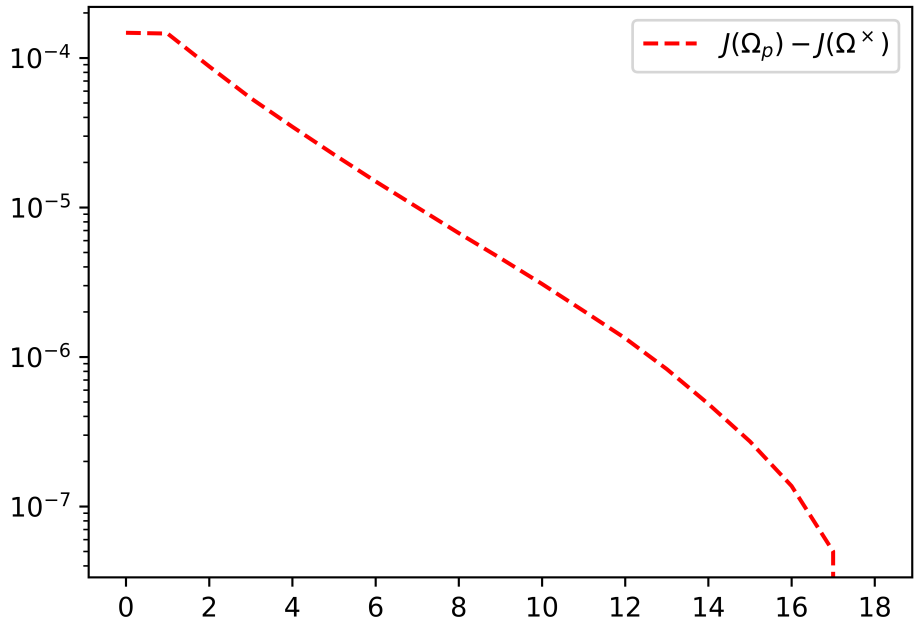

Figure 8.9 – The error to the best shape $\Omega^\times$ at every iteration of the minimization process.

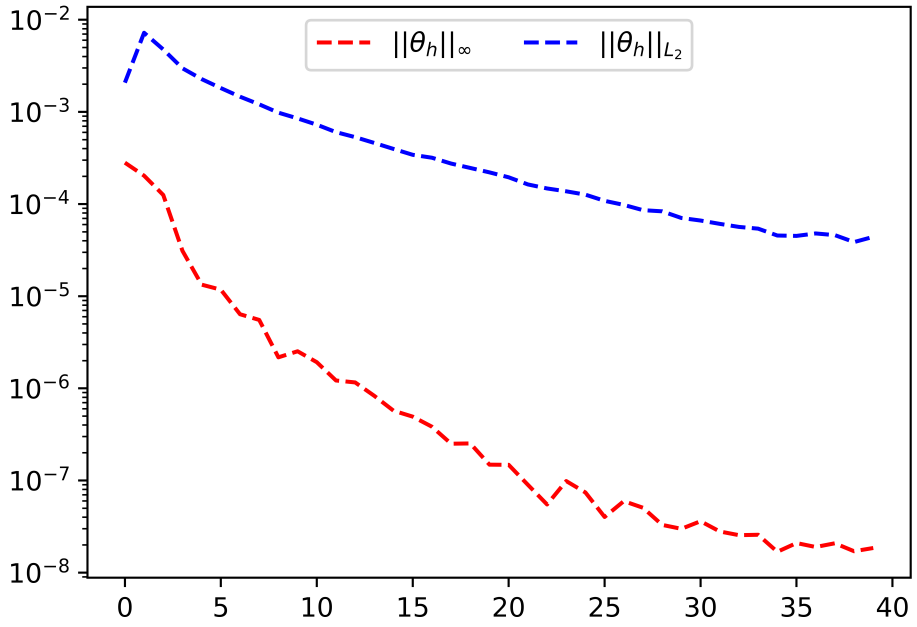

Figure 8.10 – The L_∞ and L_2 norm of the descent direction θ_h at every iteration of the minimization process.

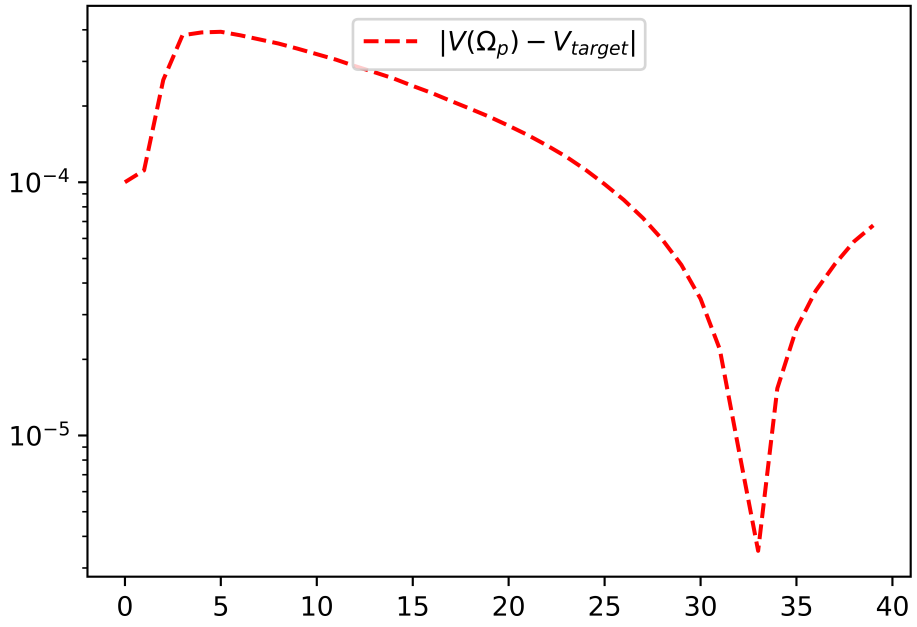

Figure 8.11 – The infeasibility of the constraint $|V(\Omega_p) - V_{target}|$.

8.3 Laplacian with a regular kernel

Let $k \in C^2(\mathbb{R}^d \times \mathbb{R}^d)$ be a symmetric (i.e. $k(x,x') = k(x',x)$) and regular kernel. In this section, we look at the shape differentials of a general energy functional

$$J(\Omega) = \int_\Omega |\nabla u|^2 dx + \int_\Omega \int_\Omega k(x,x')u(x)u(x')dxdx', \tag{8.3.1}$$

where u is a solution to the Dirichlet-Laplace problem

$$\begin{cases} -\Delta u + \int_\Omega k(\cdot,x')u(x')dx' &= C \qquad \text{in } \Omega, \\ u = 0 \qquad \text{on } \Gamma, \\ \int_\Omega u = 1. \end{cases} \tag{8.3.2}$$

The shape differentiability of the mapping $\xi \mapsto u_\xi$ is obtained through an implicit function argument and follows the same steps as in [50, Theorem 5.3.2]. We recall that u_ξ denotes the solution of (8.3.2) in the set $\Omega_\xi = (I+\xi)(\Omega)$. For a given $\xi \in W^{2,\infty}(\mathbb{R}^d,\mathbb{R}^d)$, we find that the derivative u'_ξ of $t \mapsto u_{t\xi}$ at $t=0$ satisfies

$$\begin{cases} -\Delta u'_\xi + \int_\Omega k(\cdot,x')u'_\xi(x')dx' &= C'_\xi(0) \quad \text{in } \Omega, \\ u'_\xi = -(\xi\cdot n)\partial_n u \text{ on } \Gamma, \\ \int_\Omega u'_\xi = 0. \end{cases} \tag{8.3.3}$$

We have used here that

$$\int_\Gamma (\xi\cdot n)k(\cdot,x')u(x')dx' = 0,$$

since $u = 0$ on Γ.

Let us then examine the shape derivatives of $J(\Omega)$. We multiply the first equation in (8.3.2) by u and we integrate on Ω. An integration by parts shows that $J(u_\xi) = C_{t\xi}$ (the constant C on $\Omega_{t\xi}$) and so $J'(\Omega;\xi) = C'_\xi(0)$.

Next, we multiply the first equation in (8.3.3) by u and we integrate on Ω. This yields

$$\begin{aligned} C'_\xi(0)\int_\Omega u &= -\int_\Omega u\Delta u'_\xi + \int_\Omega k(x,x')u'_\xi(x')u(x)dx'dx. \\ &= \int_\Gamma \partial_n u u'_\xi - \int_\Omega u'_\xi \Delta u + \int_\Omega k(x,x')u'_\xi(x')u(x)dx'dx. \end{aligned}$$

Now we multiply by u'_ξ the first equation in (8.3.2), we integrate on Ω and we use that k

is symmetric. We obtain that

$$C'_\xi(0) = \int_\Gamma \partial_n u u'_\xi + C \int_\Omega u'_\xi,$$

and so, with the second and third equations in (8.3.3),

$$J'(\Omega;\xi) = C'_\xi(0) = -\int_\Gamma (\xi \cdot n)(\partial_n u)^2.$$

Notice that this is the same expression as the one obtained for the Dirichlet energy earlier in (8.2.8) (up to the minus sign) . Using Theorem 8.2.1 one can see that the expression of the second order derivative is completely determined by the expression of the first order derivative, and the equation of the shape derivative of the state function u'. This means that the computation of the second order derivative is exactly the same as in the proof of Theorem 8.2.2 (up to the minus sign), and we obtain

$$\begin{aligned} J''(\Omega;\theta,\xi) = &-\int_\Gamma (\xi \cdot n)\nabla u'_\xi \cdot \nabla u - \int_\Gamma (\theta \cdot n)\nabla u'_\theta \cdot \nabla u \\ &- \int_\Gamma (\theta \cdot n)(\xi \cdot n)\Big[(\partial_n + \mathcal{H})|\nabla u|^2\Big] - \int_\Gamma Z_{\theta,\xi}|\nabla u|^2. \end{aligned} \tag{8.3.4}$$

This expression makes sense if u' is regular enough, which means if the domain Ω is regular (usually, C^3) and if the kernel k is regular enough.

To summarize, the same discretization as in subsection 8.2 can be used to perform second order shape optimization of an energy functional of type (8.3.1), assuming enough regularity both on the domain Ω and the kernel $k(x)$. Even in situations where these regularity constraints are not satisfied, for example the case where the domain Ω contains corners at the intersection of different boundary conditions, or the case when the case when the kernel k is not regular enough, we shall see in section 9.2.2 for our numerical application that the discretization (8.2.17) provides enough flexibility to get around these issues, and still hope to find an optimal shape.

Chapter 9

Mean value and variance of the optimal hull with optimized support

9.1 Theoretical results

We introduce a "bounding box", namely a bounded and connected open subset Q of the upper half plane $\{(x,z) \in \mathbb{R}^2 \ : \ z > 0\}$. We assume that Q has a Lipschitz boundary ∂Q such that $\partial Q \cap (\mathbb{R} \times \{0\})$ is a segment of the x-axis (possibly empty). We denote $\Gamma_{N,Q}$ the (relative) interior of this segment and $\Gamma_{D,Q} = \partial D \setminus \Gamma_{N,Q}$.

For instance, Q can be a half disc with a large radius and centered on the x-axis or a rectangle with one side of its boundary included in the x-axis.

We introduce the Sobolev space

$$H(Q) = \left\{ u \in H^1(Q) \ : u = 0 \text{ on } \Gamma_{D,Q} \text{ in the sense of trace} \right\},$$

equipped with the H^1 norm. For each function $u \in H^1(Q)$, we denote its support by

$$D_u = \{(x,z) \in Q \ : \ u(x,z) \neq 0\}.$$

The set D_u is unique up to a set of zero Lebesgue-measure and its area $|D_u|$ does not depend on the choice of the representative of u.

Let $a \in (0, |Q|)$ (an area) and $\mathcal{V} > 0$ (a volume). Following [26], we introduce the set

$$C_{\mathcal{V},a}(Q) = \left\{ u \in H(Q) \ : \ \int_Q u \, dxdz = \mathcal{V} \text{ and } |D_u| \leq a \right\}.$$

The set $C_{\mathcal{V},a}$ is a closed subset of $H(Q)$.

As in Section 7.1, we assume that the Kelvin wave number is a random variable

$\nu : \Omega \to \mathbb{R}$ whose probability distribution has a compact support in $(0, +\infty)$.

For $u \in H(Q)$, the functional is

$$\mathcal{J}(u) = \mathbb{E}\left[\tilde{h}(\nu)\left(2a + J_0(u) + \frac{1}{C_F} J_{wave}(u, \nu)\right)\right],$$

where $\tilde{h} : (0, +\infty) \to (0, +\infty)$ is a continuous function which depends on the fixed parameters ρ, g and C_F. The functions J_0 and J_{wave} are defined as previously, except that the integration on D is replaced by an integration on Q. That is, we have

$$J_0(u) = \int_Q |\nabla u|^2 dxdz$$

and

$$J_{wave}(u, \alpha) = \frac{8\alpha^4}{\pi} \int_1^\infty |T(u, \alpha, \lambda)|^2 \frac{\lambda^4}{\sqrt{\lambda^2 - 1}} d\lambda,$$

where T is defined for all $u \in H(Q)$, $\alpha > 0$ and $\lambda > 0$ by

$$T(u, \alpha, \lambda) = \int_Q u(x, z) e^{-i\lambda\alpha x} e^{-\lambda^2 \alpha z} dxdz.$$

We recall that the bounding box Q and the function $\tilde{h}$ are given, and that the positive parameters ρ, g, C_F, a and $\mathcal{V}$ are fixed. The problem reads:

$$\text{Find } u^\star \in C_{\mathcal{V},a}(Q) \text{ such that } \mathcal{J}(u^\star) = \min_{u \in C_{\mathcal{V},a}(Q)} \mathcal{J}(u). \tag{9.1.1}$$

The support $D_{u^\star}$ of $u^\star$ will be called on *optimal domain*. We note that $u^\star$ is generally not unique, because $\mathcal{J}$ is invariant with respect to translations along the x-axis. Moreover, the set $C_{\mathcal{V},a}(Q)$ is not convex, so that an optimal domain $D_{u^\star}$ is not necessarily unique up to translations along the x-axis.

We have:

Theorem 9.1.1. *Problem* (9.1.1) *has at least one solution* $u^\star$.

Proof. Let $(u_n)_n$ be a minimizing sequence in $C_{\mathcal{V},a}(Q)$. We have

$$\mathcal{J}(u_n) = 2a\mathbb{E}\left[\tilde{h}(\nu)\right] + \mathbb{E}\left[\tilde{h}(\nu)\right] J_0(u_n) + \frac{1}{C_F}\mathbb{E}\left[\tilde{h}(\nu) J_{wave}(u_n, \nu)\right],$$

and each term in the sum above is nonnegative. This implies that the sequence $(J_0(u_n))_n$ is bounded, and so (u_n) is bounded in $H^1(Q)$, by the Poincaré inequality. Let $q' > 5$.

By compactness, there is a subsequence still denoted (u_n) and $u^\star \in H(Q)$ such that (u_n) converges to $u^\star$ weakly in $H(Q)$, strongly in $L^{q'}(Q)$ and a.e. in Q. By Fatou's lemma, we have

$$|D_{u^\star}| = \int_Q 1_{u^\star} dxdz \leq \liminf_n \int_Q 1_{u_n} dxdz = |D_{u_n}| \leq a,$$

where 1_v denotes the characteristic function of a function $v \in H(Q)$. Thus, $u^\star$ belongs to $C_{\mathcal{V},a}(Q)$.

By lower semi-continuity of J_0, we have

$$J_0(u^\star) \leq \liminf_n J_0(u_n). \tag{9.1.2}$$

We may apply Proposition 7.2.2 with the set D replaced by Q. Since (u_n) converges strongly in $L^{q'}(Q)$, we have

$$\mathbb{E}\left[\tilde{h}(\nu) J_{wave}(u_n, \nu)\right] \to \mathbb{E}\left[\tilde{h}(\nu) J_{wave}(u^\star, \nu)\right]. \tag{9.1.3}$$

The relations (9.1.2) and (9.1.3) show that

$$\mathcal{J}(u^\star) \leq \liminf_n \mathcal{J}(u_n).$$

Since (u_n) is a minimizing sequence, this proves that $u^\star$ is a solution to problem (9.1.1). □

9.2 Numerical results

We want to compute the optimal shape for minimizing the expectation of the total water resistance $\mathcal{J}$ under volume constraint, that is we wish to solve the following problem,

$$\min_{\substack{D \in \mathcal{A}(Q) \\ |D| = a}} \mathcal{J}(D), \tag{9.2.1}$$

where $\mathcal{A}(Q)$ is the set of admissible sets in Q. Recall from (7.3.5) that solving (9.2.1) is the same as solving

$$\min_{\substack{D \in \mathcal{A}(Q) \\ |\Omega| = m}} \tilde{\mathcal{J}}(D, u_D) \tag{9.2.2}$$

where

$$\tilde{\mathcal{J}}(D,u) = \int_D |\nabla u|^2 + \frac{1}{C_F \mathbb{E}[\tilde{h}(\nu)]} \int_{D\times D} H_\alpha(x,z,x',z') u(x,z) u(x',z'),$$

and u_D is the minimizer of the problem

$$\min \left\{ \tilde{\mathcal{J}}(D,u) \ : \ u \in H(D),\ \int_D u = \mathcal{V} \right\}.$$

The shape sensitivity analysis of $\tilde{\mathcal{J}}$ is studied in subsection 8.3. We introduce the space

$$\mathcal{F}_k = \Big\{ \xi \in \mathbb{W}^{k,\infty}(\mathbb{R}^2,\mathbb{R}^2), \quad \xi \cdot n = 0 \quad \text{ on } \Gamma_{N,Q} \Big\}.$$

Then, assuming enough regularity on the domain D and the kernel H_α, for all $\theta, \xi \in \mathcal{F}_2$ the shape derivatives of $\tilde{\mathcal{J}}$ are given by

$$\tilde{\mathcal{J}}'(D;\xi) = \int_{\Gamma_{D,Q}} (\xi \cdot n)(\partial_n u)^2 \tag{9.2.3}$$

and

$$\begin{aligned} \tilde{\mathcal{J}}''(D;\theta,\xi) = &\int_{\Gamma_{D,Q}} (\theta \cdot n) \nabla u'_\xi \cdot \nabla u + \int_{\Gamma_{D,Q}} (\xi \cdot n) \nabla u'_\theta \cdot \nabla u \\ &+ \int_{\Gamma_{D,Q}} (\theta \cdot n)(\xi \cdot n) \Big[(\partial_n + \mathcal{H}) |\nabla u|^2 \Big] + \int_{\Gamma_{D,Q}} Z_{\theta,\xi} |\nabla u|^2 \end{aligned} \tag{9.2.4}$$

where

$$Z_{\theta,\xi} = D_\Gamma n\, \theta_\Gamma \cdot \xi_\Gamma - \xi_\Gamma \cdot \nabla_\Gamma (\theta \cdot n) - \theta_\Gamma \cdot \nabla_\Gamma (\xi \cdot n).$$

In what follows, we shall use the knowledge of both shape derivatives to compute the optimal shape D^*, using a first order method, the augmented Lagrangian, and the second order Newton discretization that we described earlier in Subsection 8.2. We then compare the results of the two methods to validate our computations.

For all our numerical simulations, the initial domain D_0 is taken as the half-ellipse, centered at the origin of width 2.2 and draft $T = 0.3$. The volume of the hull is fixed $\mathcal{V} = 0.06$, and we consider a uniform probability distribution on the Kelvin wave number $\alpha \in [\nu_{\min}, \nu_{\max}]$. For the sake of comparison with the results in [26], we introduce the area Froude number

$$F_r^2 = \frac{1}{\nu\sqrt{a}} = \frac{V^2}{g\sqrt{a}}$$

where a is the area of D. Thus, the bounds $\nu_{\min}, \nu_{\max}$ are computed as

$$\begin{cases} \nu_{\min} &= \dfrac{1}{\sqrt{a}Fr_{\max}^2}, \\ \nu_{\max} &= \dfrac{1}{\sqrt{a}Fr_{\min}^2}. \end{cases}$$

9.2.1 Augmented Lagrangian

In this section, we use the knowledge of the first order derivative to compute the optimal shape D^* through an augmented Lagrangian method, that is, we introduce the augmented Lagrangian :

$$L_A(D, \lambda, \mu) = \tilde{\mathcal{J}}(D) - \lambda(V(\Omega) - m) + \frac{\mu}{2}(V(\Omega) - m)^2 \tag{9.2.5}$$

where $\mu > 0$ and $\lambda \in \mathbb{R}$. The augmented Lagrangian method consists in minimizing $L_A(D, \lambda, \mu)$, where the values of λ and μ are updated at every iteration to penalize the violation of the volume constraint (see [59, section 17.3]). Using the chain rule and the expression of the shape derivative (9.2.3), and the shape derivative of the volume functional (8.2.13) we can easily deduce the shape derivative of L_A and we have

$$L'_A(\Omega, \lambda, \mu; \xi) = \int_{\Gamma_{D,Q}} (\xi \cdot n)\Big(\partial_n u^2 - \lambda + \mu(V(\Omega) - m)\Big). \tag{9.2.6}$$

Thus taking ξ such that

$$\xi \cdot n = -\big(\partial_n u^2 - \lambda + \mu(V(\Omega) - m)\big) \tag{9.2.7}$$

gives us an obvious descent direction ξ that is only defined on the boundary $\Gamma_{D,Q}$. In practice, ξ must be extended to the whole domain D through Hilbertian-extension techniques (see [7]). That is, given a mesh $\mathcal{T}_h$ approximating D, we compute a descent direction $\xi_h = (\xi_h^1, \xi_h^2) \in \mathcal{V}_h \times \mathcal{V}_h$ as a solution to the following problem

$$\begin{cases} -\operatorname{div}\Big(A\varepsilon(\xi_h)\Big) &= 0 \qquad \text{in } D \\ \xi_h \cdot n &= 0 \qquad \text{on } \Gamma_{N,Q} \\ \xi_h \cdot n &= -\big(\partial_n u^2 - \lambda + \mu(V(\Omega) - m)\big) \qquad \text{on } \Gamma_{D,Q}, \end{cases} \tag{9.2.8}$$

where $\mathcal{V}_h$ is the space of $\mathbb{P}_1$ Lagrange finite elements, A is a fourth order elasticity tensor and

$$\varepsilon(\xi_h) = \frac{1}{2}\big(\nabla\xi_h + \nabla\xi_h^T\big).$$

9.2.2 Newton algorithm

In this section, we seek to compute the optimal shape D^* Newton's method discretized following the results of sections 8.3 and 8.2, but recall that for the second order shape derivative (9.2.4) to make sense, we must have :

— $u' \in \mathbb{H}^1(D)$ which means that we should at least have the kernel $H_\alpha \in \mathbb{L}^2(D)$. This is not the case for Michell's kernel H_α, indeed, the authors in [26] prooved that H_α is only in $\mathbb{L}^{\frac{5}{4}-\epsilon}(D)$, $\epsilon > 0$.

— The boundary expression of the second order derivative given by (9.2.4) is only given for domains that are at least C^3, while D is only C^k by parts on each boundary $\Gamma_{D,Q}$ and $\Gamma_{N,Q}$, we shall always have two corners at the intersection of the boundaries, due to the different boundary conditions.

These regularity issues make it a priori difficult to attempt a second order shape optmization method. Since the boundary expression of the second order shape derivative is ill-defined, one can then try to find a different expression that takes into account the irregularity of the boundary. This is extensively studied in [52] for the case of the Dirichlet energy and volume functional, and the interested reader can find in it expressions for the second order derivative given for domains that are only Lipschitz!

In our case, it turns out that the discretization (8.1.8) gives enough flexibility to get around these issues when building the discrete Hessian matrix. Indeed,

— First, since $\theta \in \mathcal{F}_2$, the discrete Hessian shall only be constructed on the vertices of the boundary $\Gamma_{D,Q}$.

— Since our discretization is strictly dependent on the discrete normal $n_h(\mathbf{x}_i)$ on a vertex $\mathbf{x}_i$, to remain consistent, we exclude the vertices $\mathbf{x}_i$ with singularities (in this case, the first and last vertex of $\Gamma_{D,Q}$) when building the discrete Hessian. The value $\theta_h(\mathbf{x}_i)$ on these vertices is then obtained by a projection of the neighboring values $\theta_h(\mathbf{x}_{i-1}, \theta_h(\mathbf{x}_{i+1})$ on the boundary constraints of $\Gamma_{N,Q}$

$$\theta_h(\mathbf{x}_i) \cdot n_h(\mathbf{x}_i) = 0 \qquad \text{on } \Gamma_{N,Q}.$$

— Finally, while theoretically the solution u is not in $\mathbb{H}^2(D)$, we still can discretize quantities such as $\nabla^2 u$ using numerical gradients, specifically the least-squares gradient used for the discretization s above and defined in Annexe 8.2.1. This least-square gradient will enjoy higher regularity and ensures that the resulting discrete Hessian matrix is well conditioned.

These are all the tips that were used to help converge the Newton algorithm on an irregular domain with an irregular solution, and the results are given in what follows. While these tips seems complicated and a little bit technical, they are easy to implement for a trained FreeFEM user.

9.2.3 Numerical results and comparison of the two methods

Throughout this section we compute the optimal shapes on different intervals of the area Froude number Fr_a using both algorithms. The Froude number intervals are chosen so that we can compare with the numerical results in [26] obtained for the case of a constant velocity.

$Fr_a \in [2, 4]$

For high Froud numbers, the contribution of Michell's wave resistance vanishes, in which case the optimal domain is a minimizer of the viscous resistance which ressembles a half disc according to [26, Theorem 4.5].

Figure 9.1 shows that the computed optimal shapes for both Newton's algorithm and the Augmented Lagrangian ressembles a half-disc, the difference in the shapes is due to the oscillations in the Augmented Lagrangian algorithm. Indeed, one can see, both in Figure 9.1 and 9.2 that the computed L_2 and L_∞ norm have converged only for Newton's algorithm. This oscillation problem is well known for the Augmented Lagrangian and can be controlled by taking a lower limit for the incremented multiplier μ in the expression (9.2.5), but this comes at the cost of a slower convergence rate. The challenge of the Augmented Lagrangian is to take the right balance between the quadratic penalization of the constraint and the convergence of the objective. We can see in Figures 9.3 and 9.4 that the volume constraint starts oscillating after 80 iterations and before we reach the optimal solution for the expectation. This is not a problem for Newton's algorithm which manages to converge earlier. Newton's algorithm also provides a better preservation of the

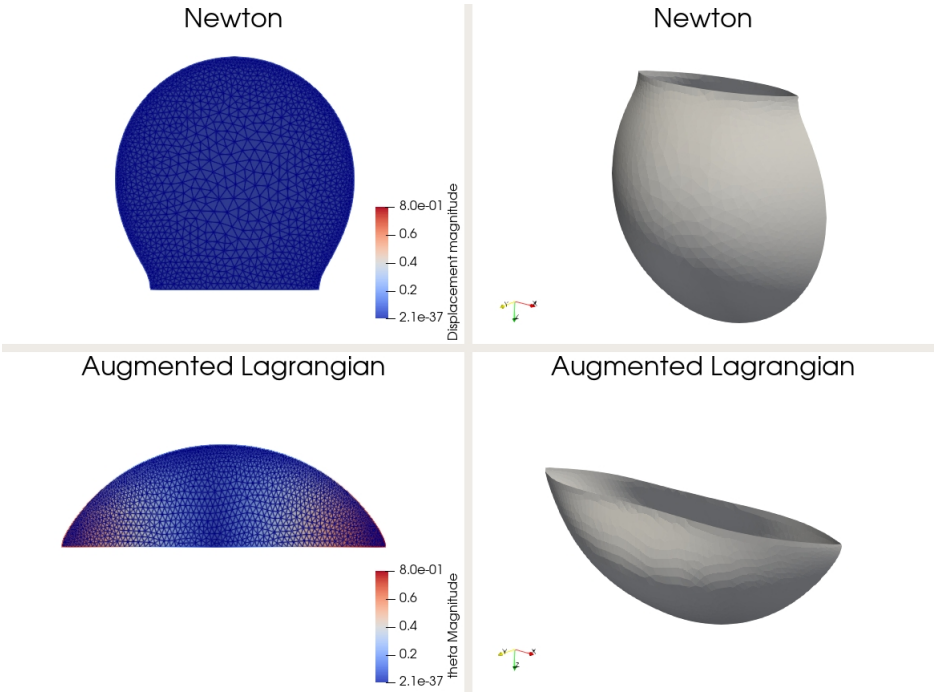

Figure 9.1 – The optimal hulls (rights) and optimal domains (left) computed with Newton's algorithm and the Augmented Lagrangian algorithm.

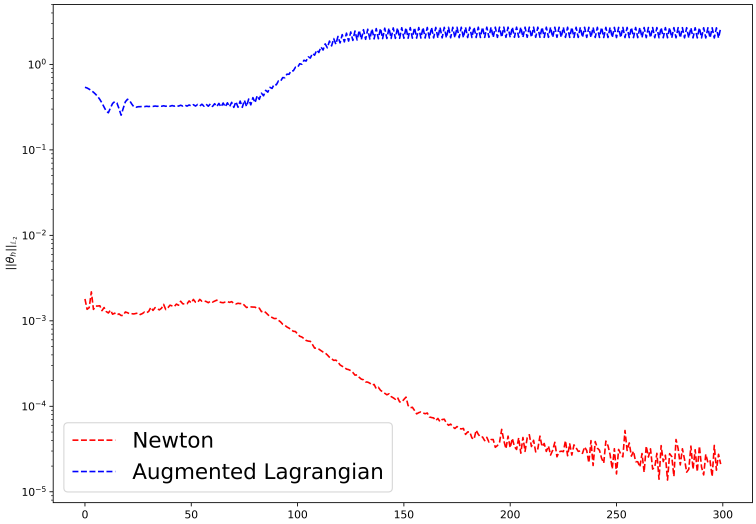

Figure 9.2 – Convergence of $\mathbb{L}_2$ norm $\|\theta_h\|_{\mathbb{L}_2}$ of the descent direction.

constraint along the optimization process, which is very important for our applications since the chosen velocity intervals are dependent on the area Froude number Fr_a which is dependent on the area of the domain D. We can see that the infeasibility of the constraint is of the order of 10^{-3} during most of the optimization process.

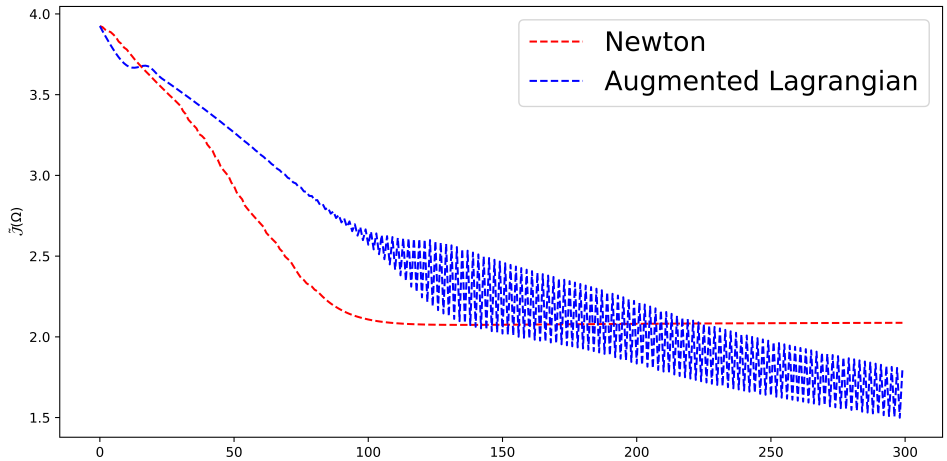

Figure 9.3 – Convergence of the normalized expectation of the total water resistance $\tilde{\mathcal{J}}$.

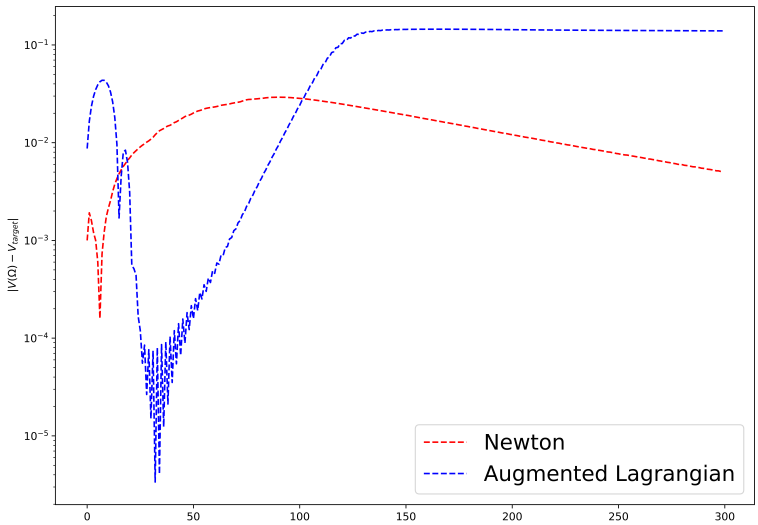

Figure 9.4 – Convergence of the volume constraint.

$Fr_a \in [1, 2]$

For Froude numbers $Fr_a \in [1, 2]$, we find no stable minimizer, in accordance with the

results of [26]. This is shown in Figure 9.5 for both algorithms. This can be thought of as the sinking of the ship, as we can see the bulbous bows getting detached from the middle of the hull causing the algorithm to crash.

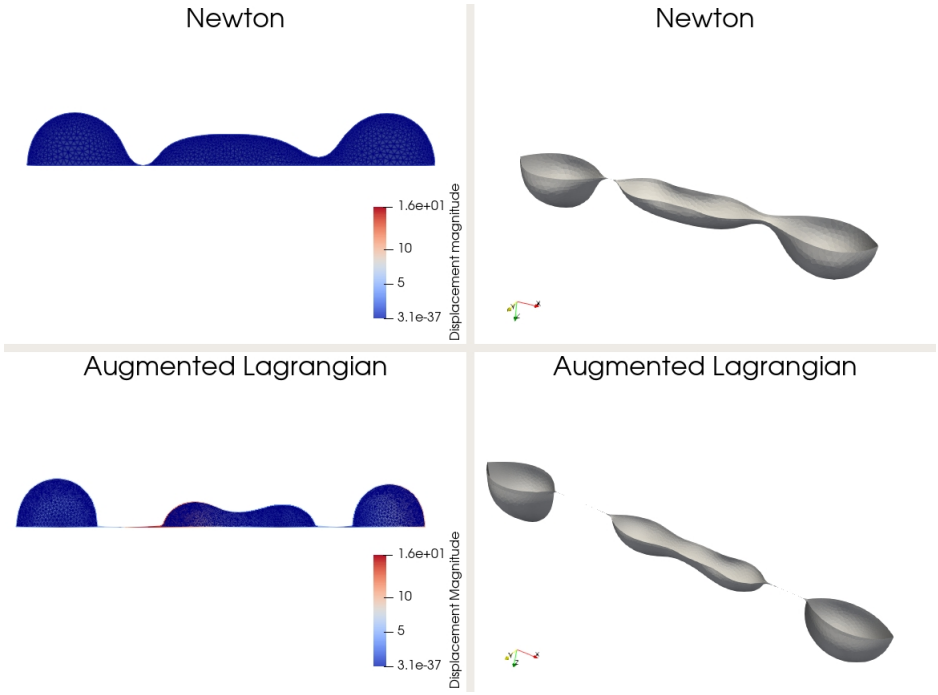

Figure 9.5 – The optimal hulls (right) and optimal domains (left) computed with Newton's algorithm and the Augmented Lagrangian algorithm.

$Fr_a \in [0.5, 1]$

The wave resistance reaches its maximum For Froude numbers in $[0.5, 1]$, thus this is the range of speed where it is most interesting to have a bulb in order to minimize the total ship's resistance, which is indeed the results obtained in [26]. Here we compute the optimal hull u^* for minimizing the expectation of the total water resistance $\tilde{\mathcal{J}}$ and we compare it to the optimal hull $\bar{u}$ for minimizing the total water resistance for an average Kelvin wave number $\alpha = \mathbb{E}(\nu)$. Figure 9.6 shows the computed optimal hulls, and we can see a slightly pronounced bulbous bow for u^* while $\bar{u}$ does not have any, and resembles more the shape of a half-disc. We then compare the resulting hulls for different Froude numbers, Figure 9.7 shows that indeed, $\bar{u}$ is optimal for $\alpha = \mathbb{E}(\nu)$, while u^* is optimal on the rest of the interval as indicated by the computed Expectations for both hulls.

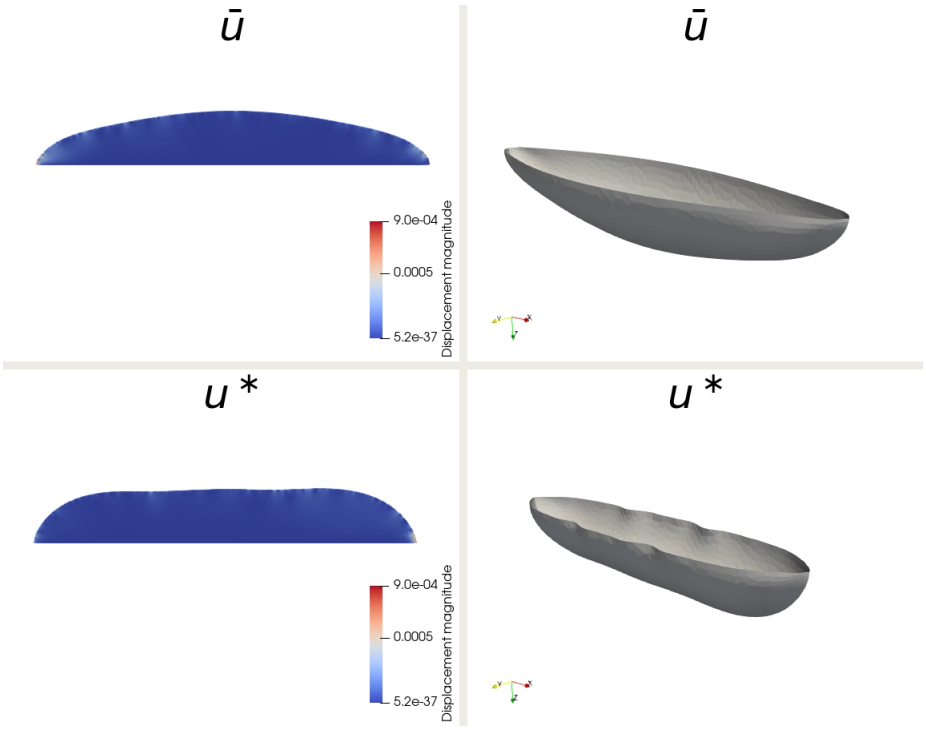

Figure 9.6 – The optimal hulls (rights) and optimal domains (left) for minimizing the total water resistance $J(\Omega, \alpha)$ and the expectation $\tilde{\mathcal{J}}(\Omega)$.

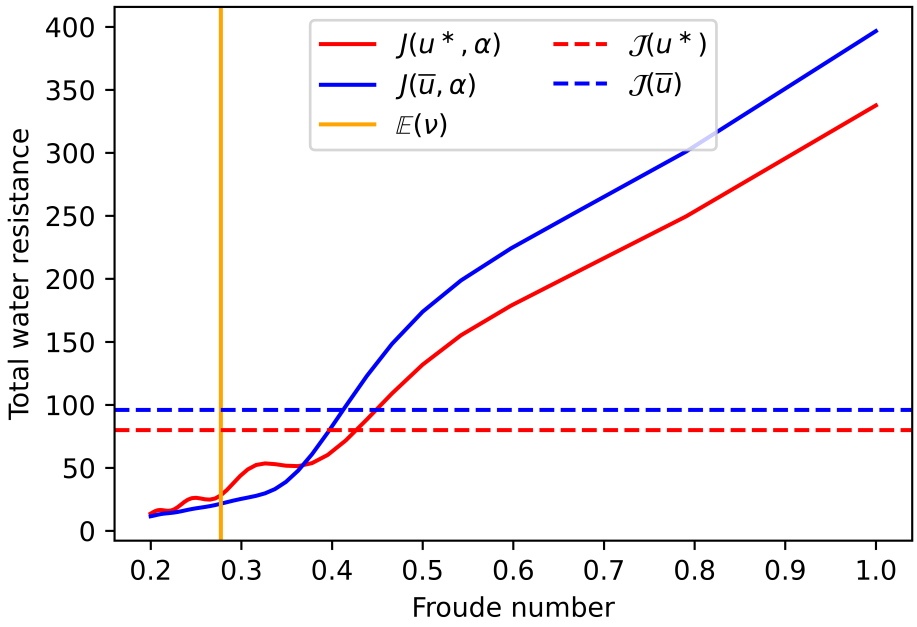

Figure 9.7 – The total water resistance for the different hulls.

$Fr_a \in [0.2, 0.5]$

For Froude numbers in $[0.2, 0.5]$, Michell's wave resistance, although small, is not accurate and is known to oscillate in the interval $[0.2, 0.35]$ which is the most interesting interval for commercial vessels. The computed optimal domain seen in Figure 9.8 is a half disc for Newton's algorithm, and while the final shapes for the augmented Lagrangian algorithm resemble a half-disc, they do not satisfy the volume constraint constraint. This is in accordance with the results in [26] for a fixed speed. Indeed, the wave resistance of a ship is small for low Froude numbers, and minimizing the ship's resistance boils down to the minimization of the viscous resistance by minimizing the wetted area of the hull, hence the spherical shape of the hull.

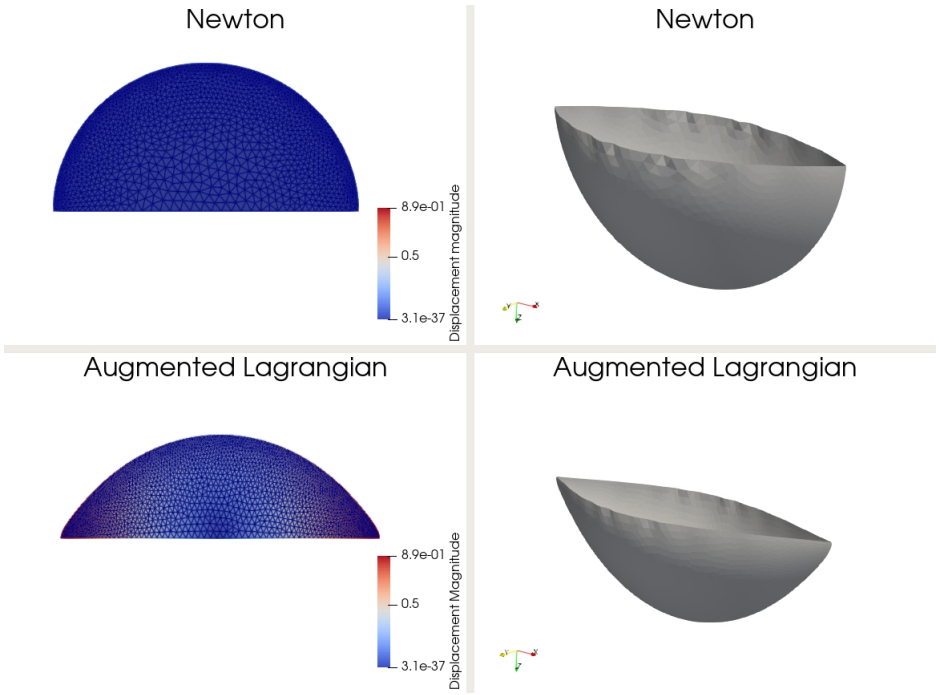

Figure 9.8 – The optimal hulls (right) and optimal domains (left) computed with Newton's algorithm and the Augmented Lagrangian algorithm.

Appendix A

NUMERICAL TOOLS

In this section we give some numerical tools, and mathematical formalism that are used throughout the chapter for building numerical methods. For a domain Ω with a boundary Γ we denote by $\mathcal{T}_h$ a triangulation of size h of Ω. We denote ny n_v the number of vertices $\mathbf{x}_i = (\mathsf{x}_i^1, \mathsf{x}_i^2)$, by n_t the number of triangles T_i and by n_{be} the number of boundary elements in $\mathcal{T}_h$. We thus have $\Omega_h = \cup_{k=1}^{n_t} T_k$ is the approximated domain of Ω and we denote by Γ_h the boundary of Ω_h.

We denote by $\mathbb{P}_k$ the set of polynomials p from $\mathbb{R}^2$ into $\mathbb{R}$ of degree less than or equal to k,

$$\mathbb{P}_k = \left\{ p(x,y) = \sum_{0<i+j\leq k} \alpha_{ij} x^i y^j \; \alpha_{ij} \in \mathbb{R} \right\},$$

and

$$\mathcal{V}_h = \left\{ u \in C(\Omega, \mathbb{R}) \middle| \forall\, T_i \in \mathcal{T}_h,\; u_{|T_i} \in \mathbb{P}_k \right\}$$

the Lagrange finite element space of continuous scalar functions that are piecewise polynomials of degree k. Let N_h be the dimension of $\mathcal{V}_h$ and we denote by $(\phi_i)_{1\leq i\leq N_h}$ a basis of $\mathcal{V}_h$ such that :

$$\begin{cases} \forall\, 1 \leq i,j \leq N_h, & \phi_i(a_j) = \delta_{ij}, \\ \forall\, u \in \mathcal{V}_h, & u(x) = \sum\limits_{i=1}^{N_h} u(a_j)\phi_i(x), \end{cases}$$

where $(a_j)_{1\leq j\leq N_h}$ are the degrees of freedom of $\mathcal{V}_h$. Recall that for $k = 1$, the degrees of freedom of $\mathcal{V}_h$ coincide with the set of vertices of the triangulation $\mathcal{T}_h$, we thus have $N_h = n_v$ and $a_i = \mathbf{x}_i$ for the space $\mathbb{P}_1$. For $k = 0$ the degrees of freedom of $\mathcal{V}_h$ coincide with the set of barycenters of the triangles T_i in $\mathcal{T}_h$.

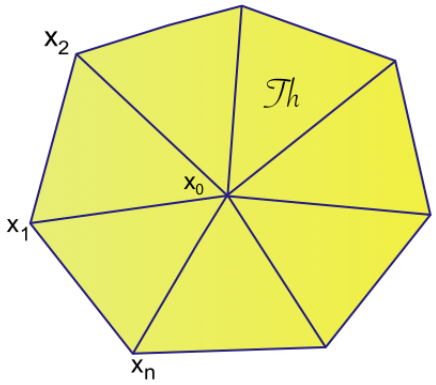

Figure A.1 – Neighborhood of a vertex $\mathbf{x}_0$ in a mesh $\mathcal{T}_h$.

A.1 Gradient of a piecewise linear function

Let $\mathcal{T}_h$ be a triangulation of a bounded domain Ω in $\mathbb{R}^2$ and u a function of $\mathcal{V}_h$, the space of $\mathbb{P}_1$ Langrange functions. Naturally, the gradient ∇u is only a $\mathbb{P}_0$ function on $\mathcal{T}_h$. i.e. it is equal to a constant value α_i on each triangle T_i. In many cases, we seek to lift this gradient to a $\mathbb{P}_1$ function defined on the vertices of $\mathcal{T}_h$ through a stable approximation.

Let $\mathbf{x}_0$ be a vertex of $\mathcal{T}_h$, and denote by $\mathbf{x}_1, \dots, \mathbf{x}_n$ the neighboring vertices as given in Figure A.1.

For a smooth function $f : \mathbb{R}^2 \to \mathbb{R}$, we have the following Taylor expansion around $\mathbf{x}_0$,

$$f(\mathbf{x}_i) \approx f(\mathbf{x}_0) + \nabla f(\mathbf{x}_0) \cdot (\mathbf{x}_i - \mathbf{x}_0), \quad \text{for } i = 1, \dots, n. \tag{A.1.1}$$

Then following [38], a good approximation of the gradient ∇u of our piecewise linear function u may be obtained by mimicking the expansion (A.1.1) for all $i = 1, \dots, n$. That is we approximate ∇u by a vector $b = (b_1, b_2)$ solution to

$$Ab = c, \tag{A.1.2}$$

where A and c are the $n \times 2$ matrix and n-dimensional vector given by :

$$A = \begin{pmatrix} \mathsf{x}_1^1 - \mathsf{x}_0^1 & \mathsf{x}_1^2 - \mathsf{x}_0^2 \\ \mathsf{x}_2^1 - \mathsf{x}_0^1 & \mathsf{x}_2^2 - \mathsf{x}_0^2 \\ \vdots & \vdots \\ \mathsf{x}_n^1 - \mathsf{x}_0^1 & \mathsf{x}_n^2 - \mathsf{x}_0^2 \end{pmatrix} \qquad \text{and} \qquad c = \begin{pmatrix} u(\mathbf{x}_1) - u(\mathbf{x}_0) \\ u(\mathbf{x}_2) - u(\mathbf{x}_0) \\ \vdots \\ u(\mathbf{x}_n) - u(\mathbf{x}_0) \end{pmatrix}. \tag{A.1.3}$$

However, problem (A.1.2) is clearly overdetermined, and in practice we search b as a solution to the least-square problem

$$A^T A b = A^T c,$$

where $A^T A$ and $A^T c$ are the 2×2 matrix and two-dimensional vector defined by

$$A^T A = \begin{pmatrix} \sum_{i=1}^{n} (\mathsf{x}_i^1 - \mathbf{x}_0^1)^2 & \sum_{i=1}^{n} (\mathsf{x}_i^1 - \mathsf{x}_0^1)(\mathsf{x}_i^2 - \mathsf{x}_0^2) \\ \sum_{i=1}^{n} (\mathsf{x}_i^1 - \mathsf{x}_0^1)(\mathsf{x}_i^2 - \mathsf{x}_0^2) & \sum_{i=1}^{n} (\mathsf{x}_i^2 - \mathsf{x}_0^2)^2 \end{pmatrix}$$

and

$$A^T c = \begin{pmatrix} \sum_{=1}^{n} (\mathsf{x}_i^1 - \mathbf{x}_0^1)(u(\mathbf{x}_i) - u(\mathbf{x}_0)) \\ \sum_{=1}^{n} (\mathsf{x}_i^2 - \mathbf{x}_0^2)(u(\mathbf{x}_i) - u(\mathbf{x}_0)) \end{pmatrix}.$$

The matrix $A^T A$ is easily seen to be invertible.

Remark A.1.1. *In practice, depending on the size h of the mesh $\mathcal{T}_h$, the matrix $A^T A$ defined above may have very small entries which will cause the degeneracy of the inverse of $A^T A$. To avoid this behavior it is often interesting to multiply both sides of problem* (A.1.4) *by a large constant before computing the inverse.*

The above procedure for approximating the gradient ∇u as a $\mathbb{P}_1$ function is pretty robust in practice. Unfortunately, it may still be affected by numerical errors, and this is a reason why it is often recommendable to smooth the resulting quantities. To this end, it is common practice to use the screened Poisson equation, i.e. for a general finite element quantity ψ defined at the vertices of $\mathcal{T}_h$, we trade ψ for the solution $u_h \in \mathcal{V}_h$ to

the following variational problem:

$$\forall\, v_h \in \mathcal{V}_h, \quad \int_\Omega (\varepsilon^2 \nabla\psi \cdot \nabla v_h + \psi v_h) dx = \int_\Omega \psi v_h dx, \tag{A.1.4}$$

where ε is chosen of the order of mesh size : $\varepsilon \approx h$.

A.2 Savitsky-Golay Filters for mesh boundary smoothing

Very often in shape optimization algorithms, where we are given a computational mesh and seek to continuously move it along the direction of finite element velocity field θ, one has to make sure that the resulting mesh is still computationally valid. To this end, one has to smooth the velocity field θ before moving the mesh through Hilbertian extension-regularization techniques (see [7] for a thorough presentation of these techniques). In practice, this technique works very well in preventing mesh degeneracy throughout the optimization process. However, in case the descent step of the optimization algorithm is big enough, this is not enough to prevent mesh degeneracy, and one has to resolve to the smoothing of the resulting mesh.

For a 3d mesh, one can find many smoothing techniques in [38] which are efficient and easy to implement. In case of a 2d mesh, it is often easier and less costly (from a computational point of view) to remesh the triangulation. This, however, only solves the problem on the interior of the domain mesh and one can still end-up with a non-smooth boundary, which can pollute the numerical computation of geometrical quantities on the boundary such as the normal to the boundary n and curvature κ. Most importantly these quantities are very crucial to the definition and use of shape gradients for first and second order shape optimization algorithms, thus one has to make sure the computations are made on a mesh with a sufficiently smooth boundary.

Here we give an easy technique for the smoothing of a 2d curves based on Savitzky-Golay Filters that we use for the smoothing of the boundary of a 2d domain. Savitzky-Golay filters are widely used in the field of digital data for the purpose of smoothing a signal without distorting its frequency, they were introduced in [66] where the authors give a set of convolution coefficients to fit successive sub-sets of adjacent data-points with a low-degree polynomial in the sense of least-squares.

This means that for a given set of data points $(y_j)_{1\leq j\leq n}$ one computes a new set of

Table A.1 – Savitzky-Golay convolution coefficients for smoothing with polynomials of order 2,3,4 and 5 for different window sizes

	Coefficients C_i				
Polynomial Degree	quadratic or cubic 2 or 3			quartic or quintic 4 or 5	
Window size m	5	7	9	7	9
-4			-21		15
-3		-2	14	5	-55
-2	-3	3	39	-30	30
-1	12	6	54	75	135
0	17	7	59	131	179
1	12	6	54	75	135
2	-3	3	39	-30	30
3		-2	14	5	-55
4			-21		15
Normalisation N	35	21	231	231	429

data points $(Y_j)_{1\leq j\leq n}$ according to the expression

$$Y_j = \frac{1}{N}\sum_{i=\frac{1-m}{2}}^{\frac{m-1}{2}} C_i y_{j+i}, \qquad \frac{m-1}{2} \leq j \leq n - \frac{m-1}{2}, \tag{A.2.1}$$

where C_i, m and N are given in Table A.1.

This can be used to construct simple and efficient smoothing algorithms by smoothing each set of coordinates separately. For a given mesh $\mathcal{T}_h$ with a boundary $\Gamma_h = \bigcup_{i=1}^{n_{be}} [\mathbf{x}_i, \mathbf{x}_{i+1}]$ consisting of n_{be} vertices $\mathbf{x}_i = (x_i, y_i)$ we have the following algorithm for computing a smooth boundary Γ_h^s :

Figure A.2 gives the results of Algorithm 1 for different iterations of the algorithm. One can see that after 2 iterations we get a smooth mesh, which gets even smoother after 10 iterations. Note that on a modern laptop this only took a fraction of a second for the whole 10 iterations.

A.3 Discrete 2d curvature κ

Shape optimization algorithms often necessitate the computation of different discrete geometric quantities, such as the normal to the boundary n, the tangent vector to the

Algorithm 1 Savitzky-Golay smoothing algorithm

Require: $\mathbf{x}_{n_{be}+1} = \mathbf{x}_1$

for $i = 1, \ldots, n_{be}$ **do**
$x[i] \leftarrow x_i$
$y[i] \leftarrow y_i$ ▷ build two arrays for the coordinates of $\mathbf{x}_i = (x_i, y_i)$
end for
for $i = 1, \ldots, n_{be}$ **do**
$x^s[i] \leftarrow X_i$
$y^s[i] \leftarrow Y_i$ ▷ Compute X_i, Y_i by the convolution (A.2.1)
end for
return $\Gamma_h^s = \bigcup_{i=1}^{n_{be}} [\mathbf{x}_i^s, \mathbf{x}_{i+1}^s]$ ▷ $\mathbf{x}_i^s = (x^s[i], y^s[i])$

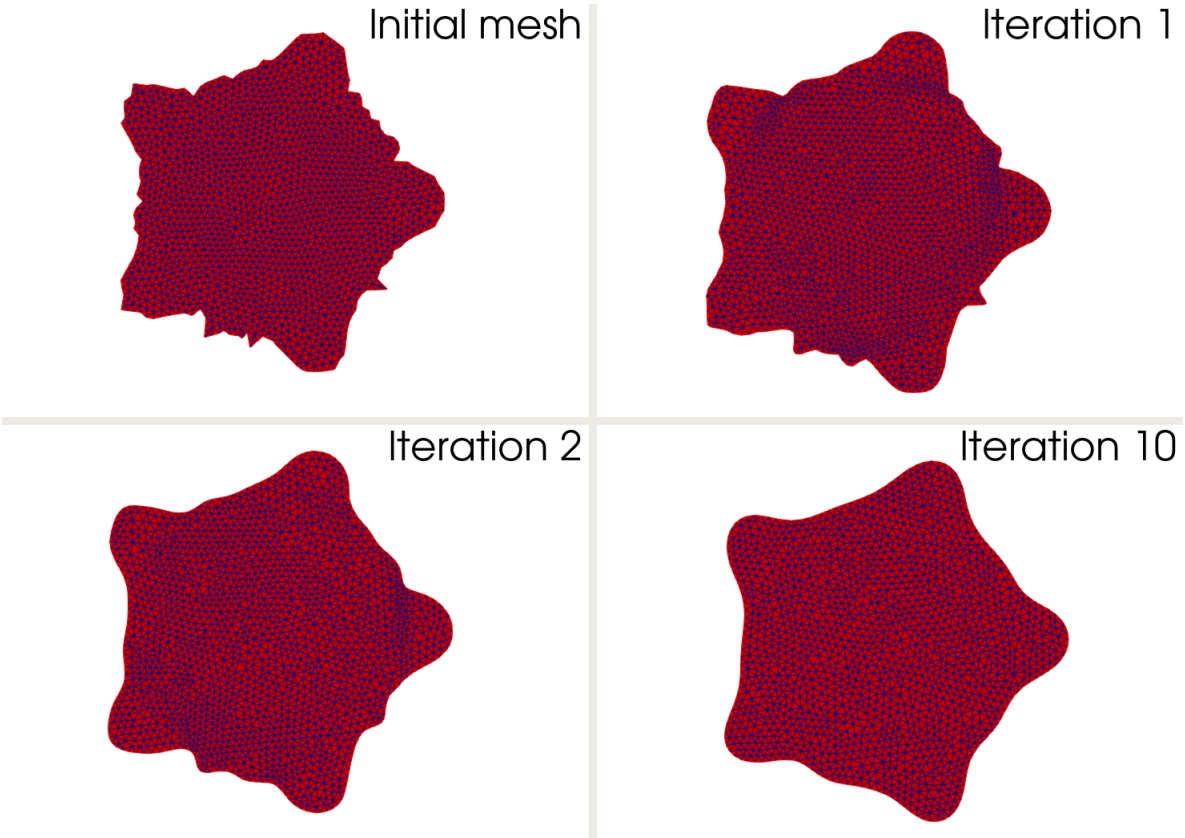

Figure A.2 – Results of mesh boundary smoothing using a Savitzky-Golay filter for a polynomial of degree 5 and a window size $m = 9$ after $1, 2$ and 10 iterations.

boundary τ and the mean curvature κ. In practice, there are many different ways to discretize any given geometric object, and depending on the applications (what properties of the geometric object we need, and would like to preserve), it is often possible to choose a discretization that exactly mimic the desired properties of the smooth geometric object.

Here, we recall a robust and efficient way to compute the discrete 2d curvature. Consider a mesh $\mathcal{T}_h$ with a boundary Γ_h as an ordered tuple $(\mathbf{x}_0, \mathbf{x}_1, \ldots, \mathbf{x}_n)$ of vertices $\mathbf{x}_i$, with $\mathbf{x}_{i+1} \neq \mathbf{x}_i$ for all i. Let $\vec{\boldsymbol{e}}_{i,i+1} = \mathbf{x}_{i+1} - \mathbf{x}_i$ denote the edge vector representing the edge between $\mathbf{x}_i$ and $\mathbf{x}_{i+1}$. For two edge vectors $\vec{\boldsymbol{e}}_{i-1,i}$ and $\vec{\boldsymbol{e}}_{i,i+1}$ we denote by θ_i the clockwise turning angle between the two vectors (see Figure A.3). We have the following formula (see [78]) for computing the discrete curvature κ_i on a vertex $\mathbf{x}_i$

$$\kappa_i = \frac{2\theta_i}{\left\|\vec{\boldsymbol{e}}_{i,i-1}\right\| + \left\|\vec{\boldsymbol{e}}_{i,i+1}\right\|}, \tag{A.3.1}$$

In addition to satisfying the basic symmetries of the curvature κ, one can easily see that formula (A.3.1) does not diverge at kinks, the only delicate matter is to compute the turning angle θ_i in a robust way. Indeed, a naive way to compute this quantity is given by the dot product identity, which gives

$$\theta_i = \cos^{-1} \frac{\vec{\boldsymbol{e}}_{i-1,i} \cdot \vec{\boldsymbol{e}}_{i,i+1}}{\left\|\vec{\boldsymbol{e}}_{i,i-1}\right\| \left\|\vec{\boldsymbol{e}}_{i-1,i}\right\|}.$$

However, this formula tends to break down for small values of θ_i, numerical error can cause the argument of $\cos^{-1}$ to exceed 1. The robust way to compute the turning angle θ_i relies on the tangent half-angle identity given by

$$\theta_i = 2\tan^{-1} \frac{\sin\theta_i}{1+\cos\theta_i} = 2\tan^{-1} \frac{(\vec{\boldsymbol{e}}_{i-1,i} \times \vec{\boldsymbol{e}}_{i,i+1}) \cdot z}{\left\|\vec{\boldsymbol{e}}_{i-1,i}\right\| \left\|\vec{\boldsymbol{e}}_{i,i+1}\right\| + \vec{\boldsymbol{e}}_{i-1,i} \cdot \vec{\boldsymbol{e}}_{i,i+1}}, \tag{A.3.2}$$

where z is the unit vector perpendicular to the plane.

In practice, it is more robust to use the *atan*2 function rather than $\tan^{-1}$, which handles better the case of small denominator. i.e :

$$\theta_i = 2\,\mathrm{atan2}\left((\vec{\boldsymbol{e}}_{i-1,i} \times \vec{\boldsymbol{e}}_{i,i+1}) \cdot z\,,\ \left\|\vec{\boldsymbol{e}}_{i-1,i}\right\| \left\|\vec{\boldsymbol{e}}_{i,i+1}\right\| + \vec{\boldsymbol{e}}_{i-1,i} \cdot \vec{\boldsymbol{e}}_{i,i+1}\right). \tag{A.3.3}$$

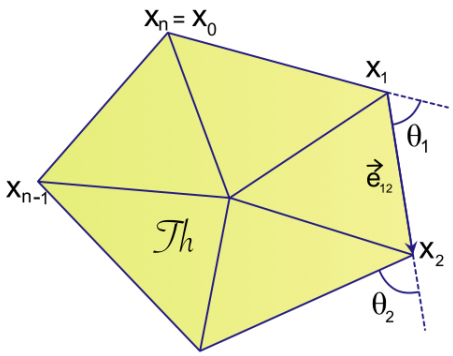

Figure A.3 – Model situation for the various elements on the boundary Γ.

BIBLIOGRAPHY

[1] R. A. Adams, *Sobolev spaces*, Pure and Applied Mathematics, Vol. 65, Academic Press [Harcourt Brace Jovanovich, Publishers], New York-London, 1975, pp. xviii+268.

[2] L. Afraites, M. Dambrine, and D. Kateb, « On second order shape optimization methods for electrical impedance tomography », *in*: *SIAM J. Control Optim.* 47.*3* (2008), pp. 1556–1590, ISSN: 0363-0129, DOI: 10.1137/070687438, URL: https://doi.org/10.1137/070687438.

[3] G. Allaire, *Boite à outils FreeFem++ pour l'optimisation de formes (géométrique et topologique).* http://www.cmap.polytechnique.fr/~allaire/freefem.html, 2008.

[4] G. Allaire, *Conception optimale de structures*, vol. 58, Mathématiques & Applications (Berlin) [Mathematics & Applications], With the collaboration of Marc Schoenauer (INRIA) in the writing of Chapter 8, Springer-Verlag, Berlin, 2007, pp. xii+278, ISBN: 978-3-540-36710-9; 3-540-36710-1.

[5] G. Allaire, *Shape optimization by the homogenization method*, vol. 146, Applied Mathematical Sciences, Springer-Verlag, New York, 2002, pp. xvi+456, ISBN: 0-387-95298-5, DOI: 10.1007/978-1-4684-9286-6, URL: https://doi.org/10.1007/978-1-4684-9286-6.

[6] G. Allaire and Ch. Dapogny, « A linearized approach to worst-case design in parametric and geometric shape optimization », *in*: *Math. Models Methods Appl. Sci.* 24.*11* (2014), pp. 2199–2257, ISSN: 0218-2025, DOI: 10.1142/S0218202514500195, URL: https://doi.org/10.1142/S0218202514500195.

[7] G. Allaire, Ch. Dapogny, and F. Jouve, « Shape and topology optimization », *in*: *Geometric partial differential equations. Part II*, vol. 22, Handb. Numer. Anal. Elsevier/North-Holland, Amsterdam, [2021] ©2021, pp. 1–132, DOI: 10.1016/bs.hna.2020.10.004, URL: https://doi.org/10.1016/bs.hna.2020.10.004.

[8] G. Allaire, P. Geoffroy-Donders, and O. Pantz, « Topology optimization of modulated and oriented periodic microstructures by the homogenization method », *in*: *Comput. Math. Appl.* 78.*7* (2019), pp. 2197–2229, ISSN: 0898-1221, DOI: 10.1016/j.camwa.2018.08.007, URL: https://doi.org/10.1016/j.camwa.2018.08.007.

[9] G. Allaire, F. Jouve, and A-M. Toader, « Structural optimization using sensitivity analysis and a level-set method », *in*: *J. Comput. Phys.* 194.*1* (2004), pp. 363–393, ISSN: 0021-9991, DOI: 10.1016/j.jcp.2003.09.032, URL: https://doi.org/10.1016/j.jcp.2003.09.032.

[10] K.J. Bai, « Overview of results », *in*: *Proceedings of the Workshop on Ship Wave-resistance Computations, I.* 1979.

[11] C. Barbarosie, « Shape optimization of periodic structures », *in*: *Computational Mechanics* 30.*3* (2003), pp. 235–246, DOI: 10.1007/s00466-002-0382-3, URL: https://www.scopus.com/inward/record.uri?eid=2-s2.0-0037297324&doi=10.1007%2fs00466-002-0382-3&partnerID=40&md5=61f4d669a937a7822ff4ececf392a625.

[12] C. Barbarosie and A.-M. Toader, « Optimization of bodies with locally periodic microstructure by varying the periodicity pattern », *in*: *Netw. Heterog. Media* 9.*3* (2014), pp. 433–451, ISSN: 1556-1801, DOI: 10.3934/nhm.2014.9.433, URL: https://doi.org/10.3934/nhm.2014.9.433.

[13] C. Barbarosie, A.-M. Toader, and S. Lopes, « A gradient-type algorithm for constrained optimization with application to microstructure optimization », *in*: *Discrete Contin. Dyn. Syst. Ser. B* 25.*5* (2020), pp. 1729–1755, ISSN: 1531-3492, DOI: 10.3934/dcdsb.2019249, URL: https://doi.org/10.3934/dcdsb.2019249.

[14] L. Birk, *Fundamentals of ship hydrodynamics: fluid mechanics, ship resistance and propulsion*, Hoboken, NJ: John Wiley & Sons, Ltd, 2019, ISBN: 978-1-118-85548-5.

[15] P. Bisegna and R. Luciano, « Variational bounds for the overall properties of piezoelectric composites », *in*: *J. Mech. Phys. Solids* 44.*4* (1996), pp. 583–602, ISSN: 0022-5096, DOI: 10.1016/0022-5096(95)00084-4, URL: https://doi.org/10.1016/0022-5096(95)00084-4.

[16] J.F. Bonnans et al., *Numerical optimization*, Second, Universitext, Theoretical and practical aspects, Springer-Verlag, Berlin, 2006, pp. xiv+490, ISBN: 3-540-35445-X.

[17] A. Braides, Γ-*convergence for beginners*, vol. 22, Oxford Lecture Series in Mathematics and its Applications, Oxford University Press, Oxford, 2002, pp. xii+218, ISBN: 0-19-850784-4, DOI: 10.1093/acprof:oso/9780198507840.001.0001, URL: https://doi.org/10.1093/acprof:oso/9780198507840.001.0001.

[18] D. Bucur, « Do optimal shapes exist? », *in*: *Milan J. Math.* 75 (2007), pp. 379–398, ISSN: 1424-9286, DOI: 10.1007/s00032-007-0074-8, URL: https://doi.org/10.1007/s00032-007-0074-8.

[19] F. Caubet, M. Dambrine, and R. Mahadevan, « Shape Derivative for Some Eigenvalue Functionals in Elasticity Theory », *in*: *SIAM Journal on Control and Optimization* 59.*2* (2021), pp. 1218–1245, DOI: 10.1137/20M1343105, eprint: https://doi.org/10.1137/20M1343105, URL: https://doi.org/10.1137/20M1343105.

[20] F. Caubet, M. Dambrine, and R. Mahadevan, « Shape sensitivity of eigenvalue functionals for scalar problems: computing the semi-derivative of a minimum », *in*: *Appl. Math. Optim.* 86.*1* (2022), Paper No. 10, 34, ISSN: 0095-4616, DOI: 10.1007/s00245-022-09827-6, URL: https://doi.org/10.1007/s00245-022-09827-6.

[21] J. Cea, « Conception optimale ou identification de formes, calcul rapide de la dérivée directionnelle de la fonction coût », *in*: *ESAIM: Mathematical Modelling and Numerical Analysis* 20.*3* (1986), pp. 371–402, ISSN: 0764-583X, 1290-3841, DOI: 10.1051/m2an/1986200303711, URL: http://www.esaim-m2an.org/10.1051/m2an/1986200303711 (visited on 09/27/2022).

[22] K. -. Chen and X. -. Feng, « CAD modeling for the components made of multi heterogeneous materials and smart materials », English, *in*: *CAD Computer Aided Design* 36.*1* (2004), Cited By :37, pp. 51–63, URL: www.scopus.com.

[23] D. Chenais, « On the existence of a solution in a domain identification problem », *in*: *J. Math. Anal. Appl.* 52.*2* (1975), pp. 189–219, ISSN: 0022-247X, DOI: 10.1016/0022-247X(75)90091-8, URL: https://doi.org/10.1016/0022-247X(75)90091-8.

[24] A. Chicco-Ruiz, P. Morin, and M. Sebastian Pauletti, « The shape derivative of the Gauss curvature », *in*: *Rev. Un. Mat. Argentina* 59.*2* (2018), pp. 311–337, ISSN: 0041-6932, DOI: 10.33044/revuma.v59n2a06, URL: https://doi.org/10.33044/revuma.v59n2a06.

[25] J. Dambrine and M. Pierre, « Continuity with respect to the speed for optimal ship forms based on Michell's formula », *in*: *Mathematical Control and Related Fields* 0 (2021).

[26] J. Dambrine and M. Pierre, « Regularity of optimal ship forms based on Michell's wave resistance », *in*: *Appl. Math. Optim.* 82.*1* (2020), pp. 23–62, ISSN: 0095-4616, DOI: 10.1007/s00245-018-9490-0, URL: https://doi.org/10.1007/s00245-018-9490-0.

[27] J. Dambrine, M. Pierre, and G. Rousseaux, « A theoretical and numerical determination of optimal ship forms based on Michell's wave resistance », *in*: *ESAIM Control Optim. Calc. Var.* 22.*1* (2016), pp. 88–111, ISSN: 1292-8119, DOI: 10.1051/cocv/2014067, URL: https://doi.org/10.1051/cocv/2014067.

[28] M. Dambrine and H. Harbrecht, « Shape optimization for composite materials and scaffold structures », *in*: *Multiscale Model. Simul.* 18.*2* (2020), pp. 1136–1152, ISSN: 1540-3459, DOI: 10.1137/19M1274638, URL: https://doi.org/10.1137/19M1274638.

[29] M. Dambrine and J. Lamboley, « Stability in shape optimization with second variation », *in*: *J. Differential Equations* 267.*5* (2019), pp. 3009–3045, ISSN: 0022-0396, DOI: 10.1016/j.jde.2019.03.033, URL: https://doi.org/10.1016/j.jde.2019.03.033.

[30] Ch. Dapogny and E. Bonnetier, *An introduction to shape and topology optimization.* https://membres-ljk.imag.fr/Charles.Dapogny/coursoptim.html, 2021.

[31] Ch. Dapogny et al., « Geometrical shape optimization in fluid mechanics using FreeFem++ », *in*: *Struct. Multidiscip. Optim.* 58.*6* (2018), pp. 2761–2788, ISSN: 1615-147X, DOI: 10.1007/s00158-018-2023-2, URL: https://doi.org/10.1007/s00158-018-2023-2.

[32] M. C. Delfour and J.-P. Zolésio, *Shapes and geometries*, Second, vol. 22, Advances in Design and Control, Metrics, analysis, differential calculus, and optimization, Society for Industrial and Applied Mathematics (SIAM), Philadelphia, PA, 2011, pp. xxiv+622, ISBN: 978-0-898719-36-9, DOI: 10.1137/1.9780898719826, URL: https://doi.org/10.1137/1.9780898719826.

[33] D. A. Di Pietro and A. Ern, *Mathematical aspects of discontinuous Galerkin methods*, vol. 69, Mathématiques & Applications (Berlin) [Mathematics & Applications], Springer, Heidelberg, 2012, pp. xviii+384, ISBN: 978-3-642-22979-4, DOI: 10.1007/978-3-642-22980-0, URL: https://doi.org/10.1007/978-3-642-22980-0.

[34] V. Dolejšié and M. Feistauer, *Discontinuous Galerkin method*, vol. 48, Springer Series in Computational Mathematics, Analysis and applications to compressible flow, Springer, Cham, 2015, pp. xiv+572, ISBN: 978-3-319-19266-6; 978-3-319-19267-3, DOI: 10.1007/978-3-319-19267-3, URL: https://doi.org/10.1007/978-3-319-19267-3.

[35] K. Eppler and H. Harbrecht, « A regularized Newton method in electrical impedance tomography using shape Hessian information », *in*: *Control Cybernet.* 34.*1* (2005), pp. 203–225, ISSN: 0324-8569.

[36] A. Ferrer, P. Geoffroy-Donders, and G. Allaire, « Stress minimization for lattice structures. Part I: Micro-structure design », *in*: *Philos. Trans. Roy. Soc. A* 379.*2201* (2021), Paper No. 20200109, 33, ISSN: 1364-503X.

[37] G. Fichera, « Existence theorems in linear and semi-linear elasticity », *in*: *Z. Angew. Math. Mech.* 54 (1974), T24–T36, ISSN: 0044-2267, DOI: 10.1002/zamm.19740541205, URL: https://doi.org/10.1002/zamm.19740541205.

[38] P.J. Frey and P-L. George, *Mesh generation*, Second, Application to finite elements, ISTE, London; John Wiley & Sons, Inc., Hoboken, NJ, 2008, p. 848, ISBN: 978-1-84821-029-5, DOI: 10.1002/9780470611166, URL: https://doi.org/10.1002/9780470611166.

[39] P. Geoffroy-Donders, G. Allaire, and O. Pantz, « 3-d topology optimization of modulated and oriented periodic microstructures by the homogenization method », *in*: *J. Comput. Phys.* 401 (2020), pp. 108994, 30, ISSN: 0021-9991, DOI: 10.1016/j.jcp.2019.108994, URL: https://doi.org/10.1016/j.jcp.2019.108994.

[40] M. Ghergu et al., « Homogénéisation et piézoélectricité. Aide à la conception d'un bio-matériau », *in*: *An. Univ. Craiova Ser. Mat. Inform.* 32 (2005), pp. 9–15, ISSN: 1223-6934.

[41] M. Ghergu et al., « Homogenization of thin piezoelectric perforated shells », *in*: *M2AN Math. Model. Numer. Anal.* 41.*5* (2007), pp. 875–895, ISSN: 0764-583X, DOI: 10.1051/m2an:2007046, URL: https://doi.org/10.1051/m2an:2007046.

[42] A. Sh. Gotman, « Study of Michell's integral and influence of viscosity and ship hull form on wave resistance », *in*: *Oceanic Engineering International* 6 (2002), pp. 74–115.

[43] P. Grisvard, *Elliptic problems in nonsmooth domains*, vol. 69, Classics in Applied Mathematics, Reprint of the 1985 original [MR0775683], With a foreword by Susanne C. Brenner, Society for Industrial and Applied Mathematics (SIAM), Philadelphia, PA, 2011, pp. xx+410, ISBN: 978-1-611972-02-3, DOI: 10.1137/1.9781611972030.ch1, URL: https://doi.org/10.1137/1.9781611972030.ch1.

[44] H. Harbrecht, « A Newton method for Bernoulli's free boundary problem in three dimensions », *in*: *Computing* 82.*1* (2008), pp. 11–30, ISSN: 0010-485X, DOI: 10.1007/s00607-008-0260-8, URL: https://doi.org/10.1007/s00607-008-0260-8.

[45] H. Harbrecht and T. Hohage, « A Newton method for reconstructing non star-shaped domains in electrical impedance tomography », *in*: *Inverse Probl. Imaging* 3.*2* (2009), pp. 353–371, ISSN: 1930-8337, DOI: 10.3934/ipi.2009.3.353, URL: https://doi.org/10.3934/ipi.2009.3.353.

[46] Z. Hashin and S. Shtrikman, « A variational approach to the theory of the elastic behaviour of multiphase materials », *in*: *J. Mech. Phys. Solids* 11 (1963), pp. 127–140, ISSN: 0022-5096, DOI: 10.1016/0022-5096(63)90060-7, URL: https://doi.org/10.1016/0022-5096(63)90060-7.

[47] J. Haslinger and J. Dvořák, « Optimum composite material design », *in*: *RAIRO Modél. Math. Anal. Numér.* 29.*6* (1995), pp. 657–686, ISSN: 0764-583X, DOI: 10.1051/m2an/1995290606571, URL: https://doi.org/10.1051/m2an/1995290606571.

[48] T. H. Havelock, « Studies in Wave Resistance: Influence of the Form of the Water-Plane Section of the Ship », *in*: *Proceedings of the Royal Society of London. Series A, Containing Papers of a Mathematical and Physical Character* 103.*723* (1923), pp. 571–585, ISSN: 09501207, URL: http://www.jstor.org/stable/94077 (visited on 09/07/2022).

[49] F. Hecht, « New development in freefem++ », *in*: *J. Numer. Math.* 20.*3-4* (2012), pp. 251–265, ISSN: 1570-2820, DOI: 10.1515/jnum-2012-0013, URL: https://doi.org/10.1515/jnum-2012-0013.

[50] A. Henrot and M. Pierre, *Shape variation and optimization*, vol. 28, EMS Tracts in Mathematics, A geometrical analysis, English version of the French publication [MR2512810] with additions and updates, European Mathematical Society (EMS), Zürich, 2018, pp. xi+365, ISBN: 978-3-03719-178-1, DOI: 10.4171/178, URL: https://doi.org/10.4171/178.

[51] A. A. Kostyukov, *Theory of ship waves and wave resistance*, Effective Communications Inc., Iowa City, Iowa, 1968.

[52] A. Laurain, « Distributed and boundary expressions of first and second order shape derivatives in nonsmooth domains », *in*: *J. Math. Pures Appl. (9)* 134 (2020), pp. 328–368, ISSN: 0021-7824, DOI: 10.1016/j.matpur.2019.09.002, URL: https://doi.org/10.1016/j.matpur.2019.09.002.

[53] J.K. Lüdeker, O. Sigmund, and B. Kriegesmann, « Inverse homogenization using isogeometric shape optimization », *in*: *Comput. Methods Appl. Mech. Engrg.* 368 (2020), pp. 113170, 16, ISSN: 0045-7825, DOI: 10.1016/j.cma.2020.113170, URL: https://doi.org/10.1016/j.cma.2020.113170.

[54] H. Mechkour, « Homogénéisation et simulation numérique de structures piézoélectriques perforées et laminées », Thèse de doctorat dirigée par Miara, Bernadette Mathématiques appliquées Marne-la-Vallée 2004, PhD thesis, 2004, 1 vol. (III–157 p.) URL: http://www.theses.fr/2004MARN0224/document.

[55] B. Miara et al., « Piezomaterials for bone regeneration design—homogenization approach », *in*: *J. Mech. Phys. Solids* 53.*11* (2005), pp. 2529–2556, ISSN: 0022-5096, DOI: 10.1016/j.jmps.2005.05.006, URL: https://doi.org/10.1016/j.jmps.2005.05.006.

[56] B. Miara et al., « Piezomaterials for bone regeneration design—homogenization approach », *in*: *J. Mech. Phys. Solids* 53.*11* (2005), pp. 2529–2556, ISSN: 0022-5096, DOI: 10.1016/j.jmps.2005.05.006, URL: https://doi.org/10.1016/j.jmps.2005.05.006.

[57] J. H. Michell, « The wave resistance of a ship », *in*: *Phil. Mag.* 5.*45* (1898), pp. 106–123.

[58] M. Mint brahim, « Méthodes d'éléments finis pour le problème de changement de phase en milieux composites », Thèse de doctorat dirigée par Azaïez, Mejdi

et Palomo Del Barrio, Elena Mecanique Bordeaux 2016, PhD thesis, 2016, URL: http://www.theses.fr/2016BORD0157/document.

[59] J. Nocedal and S.J. Wright, *Numerical optimization*, Springer Series in Operations Research, Springer-Verlag, New York, 1999, pp. xxii+636, ISBN: 0-387-98793-2, DOI: 10.1007/b98874, URL: https://doi.org/10.1007/b98874.

[60] A. Novruzi and M. Pierre, « Structure of shape derivatives », *in*: *J. Evol. Equ.* 2.*3* (2002), pp. 365–382, ISSN: 1424-3199, DOI: 10.1007/s00028-002-8093-y, URL: https://doi.org/10.1007/s00028-002-8093-y.

[61] A. Novruzi and J. R. Roche, « Newton's method in shape optimisation: a three-dimensional case », *in*: *BIT* 40.*1* (2000), pp. 102–120, ISSN: 0006-3835, DOI: 10.1023/A:1022370419231, URL: https://doi.org/10.1023/A:1022370419231.

[62] O. A. Oleinik, A. S. Shamaev, and G. A. Yosifian, *Mathematical problems in elasticity and homogenization*, vol. 26, Studies in Mathematics and its Applications, North-Holland Publishing Co., Amsterdam, 1992, pp. xiv+398, ISBN: 0-444-88441-6.

[63] O. Pantz, « Sensibilité de l'équation de la chaleur aux sauts de conductivité », *in*: *Comptes Rendus Mathematique* 341.*5* (2005), pp. 333–337, ISSN: 1631-073X, DOI: https://doi.org/10.1016/j.crma.2005.07.005, URL: https://www.sciencedirect.com/science/article/pii/S1631073X05003183.

[64] O. Pironneau, *Optimal shape design for elliptic systems*, Springer Series in Computational Physics, Springer-Verlag, New York, 1984, pp. xii+168, ISBN: 0-387-12069-6, DOI: 10.1007/978-3-642-87722-3, URL: https://doi.org/10.1007/978-3-642-87722-3.

[65] A. Savitzky, « A historic collaboration », English, *in*: *Analytical Chemistry* 61.*15* (1989), Cited By :19, 921A–923A, URL: www.scopus.com.

[66] A. Savitzky and M. J. E. Golay, « Smoothing and Differentiation of Data by Simplified Least Squares Procedures », English, *in*: *Analytical Chemistry* 36.*8* (1964), Cited By :14287, pp. 1627–1639, URL: www.scopus.com.

[67] O. Sigmund, « A new class of extremal composites », *in*: *J. Mech. Phys. Solids* 48.*2* (2000), pp. 397–428, ISSN: 0022-5096, DOI: 10.1016/S0022-5096(99)00034-4, URL: https://doi.org/10.1016/S0022-5096(99)00034-4.

[68] O. Sigmund, « Materials with prescribed constitutive parameters: an inverse homogenization problem », *in*: *Internat. J. Solids Structures* 31.*17* (1994), pp. 2313–2329, ISSN: 0020-7683, DOI: 10.1016/0020-7683(94)90154-6, URL: https://doi.org/10.1016/0020-7683(94)90154-6.

[69] O. Sigmund, « Tailoring materials with prescribed elastic properties », en, *in*: *Mechanics of Materials* 20.*4* (June 1995), pp. 351–368, ISSN: 01676636, DOI: 10.1016/0167-6636(94)00069-7, URL: https://linkinghub.elsevier.com/retrieve/pii/0167663694000697 (visited on 10/09/2022).

[70] J. Simon, « Second variations for domain optimization problems », *in*: *Control and estimation of distributed parameter systems (Vorau, 1988)*, vol. 91, Internat. Ser. Numer. Math. Birkhäuser, Basel, 1989, pp. 361–378.

[71] R. Sivapuram, P.D. Dunning, and H. Alicia Kim, « Simultaneous material and structural optimization by multiscale topology optimization », *in*: *Struct. Multidiscip. Optim.* 54.*5* (2016), pp. 1267–1281, ISSN: 1615-147X, DOI: 10.1007/s00158-016-1519-x, URL: https://doi.org/10.1007/s00158-016-1519-x.

[72] J. Sokolowski and J-P. Zolésio, *Introduction to shape optimization*, vol. 16, Springer Series in Computational Mathematics, Shape sensitivity analysis, Springer-Verlag, Berlin, 1992, pp. ii+250, ISBN: 3-540-54177-2, DOI: 10.1007/978-3-642-58106-9, URL: https://doi.org/10.1007/978-3-642-58106-9.

[73] Md. S. Tarafder, G. M. Khalil, and S. M. I. Mahmud, « Computation of wavemaking resistance of Wigley hull form using Michell's integral », *in*: *The Institution of Engineers, Malaysia* 68 (2007), pp. 33–40.

[74] E. O. Tuck, « The wave resistance formula of J. H. Michell (1898) and its significance to recent research in ship hydrodynamics », *in*: *J. Austral. Math. Soc. Ser. B* 30.*4* (1989), pp. 365–377, ISSN: 0334-2700, DOI: 10.1017/S0334270000006329, URL: https://doi.org/10.1017/S0334270000006329.

[75] E. O. Tuck, L. Lazauskas, and D. C. Scullen, *Sea wave pattern evaluation - Part 1 report: Primary code and test results (surface vessels)*, tech. rep., Applied Mathematics Department, The University of Adelaide, Australia, 1999.

[76] B. Velichkov, « Existence and regularity results for some shape optimization problems », 2013GRENM088, PhD thesis, 2013, URL: http://www.theses.fr/2013GRENM088/document.

[77] J-L. Vie, « Second-order derivatives for shape optimization with a level-set method », 2016PESC1072, PhD thesis, 2016, URL: http://www.theses.fr/2016PESC1072/document.

[78] E. Vouga, *Elementary Smooth and Discrete Differential Notes.* https://www.cs.utexas.edu/users/evouga/notes-and-code.html, 2014.

[79] J.V. Wehausen and E.V. Laitone, *Surface waves*, Handbuch der Physik, Vol. 9, Part 3, Springer-Verlag, Berlin, 1960, pp. 446–778.

SCIENCES EXACTES ET LEURS APPLICATIONS

UNIVERSITÉ DE PAU ET DES PAYS DE L'ADOUR

Titre : Optimisation de formes robuste pour la mécanique des solides et des fluides.

Mot clés : Homogénéisation, Elasticité, Piézoélectricité, Résistance de Michell, Méthode de Newton

Résumé : Cette thèse étudie des problèmes de design robuste dans les domaines de la mécanique des solides (le design de micro-structures élastique et piézoélectrique), et de la mécanique des fluides (le problème des vagues et le design de carène de bateaux). Le premier problème est étudié selon une approche déterministe (le design est performant dans toutes les configurations perturbées en optimisant le pire cas possible) ce qui est difficile à résoudre en pratique et est remplacé par une approximation du premier ordre. Nos résultats numériques suggèrent que cette approximation n'est pas efficace pour le design optimal de micro-structures élastiques. Le second problème est étudié suivant une approche stochastique (le design a une bonne performance en moyenne, en optimisant l'espérance du critère de design). Cette approche, malgré son coût élevé en calcul, est efficace et on propose un nouvel algorithme de second-ordre pour accélérer les calculs.

Title: Robust shape optimization for solid and fluid mechanics.

Keywords: Homogenization, Elasticity, Piezo-electricity, Michell's resistance, Newton's method.

Abstract: The aim of this thesis is to study some robust design problems in the fields of solid mechanics (the design of elastic and piezoelectric micros-structures), and fluid mechanics (the wave problem and the design of ship hulls). The first problem is studied following a deterministic approach (the design should perform under all perturbed configurations by looking at the worst-case possible) which is difficult to solve and has to be approximated. Numerical results suggests a first order approximation of the worst-case scenario is not very efficient for the design of elastic microstructures. The second problem is studied through a stochastic approach (the design should perform good on average under all possible perturbations by optimizing the expectancy of the design criterion), this approach, although computationally expensive, is very efficient and we propose a new second-order algorithm algorithm to speed-up the use of the stochastic approach.